

Czech Technical University in Prague  
Faculty of Information Technology  
Department of Theoretical Computer Science



## **Iris Analysis**

by

*Mikuláš Krupička*

A dissertation thesis submitted to  
the Faculty of Information Technology, Czech Technical University in Prague,  
in partial fulfilment of the requirements for the degree of Doctor.

Dissertation degree study programme: Informatics

Prague, November 2017

---

**Supervisor:**

prof. Ing. Michal Haindl, DrSc.  
Department of Pattern Recognition Department  
Institute of Information Theory and Automation of the CAS  
Pod Vodárenskou věží 4  
182 08, Praha 8  
Czech Republic

Copyright © 2017 Mikuláš Krupička



---

# Abstract and contributions

This dissertation thesis discusses the task of iris recognition. Describes its history, introduces reader to the iris recognition problem and presents current state of development and describes available iris databases. It then presents three methods to iris occlusion detection and describes novel approach to iris recognition. The dissertation thesis continues with the methods results and compares them with other top performing methods. Finally, used and implemented software is briefly discussed and the thesis is concluded with overview of contributions and topics for future research.

In particular, the main contributions of the dissertation thesis are as follows:

1. Overview of the recent state-of-the-art in the iris recognition area in all related fields.
2. Detailed description of the available iris databases and their properties.
3. Three novel methods for detecting iris occlusions. The first one uses our own publicly available ground truth database. The second method achieved first place in comparison with 97 other competing algorithms from the worldwide *NICE.I* contest. The third method was used as ground truth generation method for contestants in the *MICHE II* contest. In the last method, we presented multispectral modification of the widely used integrodifferential operator.
4. Novel approach to iris recognition. Consisting of preprocessing steps to rule out negative iris images followed with the combination of feature representation and dissimilarity computing method for pairs of iris images.
5. Publicly available ground truth masks for iris occlusions to measure the performance of different methods.

**Keywords:**

iris recognition, iris segmentation, iris features, iris databases, biometrics, pattern recognition.



---

# Acknowledgements

This work could not have been completed without support of a number of people. First of all, I would like to thank my thesis supervisor, prof. Ing. Michal Haindl, DrSc. for his kindness, support and patience. He has given me a lot of helpful advice. It has been an honour for me to be his Ph.D. student.

And also, my greatest thanks to my parents and my sister for their support and care.

---

# Contents

<b>Abbreviations</b>	<b>xiii</b>
<b>1 Introduction</b>	<b>1</b>
1.1 Motivation . . . . .	1
1.1.1 Biometric Identification . . . . .	1
1.1.2 Iris Recognition System . . . . .	2
1.2 Problem Statement . . . . .	6
1.3 Goals of the Dissertation Thesis . . . . .	6
1.4 Structure of the Dissertation Thesis . . . . .	6
<b>2 State-of-the-Art</b>	<b>9</b>
2.1 Previous Results and Related Work . . . . .	9
2.1.1 Iris Acquisition . . . . .	9
2.1.2 Iris Segmentation . . . . .	10
2.1.3 Iris Normalization . . . . .	14
2.1.4 Detection of Iris Occlusions . . . . .	15
2.1.5 Iris Features Computation . . . . .	22
2.1.6 Iris Classification . . . . .	23
2.1.7 Iris Quality Metrics . . . . .	24
2.1.8 Other Comprehensive Surveys . . . . .	25
2.1.9 Used Fundamental Image Processing Methods . . . . .	25
2.1.10 Local Binary Patterns . . . . .	26
2.1.11 Gabor Filters . . . . .	26
<b>3 Iris Databases</b>	<b>29</b>
3.1 Databases Overview . . . . .	29
3.2 Databases with Images in Near Infrared Spectrum . . . . .	29
3.2.1 CASIA . . . . .	29
3.2.2 BATH . . . . .	31

3.2.3	MMU . . . . .	31
3.2.4	ND Iris Image Dataset . . . . .	32
3.2.5	DMCS . . . . .	32
3.2.6	BioSecurID . . . . .	33
3.2.7	VISOB . . . . .	33
3.3	Databases with Images in Visible Spectrum . . . . .	34
3.3.1	UPOL . . . . .	34
3.3.2	UBIRIS . . . . .	34
3.3.3	UBIRIS.v2 . . . . .	36
3.3.4	MICHE . . . . .	36
3.4	Databases Summary . . . . .	36
3.5	Databases used in This Thesis . . . . .	38
<b>4</b>	<b>Iris Occlusions Detection</b>	<b>41</b>
4.1	Fast Occlusion Detection on Eye Images . . . . .	41
4.1.1	Overview . . . . .	41
4.1.2	Image Preprocessing . . . . .	41
4.1.3	Iris Localization . . . . .	43
4.1.4	Multispectral Iris Texture Model . . . . .	43
4.1.5	Occlusion Detection . . . . .	45
4.1.6	Occlusions Mask . . . . .	46
4.1.7	Iris Normalization . . . . .	46
4.2	Robust Iris Occlusion Detection in Challenging Images . . . . .	46
4.2.1	Overview . . . . .	46
4.2.2	Iris Localization . . . . .	47
4.2.3	Iris Occlusions and Reflection Detection . . . . .	48
4.3	Robust Iris Occlusion Detection in Face Images . . . . .	51
4.3.1	Overview . . . . .	51
4.3.2	Reflection Correction . . . . .	51
4.3.3	Iris Localization . . . . .	51
4.3.4	Iris Occlusions and Reflection Detection . . . . .	55
4.4	Methods Summary . . . . .	57
<b>5</b>	<b>Iris Recognition</b>	<b>59</b>
5.1	Our Approach . . . . .	59
5.2	Determining Eye Position . . . . .	60
5.3	Color Histogram . . . . .	61
5.4	Textural Features . . . . .	61
5.4.1	Local Binary Pattern Features . . . . .	61
5.4.2	Gabor Filters . . . . .	62
5.4.3	CAR Model . . . . .	63
5.5	Iris Classification . . . . .	64
5.6	Method Summary . . . . .	67

<b>6</b>	<b>Iris Biometrics Evaluation</b>	<b>69</b>
6.1	Performance Evaluation . . . . .	69
6.1.1	Basic Criteria . . . . .	69
6.1.2	Advanced Criteria . . . . .	69
6.1.3	ROC Plot . . . . .	70
6.2	NICE.I Contest . . . . .	71
6.3	NICE.II Contest . . . . .	72
6.4	Mobile Iris Challenge Evaluation I Contest . . . . .	73
<b>7</b>	<b>Proposed Methods Results</b>	<b>75</b>
7.1	Results for Method ‘Fast Occlusion Detection on Eye Images’ . . . . .	75
7.2	Results for Method ‘Robust Occlusion Detection in Challenging Images’ . .	75
7.3	Results for Method ‘Robust Occlusion Detection in Face Images’ . . . . .	78
7.4	Iris Recognition . . . . .	80
7.4.1	Rule-out Methods . . . . .	80
7.4.2	Iris Textural Features . . . . .	81
<b>8</b>	<b>Developed Software</b>	<b>85</b>
8.1	Created Software . . . . .	85
8.1.1	Iris Library . . . . .	86
8.1.2	Console Application . . . . .	86
8.1.3	Windows Application . . . . .	87
8.2	Ground Truth Masks for UBIRIS Database . . . . .	87
<b>9</b>	<b>Conclusions</b>	<b>91</b>
9.1	Summary . . . . .	91
9.2	Contributions of the Dissertation Thesis . . . . .	92
9.3	Future Work . . . . .	93
	<b>Bibliography</b>	<b>95</b>
	<b>Reviewed Publications of the Author Relevant to the Thesis</b>	<b>107</b>
	<b>Remaining Publications of the Author Relevant to the Thesis</b>	<b>113</b>

---

## List of Figures

1.1	Iris recognition processing pipeline. . . . .	3
1.2	The eye anatomy. . . . .	4
1.3	Necessary steps before iris recognition. . . . .	4
2.1	Iris Pipeline . . . . .	9
2.2	Iris normalization scheme . . . . .	15
2.3	The example of iris reflection. . . . .	16
2.4	The example of eyelid occlusion. . . . .	17
2.5	The example of eyelash occlusion. . . . .	17
2.6	The example of shadow caused by eyelash. . . . .	18
2.7	The example of out-of-iris occlusion. . . . .	18
2.8	The example of out of focus imperfection. . . . .	18
2.9	The example of eye partially out of image. . . . .	19
2.10	Example of creating LBP feature vector. . . . .	27
2.11	Examples of Gabor kernel. . . . .	27
3.1	Example images from CASIA-IrisV1 database. . . . .	30
3.2	Example images from CASIA-IrisV2 database. . . . .	30
3.3	Example images from CASIA-IrisV4 database. . . . .	31
3.4	Example images from MMU database. . . . .	32
3.5	Example images from VISOB database. . . . .	34
3.6	Example images from UPOL database. . . . .	35
3.7	Example images from UBIRIS database. . . . .	35
3.8	Example images from UBIRIS.v2 database. . . . .	36
3.9	Example images from MICHE database. . . . .	37
4.1	Processing scheme of method 1. . . . .	42
4.2	Detected iris regions containing all occlusion types apparent in UBIRIS database. . . . .	45
4.3	Normalized iris and its prediction error. . . . .	46
4.4	Processing scheme of method 2. . . . .	47

## LIST OF FIGURES

---

4.5	Detected reflections in iris and their corrections. . . . .	48
4.6	The intermediate results of integrodifferential Daugman operator . . . . .	49
4.7	Correcting imprecisely detected iris. . . . .	49
4.8	The visibility of pupil, iris, its occlusions and reflections in each spectral channel (red, green, blue). . . . .	50
4.9	Processing scheme of method 3. . . . .	52
4.10	Detecting iris reflections . . . . .	52
4.11	Detected rough iris region using the generalized Hough transformation . . . . .	53
4.12	Iris region defects from iPhone5 device containing four (a,b,c,d) occlusion types. . . . .	54
4.13	Output of multispectral integrodifferential operator. . . . .	55
4.14	Upper eyelid detection steps in the red spectral channel. . . . .	56
4.15	Thresholding for lower eyelid detection. . . . .	57
5.1	Schema of iris recognition method. . . . .	59
5.2	Examples of eyes with visible position. . . . .	60
5.3	Impact of rotation to iris normalization. . . . .	62
5.4	Graphs for estimating Gabor kernel. . . . .	63
5.5	Best estimated Gabor kernels (real and imaginary part). . . . .	63
5.6	PCA transformation of 3DCAR (4.1.4) parameters. . . . .	64
5.7	Schema of classification method. . . . .	65
5.8	Examples of per pixel classification result images. . . . .	65
6.1	Example of ROC curve. . . . .	71
6.2	Left is the ground truth image, center is method result image and right is diff image from the first two. . . . .	72
7.1	Eye images and the corresponding detected occlusions masks in the first method (UBIRIS database). . . . .	76
7.2	Eye images, ground truth, detected occlusions masks, and their comparison with the ground truth in the second method (UBIRIS.v2 database). . . . .	79
7.3	Selected eye images from the MICHE database and their detected defects (the third method, MICHE database). . . . .	80
7.4	Examples of LBP feature extraction on iris images. . . . .	82
7.5	Examples of PCA visualized 3DCAR (4.1.4) parameters. . . . .	82
7.6	Examples of irises convolved with Gabor kernels. The first column is input iris, the second is real part of a kernel and the third is imaginary part of a kernel. . . . .	83
8.1	First few lines from configuration file. . . . .	86
8.2	Screenshot from our ImageProcessing application. . . . .	87
8.3	Example of results of occlusion detection task in application. . . . .	88
8.4	Screen from <a href="http://iris.utia.cas.cz/">http://iris.utia.cas.cz/</a> web. . . . .	89
8.5	Publicly available ground truth masks of UBIRIS database. . . . .	90



---

## List of Tables

3.1	Detailed description of MICHE iris database. . . . .	38
3.2	Iris datasets overview . . . . .	39
5.1	Top eight alternative results from the Noisy Iris Challenge Evaluation Contest (NICE.II) [PA12]. . . . .	66
7.1	The first method performance overview. . . . .	77
7.2	The Noisy Iris Challenge Evaluation Contest [PA10] top eight results (from 97 participants) on the contest UBIRIS.v2 database compared with the presented methods and [TK12]. . . . .	78
7.3	Top eight results from the Noisy Iris Challenge Evaluation Contest [PA12] (NICE.II) compared with our individual step results. . . . .	81



---

# Abbreviations

## Common Mathematical Functions and Operators

$b_i$	the $i^{\text{th}}$ element of vector $\mathbf{b}$
$\mathbf{A}$	Matrix $\mathbf{A}$
$a_{i,j}$	Element of matrix $\mathbf{A}$ at the $i^{\text{th}}$ row, and the $j^{\text{th}}$ column
$\mathbf{A}^{-1}$	Inverse matrix to matrix $\mathbf{A}$
$\mathbf{A}^T$	Transposed matrix to matrix $\mathbf{A}$
$a \bmod b$	Remainder after dividing $a$ by $b$

## Mathematical Terminology

$\mu$	Mean value
$\sigma$	Standard deviation
$\epsilon_r$	Gaussian noise
$r = \{r_1, r_2\}$	Pair of indices (row and column)
$A_x$	Parameter matrix
$\gamma$	Process parameter matrix
$X_r$	Random variable
$X^{(r-1)}$	Process history
$Z_r$	Vector of random variables
$\Delta$	Euclidean distance

### Images related notation

$I(x, y)$	Image pixel on coordinates $x, y$
$G_\sigma(a) * \mathbf{x}$	convolution of vector $\mathbf{x}$ with 1D Gabor kernel of size $a$
$\max_{(a,b)}  f(a, b) $	maximum value when searching function $f$ for all values of $a, b$
$\rho$	Circle radius
$*$	Convolution
$\otimes$	Multispectral convolution
$\{c_x, c_y, \rho\}$	Triplet denoting circle (center coordinates and radius)
$R = \{x, y, h, w\}$	Region inside image, quartet (topleft coordinates $x, y$ and height and width of the area)
$H_a$	Histogram of image $a$

### Miscellaneous Abbreviations

<b>GHT</b>	Generalized Hough Transformation
<b>NIR</b>	Near Infra Red
<b>RGB</b>	Red-Green-Blue color channels
<b>AC</b>	Active Contours
<b>ASM</b>	Active Shape Model
<b>EM</b>	Expectation-Maximization
<b>GLCM</b>	Gray-Level Co-occurrence Matrix
<b>LBP</b>	Local Binary Patterns
<b>DCT</b>	Discrete Cosine Transform
<b>ICA</b>	Independent Component Analysis
<b>PCA</b>	Principal Component Analysis
<b>GMM</b>	Gaussian Mixture Model
<b>KNN</b>	k-nearest neighbor classifier

---

# Introduction

*In this chapter, motivation for this dissertation thesis is described along with the brief introduction to biometric identification. Particularly the biometric identification based on iris. This theme is further examined in the Chapter 2. The chapter concludes with the description of the problem we've tried to solve. The goals which we've tried to achieve and the structure of the thesis are both communicated.*

## 1.1 Motivation

For identification, people typically use their user names, passwords or identification cards. But identification card can be stolen, the password forgotten and the user name used by anybody else. So there is a big demand for improving the identification methods that are reliable, secure, fast and easy to use. Whether one wants to use ATM, pay with credit card or login to his computer account, in all these examples an reliable method for identity proof is needed.

Apart from the cases where people want to identify themselves, there are also number of cases where, on the contrary, one do not want to be known. And we want to correctly recognize them (e.g. airport security check, search for wanted persons, movement control of guarded person).

All these can be solved with the help of biometric identification methods, which will be described further.

### 1.1.1 Biometric Identification

The biometric recognition offers more reliable method for person recognition than traditional methods (described in 1.1). Since biometric identifiers are inherent to an individual, they are more difficult to steal, to manipulate or even to forget. The traits that will be used also depends on the environment conditions, the technology we can afford, how robust the results will be or how quickly we want to have the results. It can be voice, fingerprint, palmprint, iris, retina, face, handwriting, vein and others [JRN11]. They differ in ways

how to acquire them, their durability, reliability, necessary equipment for acquisition, and its costs and the evaluation.

In this text we focus on the identification using the iris because of its stability over lifetime, ease of acquisition (can be done from distance of up to several meters). Although recently was found that the iris texture slightly changes over time [FB11]. But compared to the other biometric traits it is still relatively stable over time. The eye is considered to be an internal organ (thus it is well protected from external influences). It is also visible from the outside and can be acquired without affecting the body. The idea of using the eye as an identifier is over hundred years old. In the 1882 Alphonse Bertillon started to measure body properties for the police record cards. He was also first to propose using the iris color for the person identification in 1886 [Ber86]. The idea of using an iris for a person identification was first suggested by Frank Burch in 1936 [Dau01].

Unlike classical biometrics traits described above, there are also soft biometrics traits which can be described as physical, behavioral or adhered human characteristics. They are commonly used by humans for differentiating the individuals. As stated above, their beginnings can be connected with the work done by Alphonse Bertillon in 1886 [Ber86]. These are not unique by themselves but can be well utilized in surveillance applications. Thus it is understandably one of the currently evolving science topics (see [Rei+13] for an overview).

Examples of the soft biometrics traits can be:

- *Physical*: skin color, eye color, hair color, presence of beard, presence of mustache, height, weight
- *Behavioral*: gait, keystroke
- *Adhered*: clothes color, tattoos, accessories

### 1.1.1.1 Iris Anatomy

The comprehensive description of an eye anatomy and its properties was done by Alfred Adler [Adl60]. The iris is an annual region in the eye bounded by the pupil and the sclera on the inner and outer boundaries. These features are important while searching for the iris segmentation as described in the Section 2.1.2. The visual properties of an iris are formed during the fetal body development and stabilizes in the first two years of child life. They are also believed to be unique between persons, even uncorrelated between person left and right eye [DD01]. See the Figure 1.2 for overview of an eye anatomy.

### 1.1.2 Iris Recognition System

The iris recognition undergone rapid development in the past decades [BHF13]. Still, the processing chain remained almost same. The typically conducted steps can be seen in the Figure 1.1. It is essentially a pattern matching system with the goal to match (or reject) two irises.

In particular, it consists of the following steps:

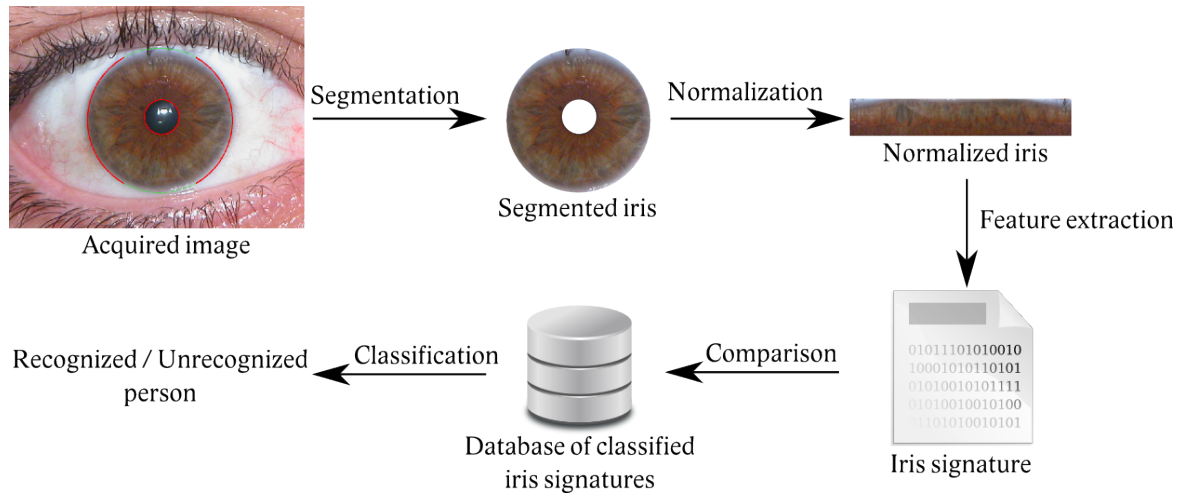


Figure 1.1: Iris recognition processing pipeline.

1. image acquisition
2. iris segmentation and occlusion detection
3. iris normalization
4. feature extraction
5. iris recognition

It is also worth to mention that the iris localization can be much harder task depending on the problem definition. Generally it is necessary to first locate the human figure, than his face and so on, see the Figure 1.3 for an brief overview. We do not take into account these problems because they are difficult tasks on their own that can be tackled separately and are out of the scope of this thesis.

### 1.1.2.1 Image Acquisition

The first step in iris recognition is capturing an image with eye. There are many different setups depending on the application. Also the image can be captured in color, grayscale or in infrared spectrum. To this day, majority of iris acquisition devices still use near-infrared images (700 – 900nm light wavelength) (see the Chapter 3).

Daugman in his paper from 2003 ([Dau04]) states that the image acquisition should use near-infrared illumination. It helps to reveal the detailed structure of heavily pigmented irises. Melanin pigment absorbs much of visible light, but reflects more of the longer wavelengths of light. He also suggests that the iris should have diameter of at least 140 pixels. The International Standards Organization (ISO) Iris Image Standard released in 2005 is more demanding, specifying the diameter of 200 pixels.

<sup>1</sup>Source: [https://en.wikipedia.org/wiki/Human\\_eye](https://en.wikipedia.org/wiki/Human_eye)

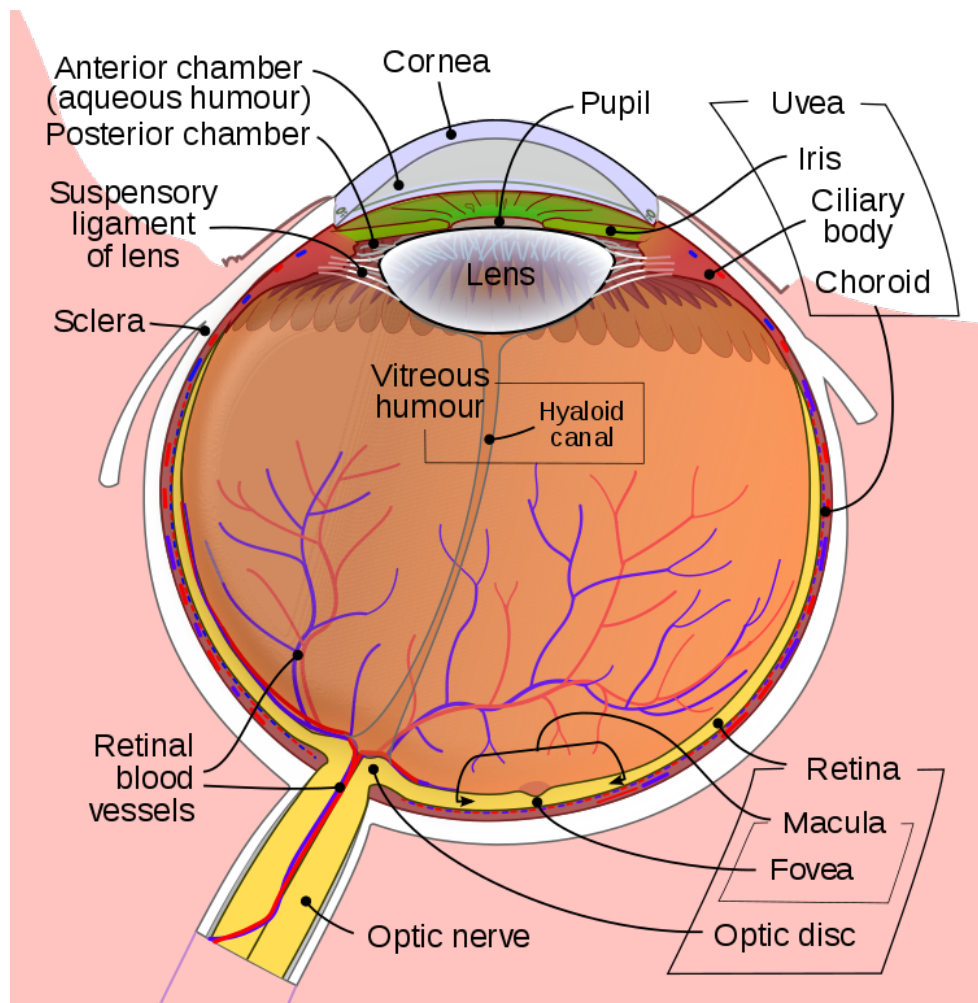


Figure 1.2: The eye anatomy<sup>1</sup>.

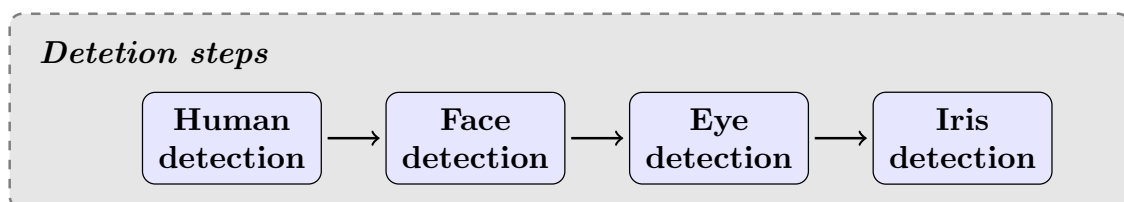


Figure 1.3: Necessary steps before iris recognition.



### 1.1.2.2 Iris Segmentation and Occlusion Detection

The captured image of the iris typically includes also eyelashes, eyelids, sclera, pupil and other unwanted parts. So the most basic step to get rid of them is to register the iris to two noncentric circles (outer and inner boundary). This process is known as the iris localization or the iris segmentation.

Subsequently it is needed to detect the occlusions in the iris texture to ensure robust system recognition. Especially for the color images. As an occlusion are understood imperfections introduced in the image during the acquisition because of environmental conditions, properties of capturing equipment, or illumination changes. There are also included parts of the eye that can obstruct iris visibility (above mentioned eyelashes, eyelids). See the Section 2.1.4 for details.

### 1.1.2.3 Iris Normalization

The normalization step was introduced by John Daugman [Dau93] to simplify the next step (see Section 2.1.3 for details). The algorithms for feature computing are typically assuming a rectangular area. Therefore the normalization is usually done to a rectangle with a fixed size to also mitigate different iris sizes due to the different head distance to the camera and the different pupil size due to the varying lighting conditions in the time of capture. This step greatly simplifies the following methods as it allows to standardize all subsequent steps to the unified iris shape.

### 1.1.2.4 Feature Computation

As stated above, the next step, given the segmented and normalized iris, is the feature computation. The purpose of feature computation is to transform the iris to compact representation format that is more suitable for comparison with other irises. These are usually called the feature vectors. Much of the current state-of-the-art development is done in this area (see Section 2.1.5).

### 1.1.2.5 Iris Recognition

And finally, the computed feature vector is compared to the database of known irises. As described in the Section 6.1, a different types of errors can occur. And therefore, although the classifier is usually true/false based, on the basis of the ROC curve we can say the probabilities of each types of the error. The result itself can be ‘recognized person’ or ‘unknown iris’.

And besides applications of the human identification, the another goal can be the recognition of various types of eye diseases. The principles of this detections can be based on the same basis as the iris recognition (iris detection with the texture analysis and following classification). But the first problem of this task is to obtain sufficient amount of and well described data. But information of this kind is currently not present in any available iris database.

### 1.2 Problem Statement

While the process explained above is well known and described, much of the well known and used methods are still focused on iris images taken from very close distance and often even with an infrared spectrum, for which the specialized equipment is needed along with the full cooperation of recognized person. Also the images taken that way are clear and without specular reflections.

This work is focusing on the processing of iris images taken from bigger distance, without the active participation of observed person and also assume that the captured iris images will be non-ideal with various types of occlusions such as eyelashes, eyelids, various reflections and others (described in Section 2.1.4). We will have to deal with images in the visual spectrum taken with the consumer hardware.

One problem not discussed in the thesis but also applicable to used methods is medical recognition. Specifically the recognition of eye diseases as glaucoma, cataract and many others. These types of problems can be supposedly detected by our methods as they make use of the iris texture analysis. However there are difficulties in obtaining such data due to the obvious reasons as the privacy protection and the expert labeling.

### 1.3 Goals of the Dissertation Thesis

1. Overview of the recent state-of-the-art in the iris recognition area in all related fields.
2. Detailed description of available iris databases and their properties.
3. Three novel methods for detecting iris occlusions specialized on different iris acquiring conditions.
4. Novel approach to iris recognition. With preprocessing steps to rule out negative iris images, a feature computation and method for computing dissimilarity for pairs of iris images.
5. Publicly available ground truth masks for iris occlusions to measure performance of different methods.

### 1.4 Structure of the Dissertation Thesis

The dissertation thesis is organized into 9 chapters as follows:

1. *Introduction*: Describes the motivation behind our efforts. There is also a list of goals of this dissertation thesis.
2. *Background and State-of-the-Art*: Introduces the reader to the necessary theoretical background and surveys the current state-of-the-art.

3. *Iris Databases*: Shows the overview of iris databases that can be used for our experiments and the chosen databases for our work.
4. *Iris Occlusions Detection*: Describes the proposed methods for detecting occlusions in the iris and covers used algorithms with their modifications against original methods.
5. *Iris Recognition*: Describes our approach to the iris recognition. Also proposes preprocessing steps to rule out negative iris images, the feature computation and method for computing dissimilarity for pairs of iris images.
6. *Iris Biometrics Evaluation*: Describes the various scoring methods for biometric evaluation. Also gives overview of several iris recognition contests used to compare our methods with others.
7. *Achieved results of proposed methods*: Shows the results of our methods in context of other approaches solving the same problem and compare them.
8. *Developed Software*: Describes software that was implemented in the process of developing our methods and presents our UBIRIS database ground truth dataset.
9. *Conclusions*: Summarizes the results of our research, describes topics for future research, and concludes the thesis.



## State-of-the-Art

In this chapter, the sections are thoroughly describing the state-of-the-art of each step of the iris recognition pipeline (see the Figure 2.1). The chapter also briefly surveys the iris quality metrics that are important for the less constrained iris setups. At the end of the chapter, the overview of recent iris related surveys is given followed with the description of the fundamental methods used further in the dissertation thesis.

### 2.1 Previous Results and Related Work

#### 2.1.1 Iris Acquisition

The image acquisition is the first step. It is typically done with the specialized camera that capture the iris in the near infra red (NIR) spectrum or with the color camera that produces the image in the visible spectrum. Both setups aim to provide good quality images because the image quality have large impact on the performance of the whole system [Dau06]. Most

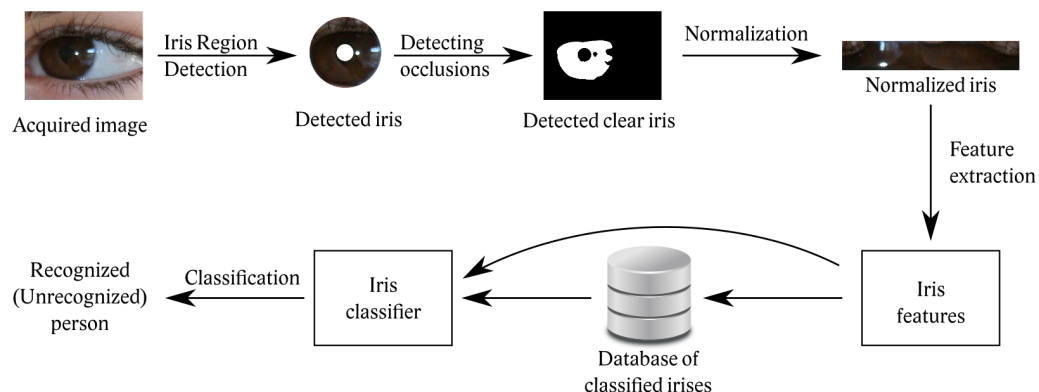


Figure 2.1: Iris Pipeline

current systems specialized on the iris capturing are in the NIR spectrum and also require the user cooperation [Way+09].

The NIR cameras operate with the light in the near infra red spectrum (wavelengths between  $700nm - 900nm$ ). Also the use of the NIR sensor has some advantages that ease the whole recognition process: the textural nuances are visible equally regardless of the iris color. Because in the visible light, the melanin in iris absorbs part of the light and subsequently changes the appearance of the captured iris. In the NIR light, the reflections from an other environmental light sources or simply the reflections of surroundings are not so apparent.

There is growing need to recognize iris images captured with more accessible color cameras. But those images are also more difficult to process as there will be bigger occlusions, more reflections and also the iris texture will be different based on iris color.

### 2.1.2 Iris Segmentation

The iris segmentation task is currently done mainly by the integrodifferential operator introduced by John Daugman [Dau93] and by circular the Hough transform proposed by Richard Wildes [Wil97]. There are also number of other methods which are not as widely used as the first two (or their modifications).

#### Integrodifferential Operator

In 1993 John Daugman [Dau93] presented the method of eye segmentation based on the integrodifferential operator (equation 2.1). This method searches through the  $\mathbb{N}^3$  space (circle radius and image coordinates). The original algorithm is thus time consuming and often modified with this improvement in mind. It also face significant difficulties when dealing with the eyelid and eyebrow overlaps, because they disrupt the upper and bottom circular intensity changes when moving to the eye center. On top of that, when the iris is not in the image at all, method still returns incorrectly found iris. For non-deformed eyes (the eyes with circular shape), its accuracy is very good. The method was originally presented on NIR images and works only in one spectral channel.

$$\max_{(\rho, r_1, r_2)} \left| G_\sigma(\rho) * \frac{\partial}{\partial \rho} \oint_{\rho, r_1, r_2} \frac{I(r_1, r_2)}{2\pi\rho} ds \right| \quad (2.1)$$

The equation 2.1 searches for outer iris boundary circle represented as vector  $[\rho, r_1, r_2]$ .  $I(r_1, r_2)$  is thus image pixel and  $\rho$  given circle radius.  $\oint_{\rho, r_1, r_2} ds$  is integrating over circle with center in  $(r_1, r_2)$  and radius  $\rho$ . Then  $\frac{\partial}{\partial \rho}$  is subsequently differentiating over range of integrated radii.  $G_\sigma(\rho)$  is convolution of sequence of differentiated radii with the Gaussian kernel. The equation thus represent the searching for maximum difference in the sums over the chosen position and radii (i.e. the highest change in circular intensity).

Some minor improvements were introduced by Nishino and Shree [NN04]. They modified the operator so that it is possible to search eye boundaries as ellipses, which can be

a considerable improvement. Especially when the eyes are rotated to the side. But the algorithm complexity rise to five dimensions (because of additional parameters for ellipse).

The similar operators were proposed by Camus [CW02] and Martin-Roche [MRSASR01]. Both their algorithms (with setup presented in articles) are faster but less accurate and are maximizing the equations that locate iris borders.

Zheng *et al.* [ZYY05] investigated segmentation in HSV space and used integrodifferential operator for pupil detection. Also presented iterative shrink and expand process minimizing average intensity for limbic boundary detection.

Kennell *et al.* [KIG06] combined the integrodifferential operator with morphological operations for pupular boundary fitting. And variance-based image binarization on pixels for limbic boundary fitting.

Grabowski and Napieralski [GN11] presented a hardware-based integrodifferential operator for faster iris fitting.

Daugman [Dau07] also presented an enhancement to precisely fitting the iris boundaries based on the active contours [BI98]. This method is designed to be performed after a regular segmentation algorithm. Since it is independent on chosen segmentation method, it can be used even after other algorithms than proposed integrodifferential operator.

Tan *et al.* [THS10] in their winning method (NICE.I [PA07]) described accelerated algorithm based on integrodifferential operator combined with gradient descent. This leads to evaluating only small fraction of possible pixels thus being a lot faster. Instead of the original operator, they proposed integrodifferential ring which determined a direction for next algorithm iteration. They also proposed additional methods for reflection removal and other occlusions which will be described in following sections.

## Circular Hough Transform

The idea of Hough transform was initially proposed by Paul Hough [Hou59] to find non-ideal objects in the parametrized space through voting procedure.

Use of the Circular Hough transform (see equation 2.2) was proposed by R. Wildes [Wil97] to be performed on an binary gradient-based edge-map. It, as well as integrodifferential operator, searches through the  $\mathbb{N}^3$  space. But the contour of the eye can be adapted to any simple shape, which can be described by the Hough transform. Because of that, finding non-circular eyes is simpler. Although this proposed improvement increases the required compute time. And this method has also problems when the iris is not present in the image at all.

$$H(r_1, r_2, \rho) = \sum_{r_1=1}^n \sum_{r_2=1}^m h(r_1, r_2, s_1, s_2, \rho) \quad (2.2)$$

where

$$h(r_1, r_2, s_1, s_2, \rho) = \begin{cases} 1 & \text{if } g(r_1, r_2, s_1, s_2, \rho) = 0 \\ 0 & \text{otherwise} \end{cases}$$

$$g(r_1, r_2, s_1, s_2, \rho) = ((r_1 - s_1)^2 + (r_2 - s_2)^2 - \rho^2) \cdot J(r_1, r_2)$$

In equation 2.2, vector  $[s_1, s_2, \rho]$  represents searched iris boundary.  $r_1$  and  $r_2$  are image coordinates,  $n$  and  $m$  are columns and rows counts in image. And  $J(r_1, r_2)$  is pixel from output mask of the edge detector.

Zuo and Schmid [ZS10] presented a method where they used the Hough transform to segment pupillary boundary. The iris image was denoised with Wiener filter, contrast enhanced and inpainted beforehand. They refined the localization with ellipse fitting and refined pupil segmentation.

Cui *et al.* [Cui+04] proposed modified Hough transform with usage of wavelet pyramid for detecting inner iris boundary in the image. For outer boundary he is proposing the integrodifferential operator (see section 2.1.2).

Ma *et al.* [MWT02] proposed a step for rough estimation of iris position by projecting the image in horizontal and vertical direction. Followed with the Circular Hough transform for accurate localization.

Filho and Costa [CFC10] used images in HSV and RGB spaces to segment iris. They firstly approximated both boundaries on selected color component (hue for outer limbic boundary and red and green for pupil boundary) by k-means clustering and further refined it with Hough transform.

## Active Contours

Active contours (AC), also called snakes, is a framework for delineating object outlines. AC is an energy minimizing spline that is influenced by some constraint typically based on an image pixels.

Ritter and Cooper [RC03] were first to propose AC approach with finding the equilibrium between an internal force favouring circularity of a boundary and external force pushing the iris boundary towards the maximum gradient.

Abhyankar and Schuckers [AS06] then proposed Active shape model which is similar to AC. They aimed to solve specifically problems with off-gaze eye images.

Daugman [Dau07] proposed an AC based approach where he described the inner and outer boundaries as Fourier series. The main problem for his approach remains as the need for initial (center) iris position.

Shah and Ross [SR09] proposed an iris segmentation scheme employing geodesic active contours to extract the iris from the surrounding structures. The proposed scheme finds the iris texture in an iterative fashion and is guided by both local and global properties of the image.

Nguyen *et al.* [NFS10] suggested rough estimation of iris position based on histogram thresholding and morphology operators and then precise iris segmentation using shrinking and expanding AC model.



Koh *et al.* [KGC10] also roughly estimated an eye position using binarization (it is assumed that the pupil have lowest intensity) followed with morphological operators. The AC is then applied to sclera and pupil boundaries.

### **Polar Transformation**

As Active contour, there are also other parameter-fitting techniques. Frequently used is polar transformation since it simplifies the task for finding the iris boundaries. An accurate iris center position is necessary though.

Du *et al.* [DIE04] proposed method that is based on adaptive thresholding and polar transformation. Initially, the pupil boundary is detected, then the image is transformed to a polar system. The second boundary is recognized as the sclera boundary. This method uses the fact, that almost all eyelash occlusions affect only the outer border. Though the method was tested only on CASIA database, which has manually highlighted pupils (with sharper edges, see Section 3.2.1).

Luengo-Oroz *et al.* [LOFA10] proposed iris segmentation that relies on the closed nested structures of iris anatomy (the sclera is brighter than the iris, and the iris is brighter than the pupil) and on its polar symmetry. The described method applies mathematical morphology for polar/radial-invariant image filtering and for circular segmentation using shortest paths from generalized gray-level distances.

### **Self Organizing Neural Network**

Liam *et al.* [LCF02] introduced a way to recognize the iris using self organizing neural networks. Evaluating neural networks is fast and this method can also reject non-iris images (instead of incorrectly recognizing eye). Unfortunately, author tested it only on the small nonpublic iris database. Also comparison with other methods is not present at all.

### **Cascade Classifier**

Cascade classifier (initially proposed by Paul Viola [VJ01]) builds upon the idea of several simpler classifiers (stages) that are applied sequentially to the region of interest until at some stage the candidate is rejected or all stages are passed. The stages are designed to reject negative regions as fast as possible. The assumption is that the vast majority of windows does not contain the object of interest. Conversely, true positives are rare and worth taking the time to verify.

He *et al.* [He+09] proposed usage of the Cascade Classifier. It is shown that this method (when properly learned) is very fast but also pixel-inaccurate. So additional step for further refinement had to be introduced (the integrodifferential operator or the Circular Hough transform discussed above).

Raja *et al.* [Raj+15] proposed a new segmentation scheme and adapted it to the smartphone based visible iris images for approximating the radius of the iris to achieve a good segmentation. They also proposed a new feature computation method based on deep sparse filtering to obtain iris features for unconstrained images.

## Morphological Operations

The morphological operations are typically used in conjunction with other techniques. Though Mira [JM03] proposed using the morphological operations alone for acquiring the iris boundaries. The used operators are: *thresholding*, *area opening*, *closing*. But proposed method is not compared with other approaches.

## EM Algorithm

Kim *et al.* [Kim+04] presented application of EM algorithm for detecting the iris in the image. They claim that the pixel intensities of the captured iris image can be classified to three Gaussian distribution components. With use of the EM algorithm is used to estimate the distribution parameters.

### 2.1.3 Iris Normalization

The iris normalization is a step proposed by Daugman in [Dau93] and is called the ‘rubber sheet model’. This step is essentially optional. But without it, further processing would be more difficult. In addition, most feature computation methods expects normalized form. It is nowadays considered a standard part of iris processing chain as it is in every method presented.

The rubber sheet model assigns each pixel  $(r_1, r_2)$  in iris, the real coordinates in the target model  $(\rho, \theta)$ . And this can be represented as

$$I(r_1(\rho, \theta), r_2(\rho, \theta)) \rightarrow I(\rho, \theta) , \quad (2.3)$$

$$r_1(\rho, \theta) = (1 - \rho) \cdot p_1(\theta) + \rho \cdot l_1(\theta) , \quad (2.4)$$

$$r_2(\rho, \theta) = (1 - \rho) \cdot p_2(\theta) + \rho \cdot l_2(\theta) , \quad (2.5)$$

with  $I(\rho, \theta)$  as coordinates in the target shape. The  $\rho$  is from the interval  $[0, 1]$  and  $\theta$  is the angle from  $[0, 2\pi]$ . So the result is the image with *width* =  $\langle 0, 2\pi \rangle$  and *height* =  $\langle 0, 1 \rangle$ . The  $r_1(\rho, \theta)$  and  $r_2(\rho, \theta)$  are defined as linear combinations of both the set of pupillary boundary points  $(p_1(\theta), p_2(\theta))$  (inner circle of the iris) and the set of limbic boundary points  $(l_1(\theta), l_2(\theta))$  (outer circle of the iris). The variables are visually explained in Figure 2.2.

So the iris normalization is basically transformation from the non-centric disc (disc defined by two non-centric circles, pupillary and limbic iris boundaries) to the rectangle (see scheme at the Figure 2.2). The transformation can be performed using the following equations:

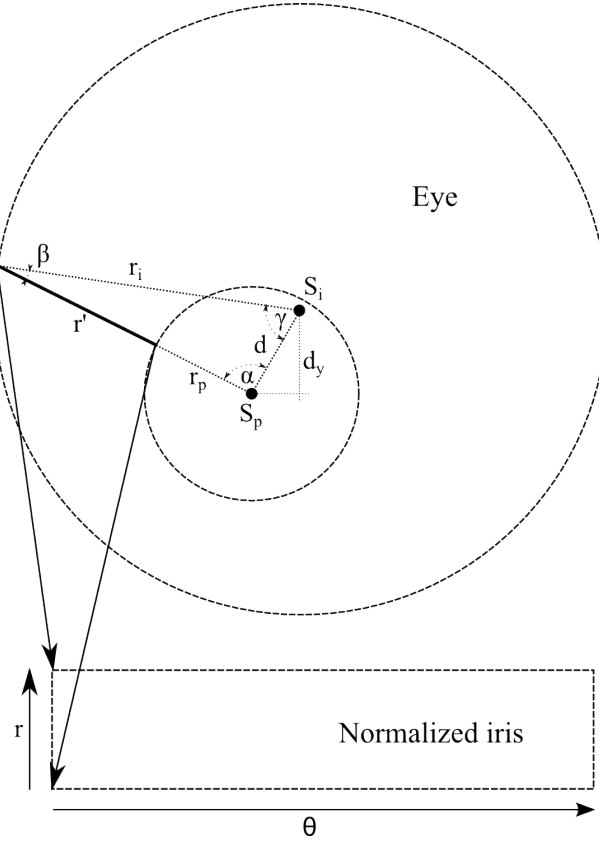


Figure 2.2: Iris normalization scheme

$$\alpha = \left| \theta - \arcsin \left( \frac{d_y}{d} \right) \right| ,$$

$$\beta = \arcsin \left( \sin \alpha \circ \frac{d}{r_i} \right) ,$$

$$\gamma = \pi - \alpha - \beta ,$$

$$r' = r_i \circ \left( \frac{\sin \gamma}{\sin \alpha} \right) - r_p .$$

### 2.1.4 Detection of Iris Occlusions

Due to the various types of occlusions which are often found in the iris (especially those acquired in an uncontrolled conditions or in a visible spectrum), additional step was introduced to improve the classification results. Its main purpose is to discard the occluded pixels from the feature computation (and therefore from classification) or deny the whole image in case of big occlusions.

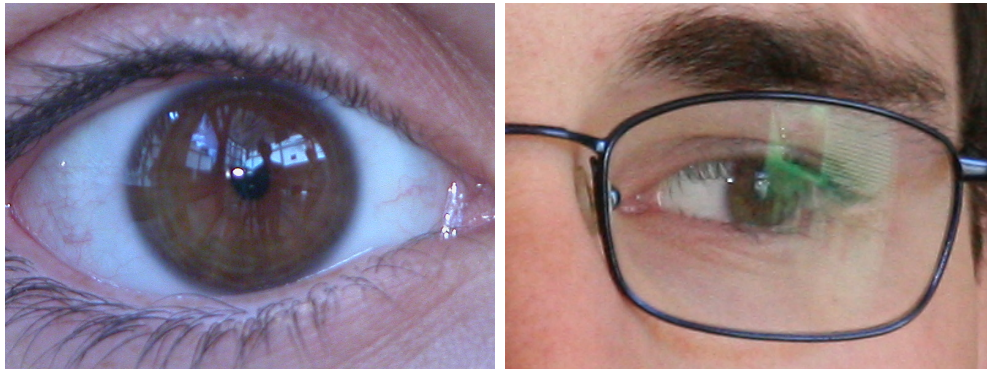


Figure 2.3: The example of iris reflection.

### 2.1.4.1 Types of Occlusions

Besides the standard types of imperfections (blur, noise, ...), the irises tend to have several specific types of occlusions. Those will be described in the following sections. These occlusions could increase the false rejection rates or even cause the failure of the segmentation method. Apart from the right image in the Figure 2.3 (which is from the UBIRIS.v2, Section 3.3.3) images in all figures under this section are taken from the UBIRIS database [PA05], described in Section 3.3.2.

**Reflection** This type of distortion highly depends on the used light spectrum and on the environmental conditions. Especially the lights surrounding the captured person, and its interaction with the environment. Also it highly depends on whether the person is wearing glasses or contact lenses (their removal can be particularly hard because of big reflection areas spreading to whole eye surroundings). The reflection distortion can appear anywhere in the iris and can have any shape as it just depends on the surrounding environment. The reflections from the lights have higher intensity than the reflections from the environment. See the examples in Figure 2.3.

**Upper and Lower Eyelid** Probably the most common type of occlusion in the iris. As this occlusion is for most people normal state of eyes. It often covers a large area of the iris and is often accompanied with an eyelashes. Due to the cause of occlusion it appears either in the upper or the lower area of the iris. See Figure 2.4 for examples.

**Eyelash** The eyelash occlusion is often concomitant to the eyelid occlusion. Mostly only to the upper eyelid. It occurs either in a form of an individual lashes (thin dark lines in the iris) or groups of lashes with their shadows on the iris (larger dark areas) as shown in examples in Figure 2.5.

**Shadows in Iris** The shadows in the iris are hard to detect because they cause only subtle changes in the iris texture and thus are difficult to remove properly as their impact

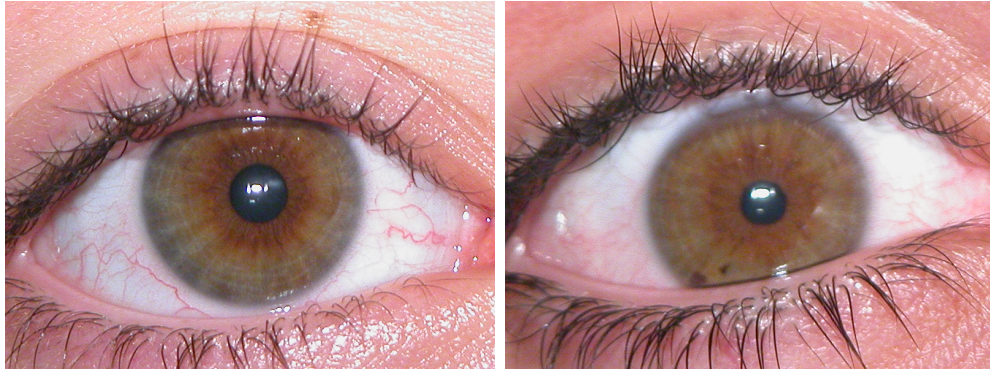


Figure 2.4: The example images with eyelid occlusions. Left image is showing the upper eyelid occlusion. And the right image is showing the lower eyelid occlusion.



Figure 2.5: The example of eyelash occlusion. In left image, there are apparent individual lashes. The right image exhibits group of lashes indistinguishable one from the other.

on the iris can be easily mistaken with true change in the iris texture. They are often accompanied with eyelashes and eyelids. These are also main cause of the shadows. See the example shown in Figure 2.6.

**Out-of-Iris** This occlusion (see Figure 2.7 for example) have a special meaning. Because when it occurs, the image should be rejected. It therefore focuses more on the segmentation step rather than on the feature computation phase. Unfortunately most of the segmentation algorithms does not have the ability to return ‘no iris found’ option.

**Out-of-Focus** Commonly occur if the capturing of the subject’s eye is done non-cooperatively. While the small out-of-focus imperfection is not a big problem, the apparent out-of-focus imperfection can cause a bigger false rejection rate. This can be partially dealt with an better image acquiring hardware. Example image in Figure 2.8.





Figure 2.6: The example of shadow caused by eyelash.

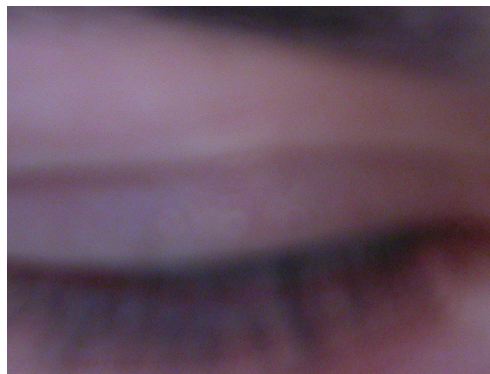


Figure 2.7: The example of out-of-iris occlusion.

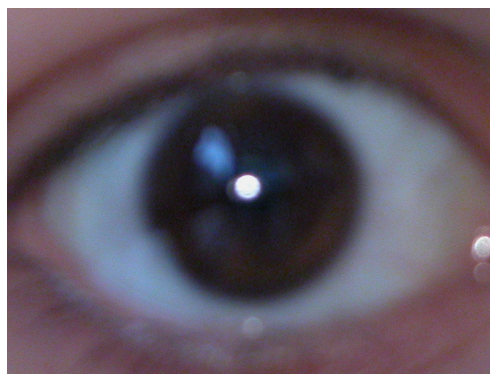


Figure 2.8: The example of out of focus imperfection.



Figure 2.9: The example of eye partially out of image.

**Partially Out of Image** Another type of imperfection is obviously done when the whole iris is not presented in the image (as in Figure 2.9). This is done when captured person unexpectedly move his head or the camera is moving. When this type of imperfection occurs, the segmentation algorithms can have problems when detecting the iris and false reject mistakes could occur. The iris finding algorithms are typically not designed for finding the partial irises.

#### 2.1.4.2 Occlusion Detection Methods

**Preprocessing** Zhu *et al.* [ZTW00] and Kim *et al.* [Kim+04] both proposed the histogram equalization to reduce the effect of nonuniform illumination.

Ma *et al.* [MWT02] also used the histogram equalization and proposed the image filtering with low-pass Gaussian filter to remove high frequency noise.

**Reflections Detection** Kong and Zhang [KZ03] proposed using the simple threshold algorithm for detecting reflection. The threshold value is based on experiments, so it most likely will be necessary to adjust this value for every different capturing settings (when capture device, lighting, environment, etc. has changed).

Sankowski *et al.* [San+06] proposed the adaptive thresholding algorithm to detect reflections. However, the adaptive threshold is detecting only the boundaries of reflections so in case of large reflections they suggest to fill in those areas as a next step. The similar method was also proposed by He *et al.* [He+09] with minor variants.

**Eyelid Detection Methods** The very basic method presented by Daugman [Dau93] simply exclude the areas where the eyelids are expected to occur. In general this approach enhances the final goal (the eyelash included in feature computation stage can have fatal impact on final system), but it also excludes the areas when the eyelid is not presented at all, thus the system is losing its robustness.

The Wildes [Wil97] proposed the localization of lower and upper eyelids by means of edge detector followed by the parametrized parabolic arc. This method is still used today

but it comes at additional computation costs. And is also highly dependent on the edge detector and its parameters. This approach was also proposed by Huang *et al.* [HLC02], Ives *et al.* [IGE04] and He *et al.* [He+09] with minor variants. The Vatsa [VSN05] suggested using similar method, Canny edge detector [Can86] followed by linear Hough transform.

Du *et al.* [DIE04] proposed the adaptive threshold operation with small window (in his case the  $7 \times 7$ ) to mask out the occluded iris regions.

**Eyelash Detection Methods** Chen *et al.* [CDJ05] proposed a method of eyelash removal based on simple thresholding and claims that the result quality highly depends on chosen image capture device. He *et al.* [He+09] proposed a similar method (applicable also on eyelid shadow) with threshold value estimation based on a statistical prediction model.

The Kong and Zhang [KZ03] proposed identifying the separable eyelashes through the energy of convolution of the image with bank of Gabor filters. The filters act similarly as an edge detector. Multiple eyelashes detection is done through the intensity variation in the selected area. If variation is small, the area is considered as an eyelash. The similar method was proposed also by Huang [HLC02].

Daugman [Dau07] proposed a method to detect eyelashes by using the statistical estimation. This method was also proposed by He *et al.* [He+09] with several improvements (eg. eyelid shadows detection).

Bachoo and Tapamo [BT05] proposed using GLCM (see Section 2.1.9.1 for description) matrices for texture analysis. They divided the image to distinctive areas ( $21 \times 21$ ) and analyzed GLCM matrix computed on each of them. They then sorted image areas to five types (skin, eyelash, sclera, pupil and iris).

**Comprehensive Occlusion Detection Methods** In his thesis, Proença [PA06] presented method based on manually detecting the occlusion masks in irises. Then compute the GLCM (see Section 2.1.9.1 for description) pixel features and train them by a Neural Network classifier. This trained classifier is then used to classify the occlusion masks of unknown irises.

Du *et al.* [DIE04] proposed simple adaptive thresholding filter to detect occluded pixels. As authors used only CASIA-IrisV1 database (see chapter 3), which has only basic occlusions, methods results are satisfactory.

Huang *et al.* [Hua+04] proposed a method to detect various types of occlusions in iris. It is based on two steps: 1) edge detection based on phase congruency, 2) the infusion of edge and region information.

Tan *et al.* [THS10] proposed method that eventually won the NICE.I contest (it is described in Section 6.2). At first they employed a clustering based coarse iris localization scheme to extract a rough position of the iris, as well as to identify non-iris regions such as eyelashes and eyebrows. An integrodifferential constellation was then constructed for the localization of pupillary and limbic boundaries. After that, a curvature model and a



prediction model based on intensity statistics between different iris regions were learned to deal with eyelids and eyelashes, respectively.

Sankowski *et al.* [San+10] presented method that obtained second place in NICE.I contest. The proposed method performs the segmentation of the iris from RGB input images. It consists of five stages. They first localize the light source reflections. Next, they fill in those reflections. Then model the iris boundaries as non concentric circles. Followed with modeling the lower eyelid boundary as a circular arc. And finally modeling an upper eyelid boundary as a line segment.

Almeida [Alm10] presented method that obtained third place in NICE.I contest. His paper describes a knowledge-based approach to the problem of locating and segmenting the iris in images. This approach is inspired in the expert system's paradigm. The algorithm involves a succession of phases that deal with image preprocessing, pupil localization, iris localization, combination of pupil and iris, eyelids detection, and filtering of reflections.

Tan and Kumar [TK12] proposed approach that works at pixel level by exploiting the localized Zernike moments at different radii to classify each pixel into iris or non-iris category. After that, they detect eyelids with fitting polynomial on edge map. And then with help of histograms constructed from various iris regions and adaptive thresholding, remove reflections, shadows and localize pupil.

Hu *et al.* [HSH15] proposed a novel method to improve the reliability and accuracy of color iris segmentation from static and mobile devices. Their method is a fusion strategy based on selection among different segmentation methods or models. They used the histogram of oriented gradients (HOG) as features, and trained an SVM-based classifier which provided the selection of given features.

### 2.1.4.3 Segmentation Quality Evaluation

Ma *et al.* [Ma+03] presented the global measure that is based on the analysis of the frequency distributions. Authors suppose, that clean irises (without any occlusions) have uniform distribution, while the occluded irises have not. The frequency analysis is also done only on the two iris subareas on the left and right from the segmented pupil.

The second method was presented by Chen *et al.* [CDJ05]. It is based on convolution of three Mexican hat wavelets (different scales) and such a quality measure itself can be either global or local.

Zuo and Schmid [ZS08] proposed an algorithm for evaluating precision of iris segmentation. They analyzed the effect of noise (low sclera contrast, occluded iris, specular reflections, low contrast images, unevenly illuminated images and out-of-focus) on iris segmentation.

Kalka *et al.* [KBC09] presented method based on probabilistic intensity and geometric features. They check pupil segmentation quality with assumption that pupil is a flat homogeneous region compared to the iris. As iris quality measure, they check the eccentricity and concentricity of the pupil and iris boundaries.

### 2.1.5 Iris Features Computation

In 2003 John Daugman [Dau93] presented his iris representation format called *IrisCode*. It is currently most widely used format for storing iris features. Many researchers proposed iris feature computation methods that followed the general format proposed by Daugman, i.e. represent iris as binary mask of 512 bits (e.g. four rows, 128 bits each). But they were looking at using something other than Gabor filter used by Daugman. The output can be visualized as rectangle image with white and black squares. The others have been using this method as basis for comparisons.

#### 2.1.5.1 IrisCode Based Methods

Ma *et al.* [MW02a] proposed minor enhancements to *IrisCode*. Vatsa *et al.* [VSN05] proposed the similar method using a log polar form of 1D Gabor filter.

Ma *et al.* [Ma+04] proposed a use of dyadic wavelet transform of 1D intensity signals around the inner part of the iris.

Tisse *et al.* [Tis+02] proposed constructing the fused image (combination of original image and its Hilbert transform) to demodulate the iris texture.

Muroñ *et al.* [MKP01] suggested to code iris through the sampling in the Fourier power spectrum.

Yao *et al.* [Yao+06] proposed modified Log-Gabor filters. They stated that ordinary Gabor filters would under-represent the components with high frequency in natural images.

Monro *et al.* [MRZ07] presented usage of discrete cosine transform (DCT) for feature computation. The DCT was applied to overlapping rectangular image windows rotated 45 degrees from the radial axis. The differences between the DCT coefficients were calculated and generated binary code.

#### 2.1.5.2 Texture Analysis Based Methods

Wildes [Wil97] chose the iris representation through the Laplacian pyramid with four different scales.

Boles and Boashash [BB98] proposed computing the iris features as the zero-crossing representations of a 1D wavelet of concentric circles at different resolutions. The similar approach was presented by Sanchez-Avila *et al.* [SASRMR02] with different classification rules.

Zhu *et al.* [ZTW00] proposed the texture analysis method based on multichannel Gabor filter and a wavelet transform.

Ali and Hassainen [AH03] introduced the iris code generation based on a wavelet transforms followed with computation of Haar features. The similar method was also proposed by Lim *et al.* [Lim+01].

Huang *et al.* [HLC02] proposed to employ the independent component analysis (ICA) to extract the iris features. They divided iris images to smaller regions and applied ICA on each.

Dorairaj *et al.* [DSF05], unlike Huang [HLC02], presented experiments on both ICA and DCA they applied those transformations to whole iris region.

Chen *et al.* [CHH09] proposed describing iris texture with modified GLCM based on looking at triples of pixels instead of pairs. They called their method 3D-GLCM.

Barra *et al.* [Bar+15] proposed method for iris authentication on mobiles by means of spatial histograms. They have tested proposed approach has on the MICHE-I iris dataset.

Santos *et al.* [San+15] presented study that focused on biometric recognition in mobile environments using iris and periocular information as the main traits. Their paper makes three main contributions. (1) They presented an iris and periocular dataset, which contains images acquired with 10 different mobile setups and the corresponding iris segmentation data. (2) They report the outcomes of device-specific calibration techniques that compensate for the different color perceptions inherent in each setup. (3) And finally, they propose the application of well-known iris and periocular recognition strategies based on classical encoding and matching techniques.

Raja *et al.* [Raj+17] proposed multi-patch deep features using deep sparse filters to obtain robust features for reliable iris recognition. They also proposed representation of them in a collaborative subspace to perform classification via maximized likelihood.

Aginako *et al.* [Agi+17b] proposed computation of local descriptors. They compute the collection of local descriptors (HOG, variants of LBP and others) and evaluated their performance by means of different classification paradigms in a 10-fold cross validation experiment.

Galdi and Dugleley [GD17] proposed Fast Iris REcognition (FIRE) algorithm designed for iris recognition on mobile phones under visible-light. It is based on the combination of three classifiers exploiting the iris color and texture information. They claim that algorithm is very fast and easily parallelisable.

Abate *et al.* [Aba+17] proposed a method that implements iris recognition in the visible spectrum through unsupervised learning by means of Self Organizing Maps (SOM). They proposed method that uses a SOM network to cluster iris features at pixel level. The discriminative feature map is obtained by using RGB data of the iris combined with the statistical descriptors of kurtosis and skewness.

Ahmed *et al.* [Ahm+17] proposed biometric matching of eye images captured by the visible spectrum smart phone cameras. They performed matching by calculating matching scores for iris codes and periocular biometric based on the Multi-Block Transitional Local Binary Patterns. The authentication scores were calculated separately, and the results were fused to improve the system performance.

Ahuja *et al.* [Ahu+17] proposed a hybrid convolution-based model for iris recognition. They compose the hybrid model as a combination of an unsupervised and a supervised convolution neural network, and augment the combination with the Root SIFT model.

### 2.1.6 Iris Classification

The classification of irises is no different from a general classification task. The irises coded to feature vectors are firstly used to train chosen classifier and then assigned

to one person (class, otherwise declined as unrecognized). In iris recognition, also as in biometrics in general it has been shown that using multiple samples for training can improve overall performance. Du [Du06] showed that increasing training samples (one to three) leads to the improved recognition rates.

The Hamming distance classifier was used for example in [Dau93], [VSN05], [SAS-RMR02], [AH03] [Tis+02] [DIE04].

The Euclidean distance classifier was used for example in [MW02a] [Ma+03], [ZTW00] [HLC02].

Few articles are using their own distance based classifier: [BB98], [Wil97].

Lim *et al.* [Lim+01] used for classification the competitive learning neural network classifier.

Aginako *et al.* [Agi+17a] proposed a novel approach for iris dissimilarity computation (firstly presented in [PA12]). They obtain the a posteriori probability for each of the considered class values from the preprocessed iris images using well-known image processing algorithms. They claim that the main novelty of the presented work remains in the computation of the dissimilarity value of two iris images as the distance between the aforementioned a posteriori probabilities.

### 2.1.7 Iris Quality Metrics

For iris images acquired in less constrained conditions it is advisable to check for captured iris quality. So while it is not part of the iris processing by itself, the iris biometric system typically evaluate at least the focus quality and possibly other factors that can worsen the system performance.

Belcher and Du [BD08] formulated iris quality metric that combined percent occlusion, percent dilatation and ‘feature information’. The ‘feature information’ is calculated from relative entropy of the iris texture when compared with a uniform distribution. Kalka *et al.* [Kal+10] forms a similar metric based on estimating defocus blur, motion blur, off-angle, occlusion, lighting, specular reflection, and iris pixel count.

Kirchen *et al.* [KGSD07] proposed probabilistic iris quality measure based on a Gaussian mixture model (GMM). They compared its behavior to two different types of noise which can corrupt the iris texture: occlusions and blurring. For occlusions, they compare their quality measure to an active contour method. And for blurred case, they compare it with a method based on Fourier transform and wavelets. Their results show that the probabilistic quality measure is independent from the kind of noise involved.

Zhou *et al.* [ZDB09] proposed addition of four modules to standard iris recognition system. A module to reject images that are generally too poor quality, a module to score segmentation quality, a module to determine if the iris are is big enough to generate iris features and a module that combines segmentation score and a quality score.

Proença [Pro11] proposes a method to assess the quality of iris samples captured in visible light and in unconstrained conditions. He determines the quality of iris biometric data according to the focus, motion, angle, occlusions, area, pupillary dilation, and levels of iris pigmentation.

### 2.1.8 Other Comprehensive Surveys

Apart from the survey in this thesis, there has been numerous attempts to cover the development in the iris biometrics area. This Section provides their summary.

The first mentionable one is survey from Bowyer *et al.* [BHF08]. their survey covers the historical development and current state of the art in image understanding for iris biometrics up to date of publication i.e. year 2007. They divided research publications to four categories according to their primary contribution to one of the topics: image acquisition, iris segmentation, texture analysis and matching of texture representations. Other research topics they covered includes experimental evaluations, image databases, applications and systems, and medical conditions that may affect the iris. They also suggested a short list of recommended readings for someone new to the field to quickly grasp the big picture of iris biometrics.

The second according to date of publication is by Jain *et al.* [JRN11]. Their title ‘Introduction to Biometrics’ is the first textbook to introduce the fundamentals of biometrics to undergraduate/graduate students. The book explore three commonly used modalities in the biometrics field, namely, fingerprint, face, and iris. Few other modalities like hand geometry, ear, and gait are also briefly discussed along with advanced topics such as multibiometric systems and security of biometric systems.

Next book, from Rathgeb *et al.* [RUW13], focuses specifically on iris. It’s called ‘Iris Biometrics: From Segmentation to Template Security’ and provides critical analysis, challenges and solutions on iris biometric research topics, including image segmentation, image compression, watermarking, advanced comparators, template protection and more. They describe at that time state-of-the-art approaches accompanied by experimental evaluations. The book has been designed as a secondary text book or reference for researchers and advanced-level students in computer science and electrical engineering.

Last survey is from Bowyer *et al.* [BHF13] and it is a continuation of the last survey by this author ([BHF08]). This new survey is intended to update the previous one, and covers iris biometrics research over the period of roughly 2008–2010.

### 2.1.9 Used Fundamental Image Processing Methods

#### 2.1.9.1 GLCM

The Gray-level co-occurrence matrix [HSD73] is a matrix that is defined to describe spatial relationships of pixels in given image (or area in image).

The GLCM have two parameters. Namely:  $(\Delta r_1, \Delta r_2), p$ . The  $(\Delta r_1, \Delta r_2)$  represent offset for which the matrix is computed. And the  $d$  parameter represents the number of a different values pixels can have and consequently the size of the  $C$  matrix (which is then  $d \times d$ ).

The GLCM matrix is then defined as:

$$C_{\Delta r_1, \Delta r_2}(i, j) = \sum_{r_1=1}^n \sum_{r_2=1}^m \begin{cases} 1, & \text{if } I(r_1, r_2) = i \text{ and } I(r_1 + \Delta r_1, r_2 + \Delta r_2) = j \\ 0, & \text{otherwise} \end{cases}, \quad (2.6)$$

where  $r_1$  and  $r_2$  are the pixel coordinates in the image  $I$  and the  $(\Delta r_1, \Delta r_2)$  define the offsets from  $(r_1, r_2)$  positions for which this matrix is calculated, then  $i$  and  $j$  are the pixel values. And the  $I(r_1, r_2)$  indicates the value at pixel  $(r_1, r_2)$ .

From the GLCM matrix can be computed number of features. Energy, Entropy, Contrast or Homogeneity to name a few. Comprehensive listing with definitions can be found in original article from Robert Haralick [HSD73].

### 2.1.10 Local Binary Patterns

The Local Binary Patterns (LBP) is a feature computation method that was first published in the 1994 by Ojala *et al.* [OPH94]. It has been found to have great power for the texture description. The LBP is essentially the feature vector that is created in the following way:

$$LBP_{P,R} = \sum_{p=0}^{P-1} s(v_r - v_c) 2^p, \quad (2.7)$$

$$s(x) = \begin{cases} 1 & \text{for } x \geq 0 \\ 0 & \text{for } x < 0 \end{cases}, \quad (2.8)$$

where  $P$  denotes the length of the feature vector,  $R$  radius for the comparison values (see Figure 2.10 for overview) and  $v_c$  and  $v_r$  denotes center and compared pixels. The feature vector can now be processed using any suitable classifier.

### 2.1.11 Gabor Filters

Gabor filters are thought to be similar to how cells in human visual system works [Mar80]. Their impulse response is defined by a sinus function (a plane for 2D Gabor filters) multiplied by a Gaussian function [FS89] (See Figure 2.11 for 2D example). The filter has a real and an imaginary component representing orthogonal directions. The two components then may be used individually or together as complex number. John Daugman defined Gabor filter as [Dau85]:

$$g_{\lambda, \theta, \psi, \sigma, \gamma}(r_1, r_2) = \exp\left(-\frac{r_1'^2 + \gamma^2 r_2'^2}{2\sigma^2}\right) \cos\left(2\pi \frac{r_1'}{\lambda} + \psi\right), \quad (2.9)$$

$$r_1' = r_2 \cos(\theta) + r_1 \sin(\theta), \quad (2.10)$$

$$r_2' = -r_1 \sin(\theta) + r_2 \cos(\theta). \quad (2.11)$$

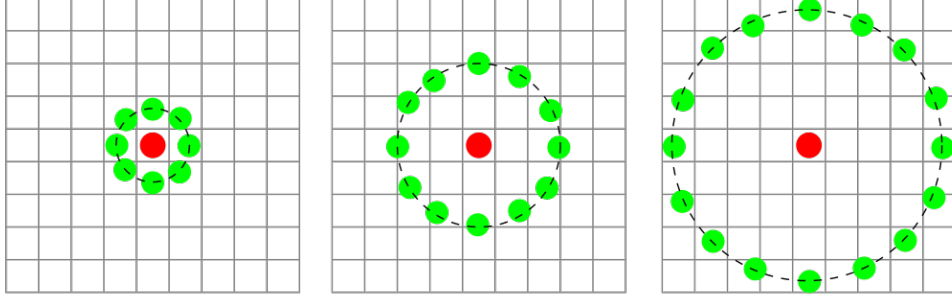
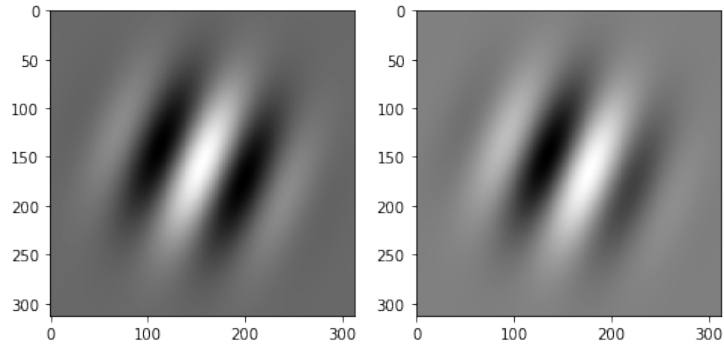

 Figure 2.10: Example of creating LBP feature vector.<sup>1</sup>


Figure 2.11: Examples of Gabor kernel.

The half-response spatial frequency bandwidth  $b$  and the ratio  $\sigma/\lambda$  are related as follows:

$$b = \log_2 \frac{\frac{\sigma}{\lambda}\pi + \sqrt{\frac{\ln 2}{2}}}{\frac{\sigma}{\lambda}\pi - \sqrt{\frac{\ln 2}{2}}}, \quad (2.12)$$

$$\frac{\sigma}{\lambda} = \frac{1}{\pi} \sqrt{\frac{\ln 2}{2}} \cdot \frac{2^b + 1}{2^b - 1}, \quad (2.13)$$

where  $\lambda$  represents the wavelength and  $1/\lambda$  the spatial frequency of the cosine factor,  $\theta$  the orientation of the normal to the parallel stripes of a Gabor function  $\psi$  is the phase offset,  $\sigma$  is the standard deviation of the Gaussian envelope and  $\gamma$  is the spatial aspect ratio, and specifies the ellipticity of the support of the Gabor function. It has been found to vary in a limited range of  $0.23 < \gamma < 0.92$ . The ratio  $\sigma/\lambda$  determines the spatial frequency bandwidth. And  $r_1, r_2$  denotes coordinates in the Gabor kernel.

<sup>1</sup>Source: [https://en.wikipedia.org/wiki/Local\\_binary\\_patterns](https://en.wikipedia.org/wiki/Local_binary_patterns)





---

## Iris Databases

*This chapter surveys available iris databases and gives an overview of each along with the image samples for several of them. It focuses specifically on the iris image databases in the visible spectrum. The chapter concludes with the substantiation of the chosen databases. The important part is also the table (3.2) with each database presented and comparison of their properties.*

### 3.1 Databases Overview

There are number of iris databases as they were developed during the time and as they were focused on the different scenarios and approaches. Most of them provide images captured in a near infrared spectrum (wavelengths between  $700nm - 900nm$ ) and therefore are only monospectral. Only few of them provide color images. There is no database that would provide both NIR and RGB images of the eye captured at the same time (or essentially any other variant that would provide either NIR spectrum or RGB spectrum). Also most were captured indoors with the artificial lighting. For overview of all databases see the Table 3.2 and for overall summary, the Section 3.4.

### 3.2 Databases with Images in Near Infrared Spectrum

#### 3.2.1 CASIA

The CASIA currently represents four databases from the Chinese Academy of Sciences [Cen]. The first version was one of the first databases widely used. Images in all four versions are monospectral, taken in NIR.

CASIA Iris Image Database Version 1.0 (CASIA-IrisV1) includes 756 iris images from 108 eyes. For each eye, 7 images are captured in two sessions with their proprietary device CASIA close-up iris camera, where three samples are collected in the first session and four in the second session. All images are stored as BMP format with resolution  $320*280$ . The

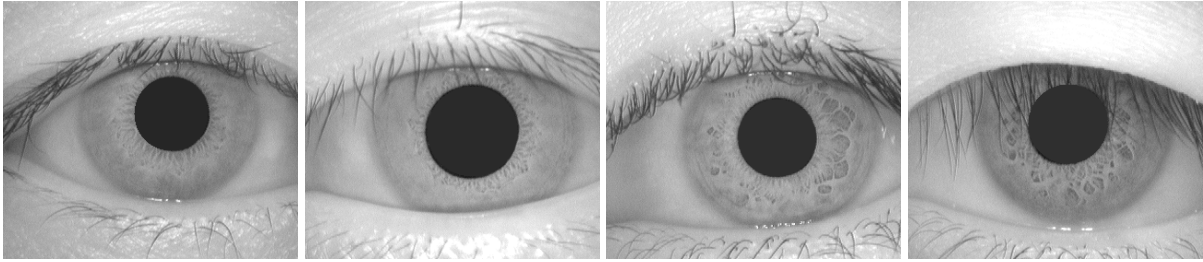


Figure 3.1: Example images from CASIA-IrisV1 database.

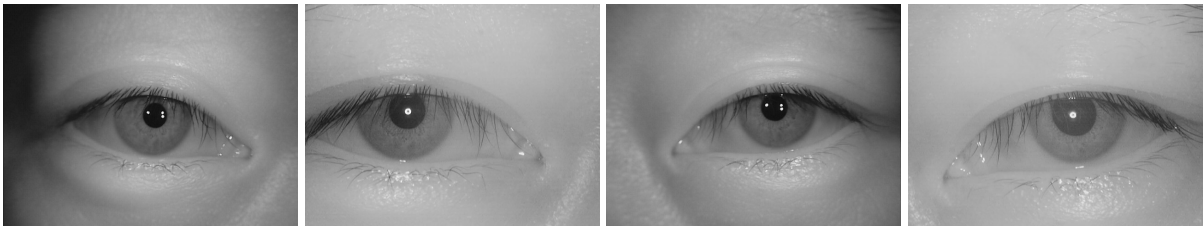


Figure 3.2: Example images from CASIA-IrisV2 database. Odd columns are from device 1, even columns from device 2.

pupil regions of all iris images in CASIA-IrisV1 were automatically detected and replaced with a circular region of constant intensity to mask out the specular reflections from the NIR illuminators. Such editing clearly makes iris boundary detection much easier but has minimal or no effects on other components of an iris recognition system, such as feature extraction and classifier design. See examples in Figure 3.1.

CASIA Iris Image Database Version 2.0 (CASIA-IrisV2) includes two subsets captured with two different devices: Irisspass-h developed by OKI and their proprietary device CASIA-IrisCamV2. Each subset includes 1200 images from 60 classes. See examples in Figure 3.2.

CASIA-IrisV3 includes three subsets which are labelled as CASIA-Iris-Interval, CASIA-Iris-Lamp, CASIA-Iris-Twins. CASIA-IrisV3 contains a total of 22,034 iris images from more than 700 subjects. All iris images are 8 bit grey-scale JPEG files, collected under near infrared illumination. Almost all subjects are Chinese except a few exceptions in CASIA-Iris-Interval. Because the three data sets were collected in different times, only CASIA-Iris-Interval and CASIA-Iris-Lamp have a small overlap in subjects.

CASIA-IrisV4 is an extension of CASIA-IrisV3 and contains six subsets. The three subsets from CASIA-IrisV3 are CASIA-Iris-Interval, CASIA-Iris-Lamp, and CASIA-Iris-Twins respectively. The three new subsets are CASIA-Iris-Distance, CASIA-Iris-Thousand, and CASIA-Iris-Syn. CASIA-IrisV4 contains a total of 54,601 iris images from more than 1,800 genuine subjects and 1,000 synthesized subjects. All iris images are 8 bit grey-level JPEG files, collected under near infrared illumination or synthesized. The six data sets were collected or synthesized at different times and CASIA-Iris-Interval, CASIA-Iris-Lamp, CASIA-Iris-Distance, CASIA-Iris-Thousand may have a small inter-subset overlap in sub-

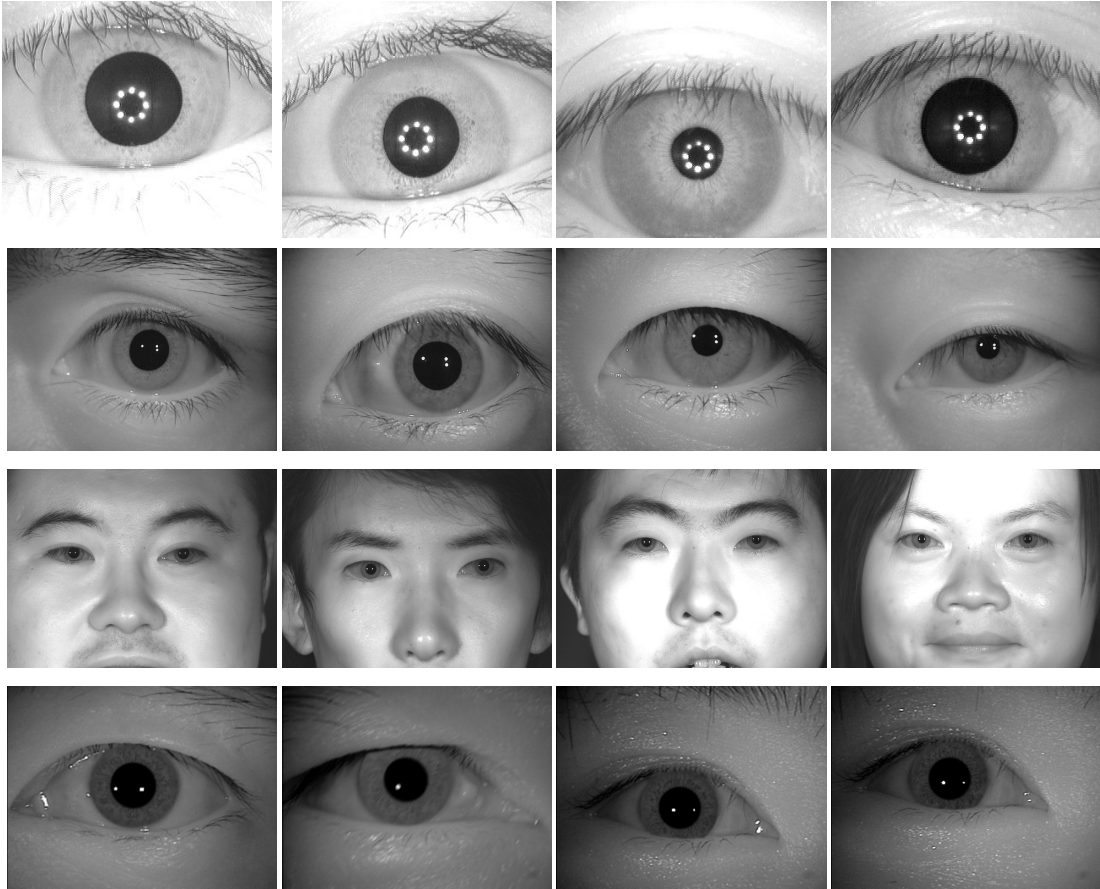


Figure 3.3: Example images from CASIA-IrisV4 database. Each row is from different subset. From top to down it is: Interval, Lamp, Distance, Synthetic.

jects. See examples in Figure 3.3.

#### 3.2.2 BATH

BATH is database from University of Bath [Uni]. Database contains 1000 images from 50 eyes with 20 images taken from each eye. All images has resolution 1280x720 pixels and are only in gray-scale.

#### 3.2.3 MMU

From Multimedia University [Mul], there are two databases (MMU1 and MMU2). The MMU1 iris database contributes a total number of 450 iris images which were taken using LG IrisAccess 2200 device (camera) from 45 persons. This camera is semi-automated and it operates at the range of 7-25 cm. The follow up, MMU2 iris database consists of 995 iris

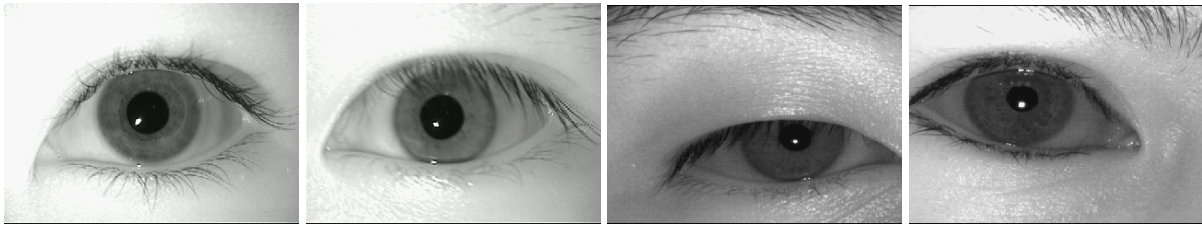


Figure 3.4: Example images from MMU database. First two images are from MMU1 database, second two are from MMU2.

images. The iris images are collected using device Panasonic BM-ET100US Authenticam and its operating range is even farther with a distance of 47-53 cm away from the user. These iris images are contributed by 100 volunteers with different age and nationality. They come from Asia, Middle East, Africa and Europe. Each of them contributes 5 iris images for each eye. There are 5 left eye iris images which are excluded from the database due to cataract disease. Image resolution in database is 320x240 pixels. All images are taken in NIR. See examples in Figure 3.4.

#### 3.2.4 ND Iris Image Dataset

All images in the ND 2004-2005 iris image dataset [Phi+10] were acquired using the same LG 2200 iris biometrics system. The LG 2200 uses near-infrared illumination of the eye. The dataset contains 64,980 images corresponding to 356 unique subjects, and 712 unique irises. The age range of the subjects is 18 to 75 years old. 158 of the subjects are female, and 198 are male. 250 of the subjects are Caucasian, 82 are Asian, and 24 are other ethnicities. None of the images correspond to subjects wearing glasses during image acquisition. However, a significant fraction of the subjects wore contact lenses. The ND 2004-2005 iris image data acquisition is large enough that many real-world conditions occur that may present challenges for iris biometrics systems. There are some images that have noticeable blur, and some in which the iris region is substantially occluded. There are some images in which the iris region is cut off at the image boundary. While most iris images are acquired in a near straight-on view, another real-world condition that occurs is ‘off-axis’ images, where the subject’s view direction is not orthogonal/perpendicular to the optical axis of the camera.

#### 3.2.5 DMCS

The DMCS (DMCS - Department of Microelectronics and Computer Science) database was initially designed for the Iris Finder program [San+06]. This database has been established by the authors of Iris Finder. At the time of article’s publication it contained 141 images of left and right eyes of 4 persons. It is worth mentioning that photos were taken not at once, but in three consecutive sessions during 6 months. The images are colour with 8

bits per pixel for each red, blue and green components. The photos dimension equals 3072 pixels x 2048 pixels. The acquisition was performed using Canon EOS 10D camera (6.3 Megapixel CMOS sensor). Instead of using standard lens the camera was connected to Kontron Fundus Camera - a medical device intended for diagnosis in ophthalmology. The images are stored in the raw format.

The database itself is however not publicly released.

### 3.2.6 BioSecurID

BioSecurID [Fie+10] is multimodal biometric database, acquired in the framework of the BioSecurID project. A new multimodal biometric database, is presented together with the description of the acquisition setup and protocol. The database includes eight unimodal biometric traits, namely: speech, iris, face (still images, videos of talking faces), handwritten signature and handwritten text (on-line dynamic signals, off-line scanned images), fingerprints (acquired with two different sensors), hand (palmprint, contour-geometry) and keystroking. The database comprises 400 subjects and presents features such as: realistic acquisition scenario, balanced gender and population distributions, availability of information about particular demographic groups (age, gender, handedness), acquisition of replay attacks for speech and keystroking, skilled forgeries for signatures, and compatibility with other existing databases. All these characteristics make it very useful in research and development of both unimodal and multimodal biometric systems.

### 3.2.7 VISOB

Visible light mobile Ocular Biometric (VISOB) Dataset ICIP2016 Challenge Version is a publicly available database [Rat+16] consisting of eye images from 550 healthy adult volunteers acquired using three different smartphones i.e., iPhone 5s, Samsung Note 4 and Oppo N1. The iPhone was set to capture bursts of still images at 720p resolution, while the the Samsung and Oppo devices were capturing bursts of still images at 1080p resolution using pixel binning. Volunteers' data were collected during two visits (Visit 1 and Visit 2), 2 to 4 weeks apart. At each visit, volunteers were asked to take selfie like captures using front facing cameras of the aforementioned three mobile devices in two different sessions (Session 1 and Session 2) that were about 10 to 15 minutes apart. The volunteers used the mobile phones naturally, holding the devices 8 to 12 inches from their faces. For each session, a number of images were captured under three lighting conditions: regular office light, dim light (office lights off but dim ambient lighting still present), and natural daylight settings (next to large sunlit windows). The collected database was preprocessed to crop and retain only the eye regions of size 240 x160 pixels using a Viola-Jones based eye detector. See examples in Figure 3.5.



Figure 3.5: Example images from VISOB database. Each row is from different lighting conditions. From top to down it is: natural daylight, dim light and office light. Also first column is from iPhone 5s, second from Oppo N1 and third from Samsung Note 4 devices.

## 3.3 Databases with Images in Visible Spectrum

### 3.3.1 UPOL

UPOL is database from University of Olomouc [DM]. Small but high quality database contain iris images of three persons (64x left eye, 64x right eye). Images were scanned by device TOPCON TRC50IA which is specialized retina scan device which resulted in high quality images almost without any imperfections. This database has great value for research of iris patterns or characteristics but not so usable when need of images from common capture device. See examples in Figure 3.6.

### 3.3.2 UBIRIS

The aim of UBIRIS database [PA05] is to provide images with different types of occlusions, simulating image captured with or without minimal collaboration from the subjects, pretending to become an effective resource for the evaluation and development of robust



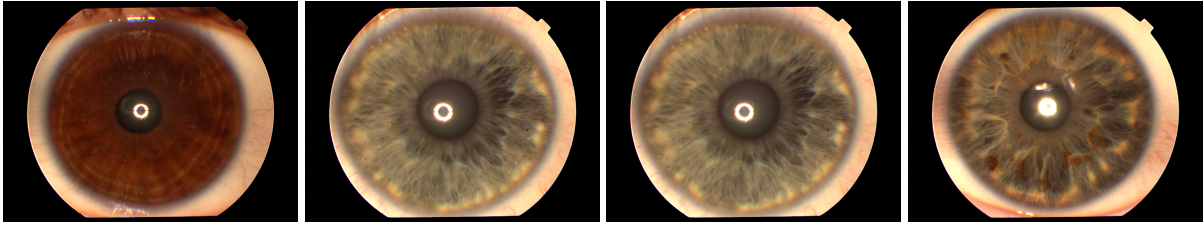


Figure 3.6: Example images from UPOL database.

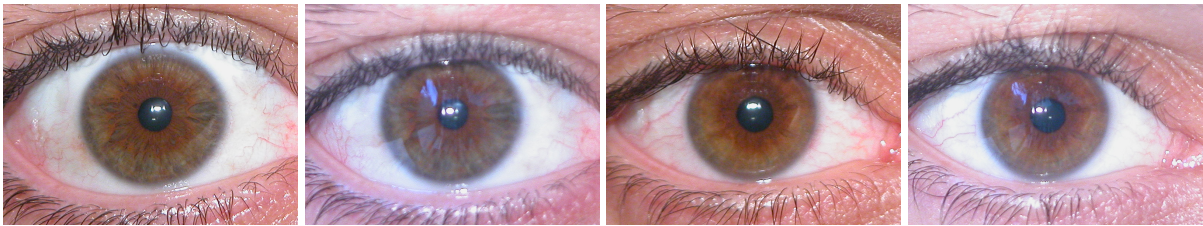


Figure 3.7: Example images from UBIRIS database.

iris identification methodologies. UBIRIS database is composed of 1877 images collected from 241 persons during September, 2004 in two distinct sessions. It was constituted as the world's largest public and free available iris database at its release date (2005). See examples in Figure 3.7.

For capturing was used a Nikon E5700 camera with software version E5700v1.0, 71mm focal length, 4.2 F-Number, 1/30 sec. exposure time, RGB color representation and ISO-200 ISO speed. Images dimensions were 2560x1704 pixels with 300 dpi horizontal and vertical resolution and 24 bit depth. They were saved in JPEG format with lossless compression and resolution 800x600 pixels. For the first image capture session, the enrollment, they tried to minimize imperfection factors, specially those relative to reflections, luminosity and contrast, by means of the framework installed inside a dark room. In the second session they changed the capture location in order to introduce natural luminosity factor. This enabled the appearance of heterogeneous images with respect to reflections, contrast, luminosity and focus problems. Images collected at this stage pretend to simulate the ones captured by a vision system without or with minimal active collaboration from the subjects. All images from both sessions are classified with respect to three parameters ('Focus', 'Reflections' and 'Visible Iris') in a three value scale ('Good', 'Average' and 'Bad'). This classification was obtained manually and the results were: focus (Good = 73.83%, Average = 17.53%, Bad = 8.63%), reflections (Good = 58.87%, Average = 36.78%, Bad = 4.34%) and visible iris (Good = 36.73%, Average = 47.83%, Bad = 15.44%). There are in total 1877 images from 241 persons.



Figure 3.8: Example images from UBIRIS.v2 database.

#### 3.3.3 UBIRIS.v2

The major purpose of the UBIRIS.v2 database [Pro+10] is to constitute a new tool to evaluate the feasibility of visible wavelength iris recognition under far from ideal imaging conditions. In this scope, the various types of non-ideal images, imaging distances, subject perspectives, and lighting conditions existent on this database could be of strong utility in the specification of the visible wavelength iris recognition feasibility and constraints.

The database contains over 11000 images captured in realistic conditions. Images has more occlusions, same as first UBIRIS with additional at-a-distance and on-the-move imperfections. See examples in Figure 3.8.

#### 3.3.4 MICHE

MICHE-I [Mar+15] is iris biometric dataset captured under uncontrolled settings using mobile devices. The key features of the MICHE-I dataset are a wide and diverse population of subjects, the use of different mobile devices for iris acquisition, realistic simulation of the acquisition process (including noise), several data capture sessions separated in time, and image annotation using metadata. The aim of MICHE-I dataset was to make up the starting core of a wider dataset, with the further aim to address interoperability, both in the sense of matching samples acquired with different devices and of assessing the robustness of algorithms to the use of devices with different characteristics. See details in Table 3.1. See examples in Figure 3.9.

The dataset is available through authors website<sup>1</sup>. Password, needed to unpack the data, is obtainable by email.

### 3.4 Databases Summary

The table with summary of the databases can be seen in 3.2. Apart from two, all of the databases have images taken indoor. Most of them have images captured in the infrared spectrum (one is in grayscale) and minority (5) is in the visible spectrum. All color databases (apart from UBIRIS) have images taken with mobile cameras. The UBIRIS used

---

<sup>1</sup><http://biplab.unisa.it/MICHE/>





Figure 3.9: Example images from MICHE database. Each row is from different subset. From top to down it is: iPhone5, SamsungGalaxyS4, SamsungGalaxyTab2. Also odd columns are from indoor and even columns are from outdoor environment.

	(Number of images) Resolution	Distance [cm]
<b>iPhone5</b>	(1262)	
Front camera	$960 \times 960, 960 \times 1280$	$\approx 10$
Rear camera	$1536 \times 2048, 2448 \times 2448$ $2448 \times 3264$	$\approx 13$
<b>Samsung Galaxy S4</b>	(1297)	
Front camera	$1080 \times 1920$	$\approx 10$
Rear camera	$2320 \times 4128$	$\approx 13$
<b>Samsung Galaxy Tab2</b>	(632)	
Front camera	$640 \times 480$	$\approx 5$

Table 3.1: Detailed description of MICHE iris database.

Nikon E5700 camera. Rest of the databases used non-consumer hardware because of the NIR spectrum.

Most of the databases have several hundreds of subjects (only CASIA-Iris-Thousand has more and four of the databases have less than hundred). Most databases also have tenths of images per subject. The UPOL database have most images per subject (64) but it also have only 3 subjects total. Minimum images per subject is 5. The databases have usually several thousands images overall. Most databases have resolution  $640 \times 480$  or below. Only two have Full HD resolution ( $1920 \times 1080$ ) or more.

### 3.5 Databases used in This Thesis

As this thesis focuses on modern trend of the iris recognition in the visual spectrum with the images taken in unconstrained conditions and without active participation of subjects, our choice was limited only to databases with color images. The databases in visible spectrum are UBIRIS [PA05], UBIRIS.v2 [Pro+10], MICHE [Mar+15], UPOL [DM] and VISOB [Rat+16]. The VISOB database have too small images for our purposes. The UPOL is database almost without occlusions with irises captured in near ideal conditions. The UBIRIS database is a good intermediate challenge that have good resolution of iris images, but many occlusions as reflections, eyelids and eyelashes. On the other hand UBIRIS.v2 is database focused mainly on different types of occlusions in challenging, smaller resolution. The MICHE database is focused on big high quality images taken by people themselves with lots of occlusions. With sometimes even big parts of faces included in the image. Therefore, for the experiments, the UBIRIS database was chosen mainly for the first method and the UBIRIS.v2 database and the MICHE database were used for advanced occlusion detection.

Name	Environment	Captured spectrum	Images count	Images per eye	Subjects count	Image resolution
CASIA-IrisV1	Indoor	NIR	756	7	108	320x280
CASIA-IrisV2	Indoor	NIR	2400	40	120	640x480
CASIA-Iris-Interval	Indoor	NIR	2639	10	249	320x280
CASIA-Iris-Lamp	Indoor	NIR	16212	20	411	640x480
CASIA-Iris-Twins	Outdoor	NIR	3183	10	200	640x480
CASIA-Iris-Distance	Indoor	NIR	2567	10-20	142	2352x1728
CASIA-Iris-Thousand	Indoor	NIR	20000	10	1000	640x480
BATH	Indoor	Grayscale	1000	20	50	1280x720
MMU1	Indoor	NIR	450	5	45	320x240
MMU2	Indoor	NIR	995	5	100	320x240
UPOL	Indoor	RGB	192	64	3	576x768
UBIRIS	Indoor	RGB	1877	10	241	800x600
UBIRIS.v2	Indoor	RGB	11000	15	261	400x300
ND Iris Image	Indoor	NIR	64980	?	356	?
MICHE	In & Out-door	RGB	3191	50	75	640x480, 960x1280, 1920x1080
VISOB	Indoor	NIR	64980	50-100	550	240x160

Table 3.2: Iris datasets overview



---

# Iris Occlusions Detection

*We've developed three methods for better detection of irises in the image. And subsequently also to detect areas with occlusion in them. Each method was developed for a different problem specification. The first one is fastest but also uses least difficult (of the tree) images (the UBIRIS database). The second method uses the UBIRIS.v2 database and the third method builds on top of UBIRIS.v2 and MICHE databases.*

## 4.1 Fast Occlusion Detection on Eye Images

The first method was published at the International Conference BTAS in 2013 [A.1]. The occlusion detection is based on the multispectral causal autoregressive model. This method works well on UBIRIS and UBIRIS.v2 databases (Sections 3.3.2 for UBIRIS or 3.3.3 for UBIRIS.v2 respectively). The UBIRIS images are better quality and generally less difficult than the other two selected databases.

### 4.1.1 Overview

Our first method basically uses the integrodifferential operator (described in Section 2.1.2) for iris finding and the adaptive 3D causal simultaneous auto-regressive model (see Section 4.1.4 for description) for occlusion detection. See the method diagram at Figure 4.1.

### 4.1.2 Image Preprocessing

Since the UBIRIS database (described in Section 3.3.2, which we are using in this method) have color images and couple of methods we are using expects monospectral images, we are also converting the color images to grayscale with the following formula:

$$Y = 0.299 * R + 0.587 * G + 0.114 * B , \quad (4.1)$$

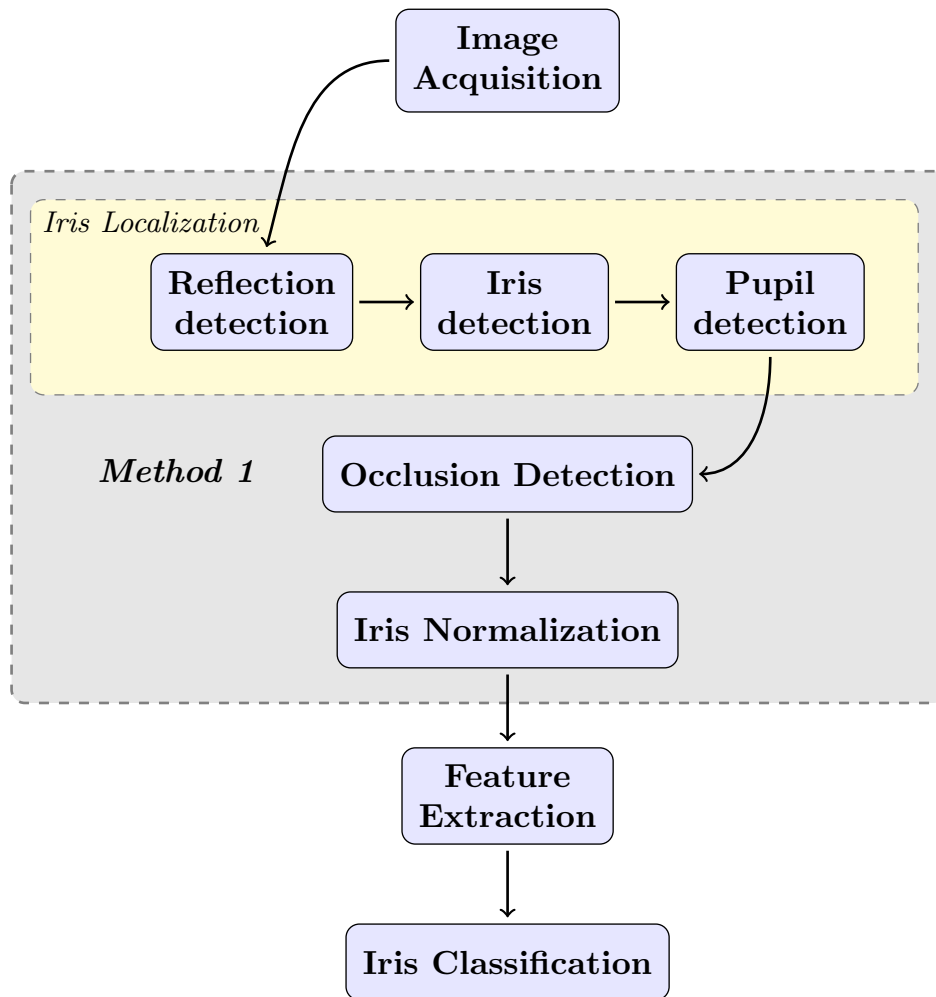


Figure 4.1: Processing scheme of method 1.

where  $Y$  is resulting gray-scale pixel (luma, see paragraph below for brief description) and  $R, G, B$  are color channels (red, green and blue) from original image. This transformation is to compute the luma from color image. The formula was used whenever some algorithm used monospectral images and source images was color in RGB (and it is not stated otherwise).

**Luma** The Luma is the weighted sum of RGB components. The proportion numbers came from *ITU-R Recommendation BT.601* a standard originally issued in 1982 by the CCIR (an organization which has since been renamed as the International Telecommunication Union – Radiocommunication sector). So the luma represents the brightness in an image and is typically paired with the chrominance. As such, the luma represents the

achromatic image, while the chroma components represent the color information.<sup>1</sup>

Since the reflections present in eye images can substantially obstruct the iris localization, it is necessary to perform the search for light reflections. It is done through the adaptive thresholding in blue spectral channel. According to our experiments, they are most visible here. The threshold value for each pixel is the weighted sum of neighborhood pixels where weights are a Gaussian window values. The resulting binary mask is then firstly slightly dilated to ensure full coverage of the reflections and than the detected reflective regions are filled using the inpainting algorithm presented in [Tel04] (see Figure 4.5 for example). Since this thresholding is done only for better iris localization, it is not that important that true iris texture remains untouched. Instead it is desirable for the reflection detection to be more robust than precise.

### 4.1.3 Iris Localization

The eye area is found using the original integrodifferential Daugman operator [Dau93] as described in the Section 2.1.2. The image used for this task is the output from previous step, thus with inpainted reflections and monospectral.

### 4.1.4 Multispectral Iris Texture Model

For occlusions detection, our first assumption was that the multispectral iris texture can be represented by the adaptive 3D causal simultaneous auto-regressive model [Hai12; HŠ92]:

$$X_r = \sum_{s \in I_r^c} A_s X_{r-s} + \epsilon_r \quad , \quad (4.2)$$

where  $\epsilon_r$  is a white Gaussian noise vector with zero mean, and a constant but unknown covariance matrix  $\Sigma$  and  $r = \{r_1, r_2\}, s = \{s_1, s_2\}$  are multiindices with the row and column indices, respectively. The noise vector is uncorrelated with data from a causal neighborhood  $I_r^c$ ,

$$A_{s_1, s_2} = \begin{pmatrix} a_{1,1}^{s_1, s_2}, \dots, a_{1,d}^{s_1, s_2} \\ \vdots, \ddots, \vdots \\ a_{d,1}^{s_1, s_2}, \dots, a_{d,d}^{s_1, s_2} \end{pmatrix} \quad , \quad (4.3)$$

are  $d \times d$  parameter matrices where  $d$  is the number of spectral bands.  $r, r-1, \dots$  is a chosen direction of movement on the image lattice (e.g. scanning lines rightward and top to down). This model can be analytically estimated using numerically robust recursive statistics hence it is exceptionally well suited for possibly real-time texture defect detection applications. The model adaptivity is introduced using the standard exponential

<sup>1</sup>Full description can be read in [https://en.wikipedia.org/wiki/Luma\\_\(video\)](https://en.wikipedia.org/wiki/Luma_(video)).

forgetting factor technique in the parameter learning part of the algorithm. The model can be alternatively written in the matrix form

$$X_r = \gamma Z_r + \epsilon_r , \quad (4.4)$$

where  $\gamma = [A_1, \dots, A_\eta]$ ,  $\eta = \text{card}(I_r^c)$  is a  $d \times d\eta$  parameter matrix and  $Z_r$  is a corresponding vector of  $X_{r-s}$ . To evaluate the conditional mean values  $E\{X_r | X^{(r-1)}\}$ , where  $X^{(r-1)}$  is the past process history, the one-step-ahead prediction posterior density  $p(X_r | X^{(r-1)})$  is needed. If we assume the normal-gamma parameter prior for parameters in (4.2) this posterior density has the form of Student's probability density with  $\beta(r) - d\eta + 2$  degrees of freedom, where the following notation is used:

$$\beta(r) = \beta(0) + r - 1 , \quad (4.5)$$

$$\hat{\gamma}_{r-1}^T = V_{zz(r-1)}^{-1} V_{zx(r-1)} , \quad (4.6)$$

$$V_{r-1} = \begin{pmatrix} \tilde{V}_{xx(r-1)} & \tilde{V}_{zx(r-1)}^T \\ \tilde{V}_{zx(r-1)} & \tilde{V}_{zz(r-1)} \end{pmatrix} + I , \quad (4.7)$$

$$\tilde{V}_{uw(r-1)} = \sum_{k=1}^{r-1} U_k W_k^T , \quad (4.8)$$

$$\lambda(r) = V_{x(r)} - V_{zx(r)}^T V_{z(r)}^{-1} V_{zx(r)} , \quad (4.9)$$

where  $\beta(0) > 1$  and  $U, W$  denote either  $X$  or  $Z$  vector, respectively. If  $\beta(r-1) > \eta$  then the conditional mean value is

$$E\{X_r | X^{(r-1)}\} = \hat{\gamma}_{r-1} Z_r , \quad (4.10)$$

and it can be efficiently computed using the following recursion

$$\hat{\gamma}_r^T = \hat{\gamma}_{r-1}^T + \frac{V_{z(r-1)}^{-1} Z_r (X_r - \hat{\gamma}_{r-1} Z_r)^T}{1 + Z_r^T V_{z(r-1)}^{-1} Z_r} . \quad (4.11)$$

The selection of an appropriate model support ( $I_r^c$ ) is important to obtain good iris representation. If the contextual neighborhood is too small it can not capture all details of the random field iris model. Inclusion of the unnecessary neighbors on the other hand adds to the computational burden and can potentially degrade the performance of the model as an additional source of noise. The optimal Bayesian decision rule for minimizing the average probability of decision error chooses the maximum posterior probability model, i.e., a model  $M_i$  corresponding to

$$\max_j \{p(M_j | X^{(r-1)})\}$$

can be found analytically [Hai12; HŠ92].



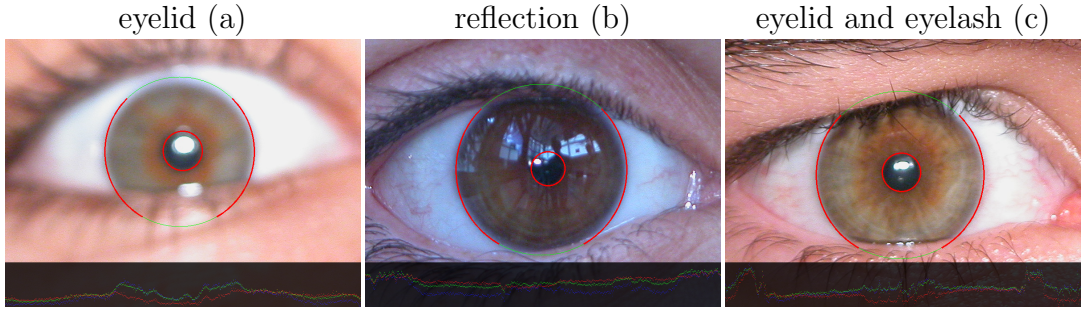


Figure 4.2: Detected iris regions containing all occlusion types apparent in UBIRIS database.

### 4.1.5 Occlusion Detection

The iris occlusions (Figure 4.2) are detected pixel-wise. Single multispectral pixels are classified as belonging to the occluded (non-iris) area based on their corresponding prediction errors. If the prediction error is larger than the adaptive threshold:

$$|\tilde{E}\{X_r | X^{(r-1)}\} - X_r| > \frac{\alpha}{l} \sum_{i=1}^l \left| \tilde{E}\{X_{r-i} | X^{(r-i-1)}\} - X_{r-i} \right|, \quad (4.12)$$

then the pixel  $r$  is classified as a detected occluded pixel. The parameter  $l$  in (4.12) is a process history length of the adaptive threshold and the constant  $\alpha = 2.7$  was found experimentally.

The one-step-ahead predictor

$$\tilde{E}\{X_r | X^{(r-1)}\} = \hat{\gamma}_s Z_r, \quad (4.13)$$

differs from the corresponding predictor (4.10) in using parameters  $\hat{\gamma}_s$  which were learned only in the expected flawless texture area ( $s < r$ ). The small learning flawless texture cutout is found automatically inside reflection-less iris area. The whole algorithm is extremely fast because the adaptive threshold is updated recursively:

$$|\epsilon_{r+1}| > \frac{\alpha}{l} \left[ \sum_{i=0}^{l-1} |\epsilon_{r-i}| \right], \quad (4.14)$$

where  $\epsilon_r$  is the prediction error

$$\epsilon_r = \tilde{E}\{X_r | X^{(r-1)}\} - X_r,$$

and  $\hat{\gamma}_s$  is the parametric matrix which is not changing. Hence the algorithm can be easily applied in real time iris defect detection.

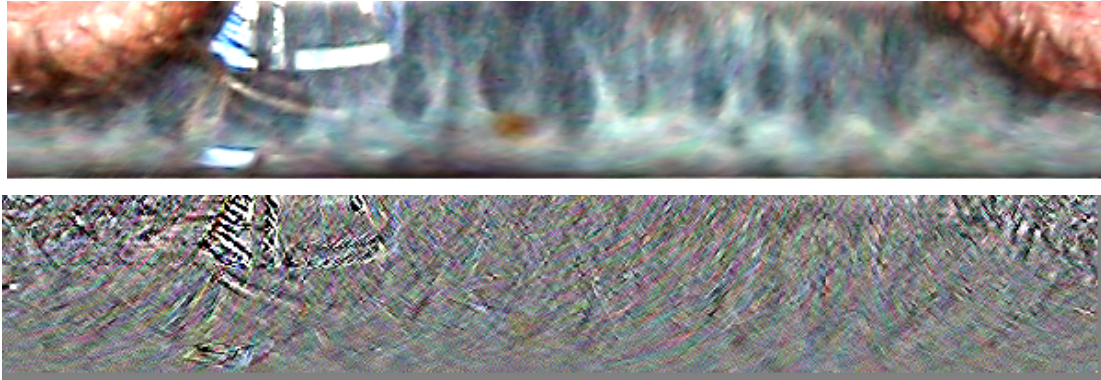


Figure 4.3: Normalized iris and its prediction error.

### 4.1.6 Occlusions Mask

The result of the previous section is taken as mask representing the detected occlusions in a given iris (for examples see Section 4.1.5). In Figure 4.3 can be seen the normalized iris and its prediction error before thresholding.

### 4.1.7 Iris Normalization

The iris normalization is done exactly as described in Section 2.1.3. In transformation to new coordinates, the bicubic interpolation is used.

The output of method in form of iris occlusion masks is compared with other methods and can be seen in Section 7.1.

## 4.2 Robust Iris Occlusion Detection in Challenging Images

The second method was published at the International Conference SITIS in 2014 [A.2]. It improves techniques from the first method (4.1), the iris localization and the defect detection and combines them with several new techniques designed for better detection of iris occlusions in specific areas. This second method is designed for UBIRIS.v2 database (described in Section 3.3.3). It's images are similar to UBIRIS but overall more challenging as they are smaller and contain more occlusions of all kinds.

### 4.2.1 Overview

The first step is same as in previous method, removal of reflections. The iris localization part is modified from previous method and described in 4.2.2. Then the iris normalization is performed, again as described in Section 2.1.3. On the contrary, the occlusion detection is completely reworked with additional algorithms as described in Section 4.2.3. As is shown

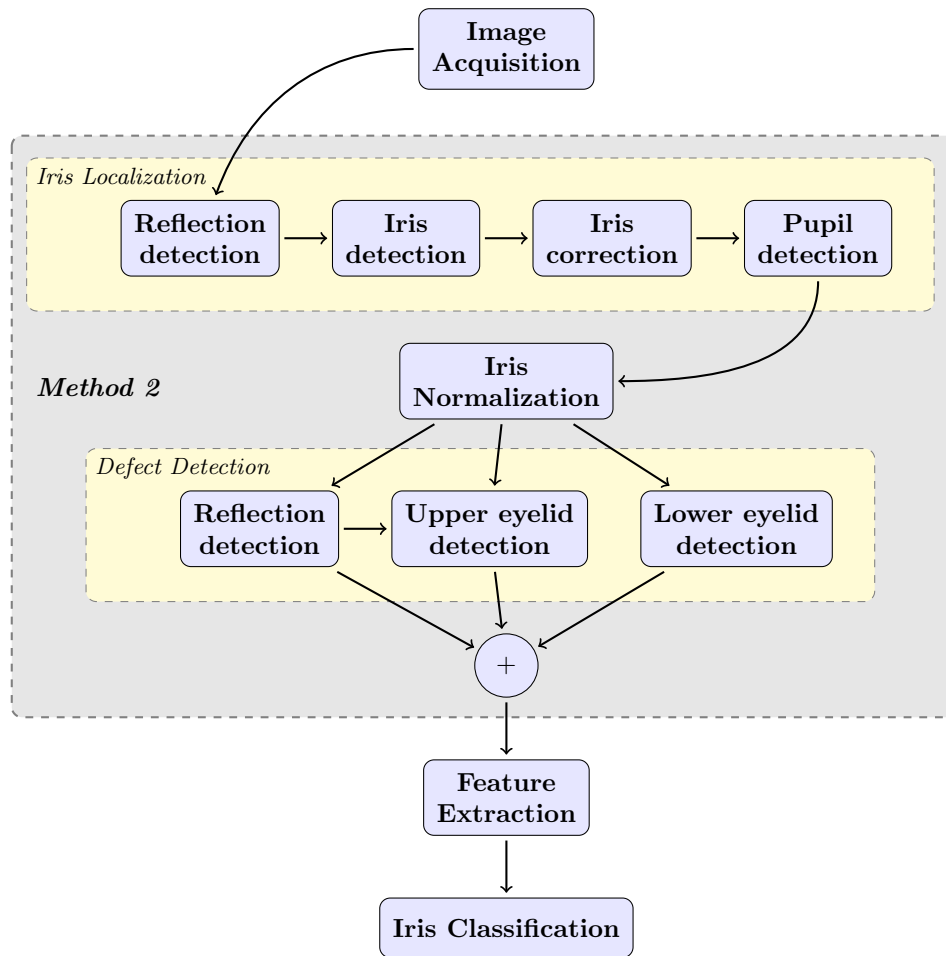


Figure 4.4: Processing scheme of method 2.

in the diagram in Figure 4.4, the outputs of all three occlusion finding methods (reflection detection, upper and lower eyelid detections) are binary masks and are combined together to form the result of the whole method.

### 4.2.2 Iris Localization

The iris occlusions (Fig.4.2) detection starts with searching for the reflections (Fig.4.5-left) in the blue spectral channel where they are the most visible (according to our extensive experiments) using the adaptive threshold. The binarization threshold is obtained using the cross-correlation between pixel-centered windows and the Gaussian window. The resulting binary mask is firstly slightly dilated (Fig.4.5-middle) to ensure full coverage of the reflections and then the detected reflective regions are corrected (Fig.4.5-right) using the inpainting algorithm presented in [Tel04]. The corrected image is subsequently used to detect the iris location in the image. The eye area is found using the modified integrodif-

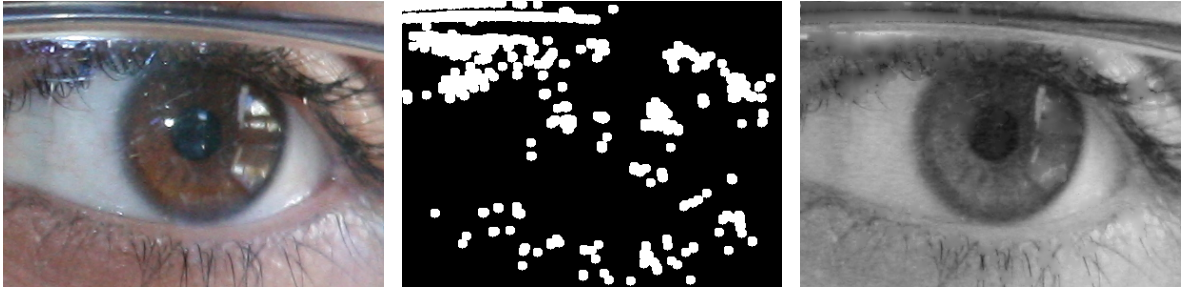


Figure 4.5: Detected reflections in iris (middle) and their corrections.

ferential Daugman operator [Dau93]:

$$\max_{\rho, \tilde{r}_1, \tilde{r}_2} \left| G_\sigma(\rho) * \frac{\partial}{\partial \rho} \oint_{\rho, \tilde{r}_1, \tilde{r}_2} Y_{r,B} 2\pi \rho ds d\rho \right|, \quad (4.15)$$

where  $r = \{r_1, r_2\}$ ,  $s = \{s_1, s_2\}$  are multiindices with the row and column indices,  $\tilde{r}$  the radius centre,  $\rho$  is the radius,  $Y_{r,B}$  is the blue component of the  $r$ -th eye pixel, and  $G_\sigma(\rho)$  denotes a Gaussian filter of scale  $\sigma$ . However the circle integral is not taken for full circle but only for degrees from  $0^\circ$  to  $45^\circ$  and from  $135^\circ$  to  $360^\circ$ . This is to better deal with possible upper eyelid occlusions in the image (which would otherwise obviously obstruct the correct localization of iris region). Fig.4.6-a illustrates local maxima (white dots) in the accumulator of this operator. Fig.4.6-b is the corresponding maximal value of radius for each pixel. Fig. 4.6-c is accumulator of the integrodifferential operator for pupil (only small area when iris boundary is known). And Fig.4.6-d image shows the localized iris regions where the outer circle correspond to the global maxima of iris accumulator (the smaller circle corresponds to the pupil accumulator described below).

The next step is the pupil detection in the red spectral channel to separate the iris region due to its best separability spectrum. The inner circle representing the pupil border is found in a similar way as the iris location described above, but in its respective smaller area (as can be seen in Fig. 4.6-c). The pupil is detected using the original (unmodified) Daugman operator inside the iris region. Detected iris region is then verified by checking the candidate pupil region mean with comparison of the closest left and right neighborhood iris regions. This is to deal with possible mislocalization of the iris border as can be seen in Fig. 4.7.

### 4.2.3 Iris Occlusions and Reflection Detection

Once we locate the iris region, this region is then normalized to rectangular shape (see Section 2.1.3 for method details) and we subsequently search for each of the selected occlusions (as can be seen in Fig.2.1). Possible occlusions are searched in the red spectral channel and reflections in the blue spectral channel, respectively (see Figure 4.8 for example). The resulting iris occlusion mask is results of these three methods combined.

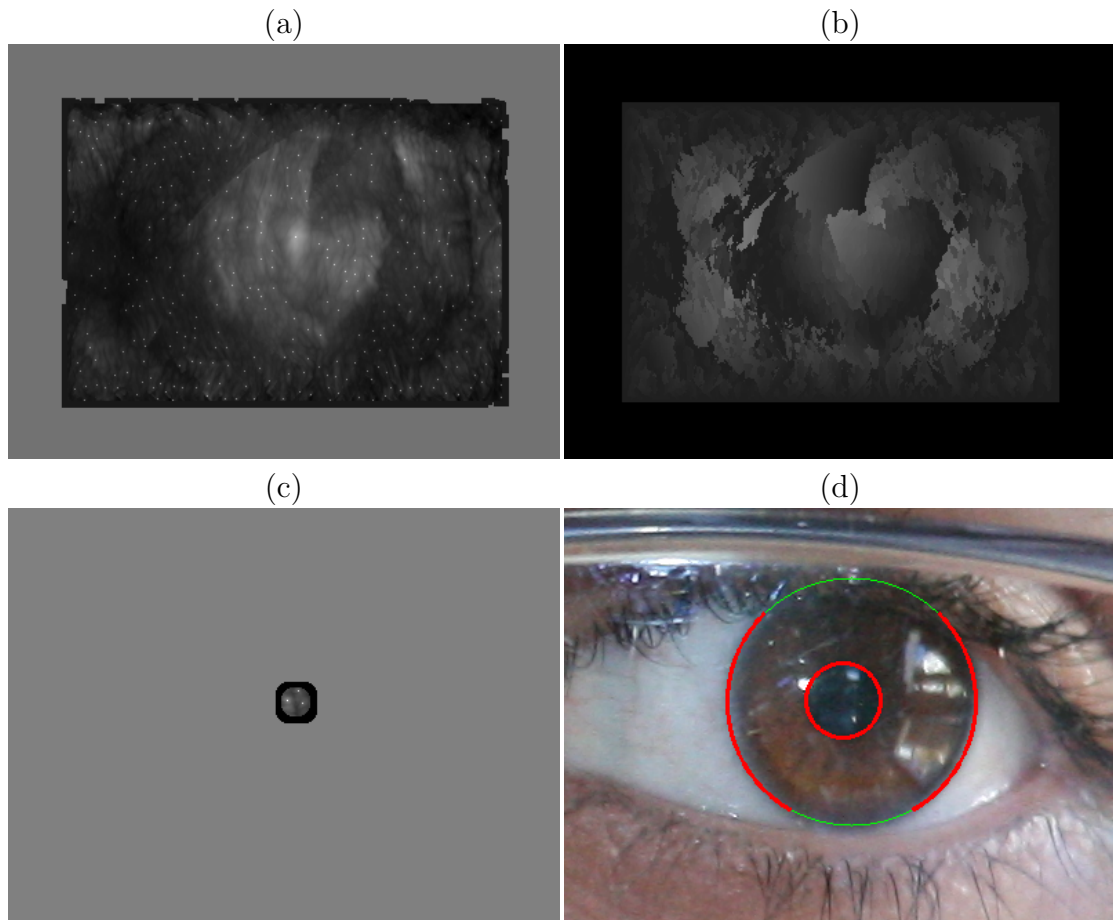


Figure 4.6: The accumulator of the integrodifferential Daugman operator (4.15) in the blue spectral channel (a), the corresponding maximal radius for each pixel (b), accumulator of the integrodifferential operator for pupil (c) (only small area when iris boundary is known) and the resulting iris localization (d).

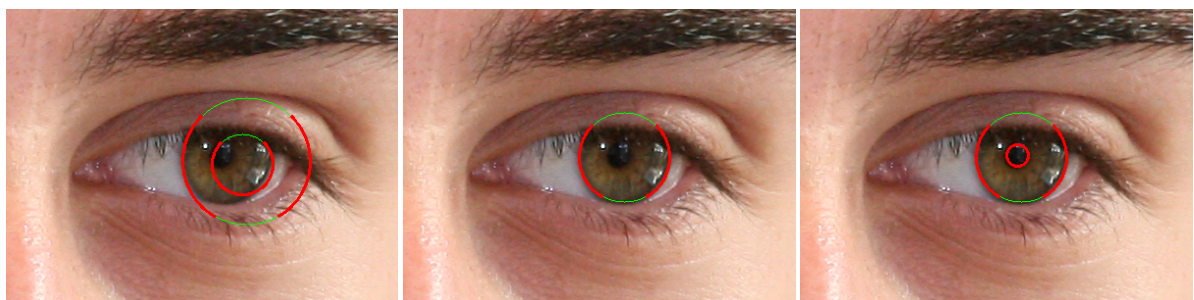


Figure 4.7: Imprecisely detected iris region (left), its correction (middle) and the corrected pupil (right).



Figure 4.8: The visibility of pupil, iris, its occlusions and reflections in each spectral channel (red, green, blue).

### 4.2.3.1 Upper Eyelid

The upper eyelid (Fig.4.2-c) is detected using vertically swapped image so that a potential upper eyelid is completely located in the center of image (otherwise it would be split in half at the corners of normalized iris image and the polynomial fitting would be slightly more complicated and slower). Subsequently the rays from  $0^\circ$  to  $180^\circ$  from the top center point are drawn. These rays are convolved with differential kernel and the maximum is located on each of them. The third order fitted polynomial then denotes the upper eyelid occlusion region border.

### 4.2.3.2 Lower Eyelid

Most iris images are not obstructed with the lower eyelid. The occasional lower eyelid occlusions (Fig.4.2-a) are detected using mean and standard deviation estimates  $\mu_{le}$  and  $\sigma_{le}$  of the top center region. Rows are in the range of  $r_1 \in \langle 0; \frac{N}{2} \rangle$  and columns  $r_2 \in \langle \frac{M}{4}; \frac{3M}{4} \rangle$ , where  $N$  ( $M$ ) is number of rows (columns) in the normalized iris image. If the standard deviation is larger than 25% of  $\mu_{le}$ , i.e.,

$$\sigma_{le} > \frac{\mu_{le}}{4} ,$$

then the lower eyelid is detected by simple thresholding with the threshold  $\tau = \mu + \frac{\sigma_{le}}{2}$ . The topmost central region in result mask from thresholding is detected as the lower eyelid.

### 4.2.3.3 Iris Reflections

The precise localization of reflections (Fig.4.2-b) is based on the fusion of similar adaptive thresholding (without dilatation) as in section 4.2.2 and detection based on the multispectral Markovian iris texture model (as presented in Section 4.1.5).



## 4.3 Robust Iris Occlusion Detection in Face Images

The third method was published in the Pattern Recognition Letters journal in 2015 [A.3] and as best current method was used as ground truth generation method in MICHE-II contest. It builds on the second method (4.2) and improves mainly iris localization part as this part is more challenging in the used database than in previous ones. In this method, MICHE database (described in Section 3.3.4) was used. Its images usually contain bigger area around eye (around half of the face) so additional steps to ensure the correct iris localization were needed. Also the images pose additional difficulty from the bigger resolution and better sharpness with many reflections coming from moist drops on the face. Those can also obstruct the overall eye localization. This method is also the only one that can detect missing eye and reject image all together.

### 4.3.1 Overview

As stated above, the images in MICHE database used in this method often contain big parts of the surrounding eye area (up to half of the face). So the new step needed to be introduced to find rough eye area because the integrodifferential operator alone often found incorrect maxima. Also new modified (multispectral) integrodifferential operator was introduced. The occlusion detection part remained largely unchanged. See Figure 4.9 for method diagram.

### 4.3.2 Reflection Correction

Similarly as in the second method, this one starts with searching for reflections (Figures 4.10-a and 4.12-c) in the blue spectral channel where they are most visible using an adaptive threshold. The binarization threshold is obtained using the cross-correlation between pixel-centered windows and the Gaussian window. The resulting binary mask is firstly slightly dilated (Fig.4.10-c) to ensure full coverage of reflections and then the detected reflective regions are corrected (Fig.4.10-d) using the inpainting algorithm presented in [Tel04].

The corrected multispectral image is subsequently used to detect eye location in the image.

### 4.3.3 Iris Localization

The iris occlusion detection requires to localize the eye region in the acquired image which is complicated with variable source image resolution and large differences in the captured face portion. The accurate iris region is recognized using a two step procedure with rough localization using the generalized Hough transformation (GHT) (to detect eye) subsequently elaborated by a modified integrodifferential Daugman operator (to localize iris).

#### 4. IRIS OCCLUSIONS DETECTION

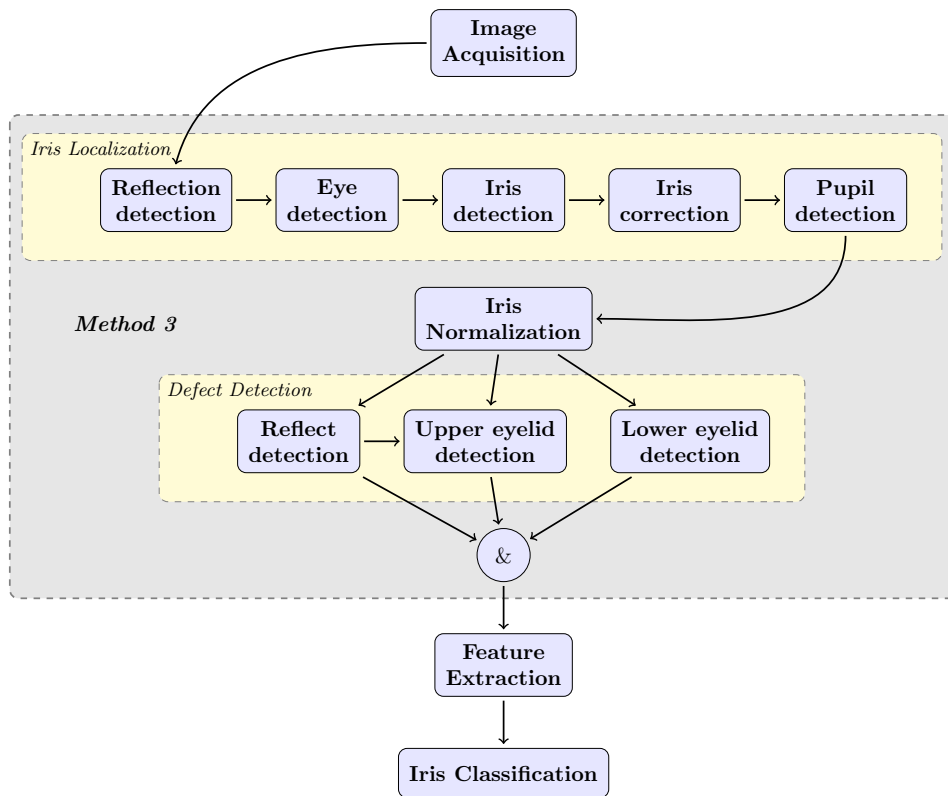


Figure 4.9: Processing scheme of method 3.

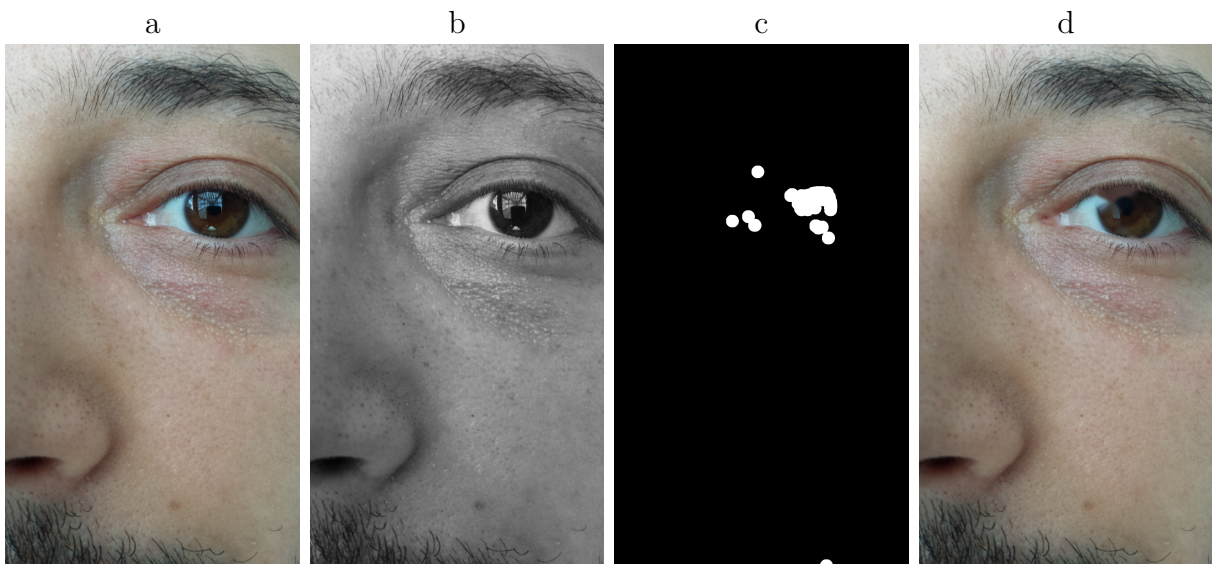


Figure 4.10: Iris detected reflections: source image (a), blue channel (b), detected reflections (c), and their corrections(d).



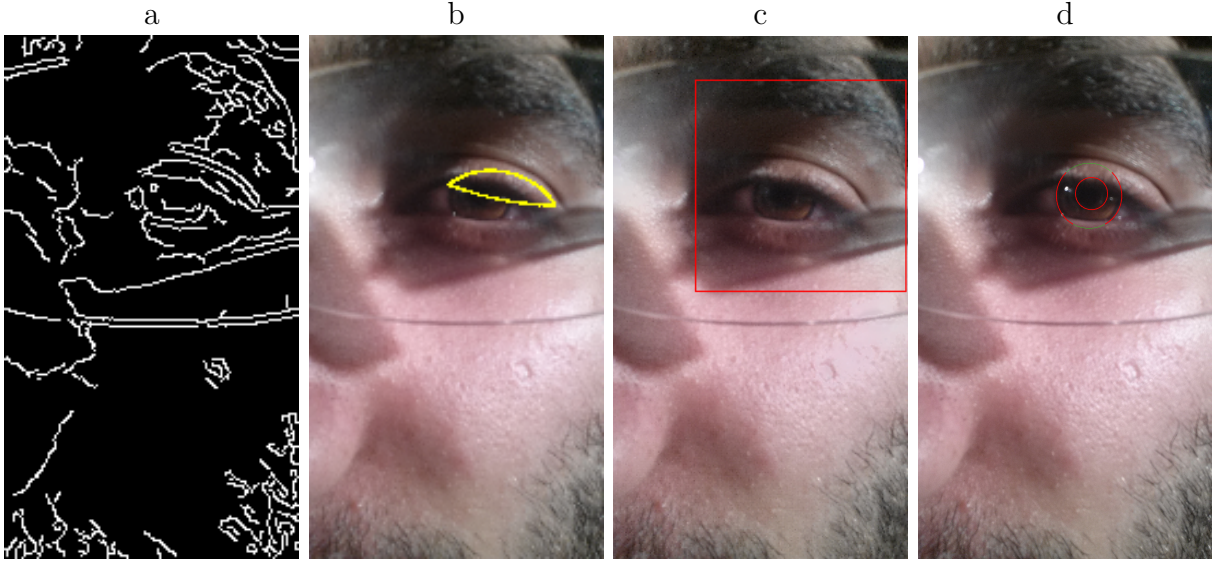


Figure 4.11: Detected rough iris region using the generalized Hough transformation: Canny detector(a), GHT mask(b), search window(c), detected iris(d).

#### 4.3.3.1 Eye Localization

The generalized Hough transformation [Bal81] is used to detect approximate eye region on a sub-sampled, reflection corrected image. The rough scale image has the width in the range 200 – 400 pixels because the corresponding sub-sampling step is selected to avoid non-lattice pixel positions interpolation. Down-scaled images speed up the processing time. A binary eye template for GHT is created as the intersection of two circles which are parameterized by the length  $c$  of their common chord. It is subsequently rescaled to handle variable image resolution. We assume the ratios of both circular segments altitudes  $h_1, h_2$  to this chord to be fixed

$$k_1 = \frac{c}{h_1} = 4.8 \text{ ,}$$

$$k_2 = \frac{c}{h_2} = 15.8 \text{ .}$$

The corresponding circles radii can be computed from

$$R_i = \frac{c^2}{8h_i} + \frac{h_i}{2} = c \frac{k_i^2 + 4}{8k_i} \quad i = 1, 2 \text{ .} \quad (4.16)$$

This template (Fig.4.11-b) is rotated in the range of  $\pm 15^\circ$ .

#### 4.3.3.2 Refined Iris Localization

The accurate eye area is found using the integrodifferential Daugman operator [Dau93] generalized from monospectral into the multispectral formulation (4.17) to exploit all available

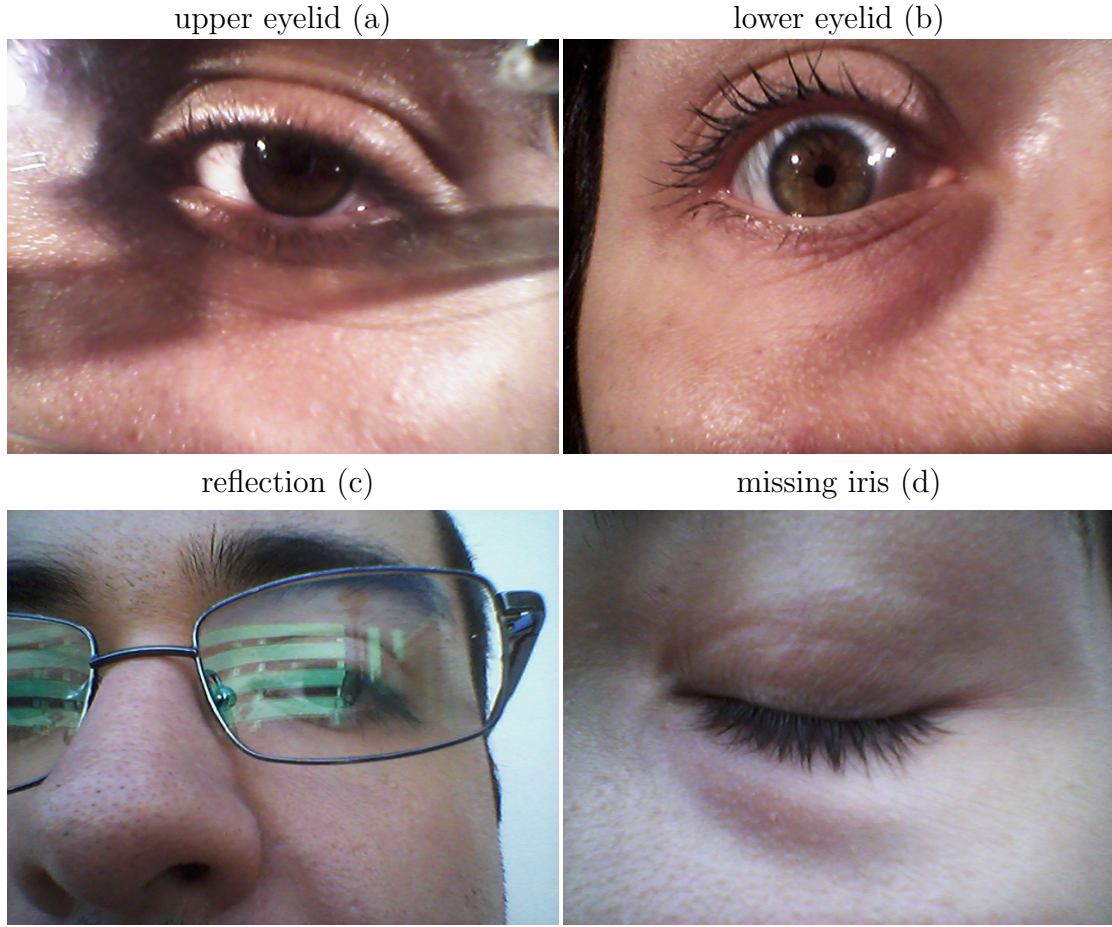


Figure 4.12: Iris region defects from iPhone5 device containing four (a,b,c,d) occlusion types.

information. The multispectral Daugman operator is

$$\max_{\rho, \tilde{r}_1, \tilde{r}_2} \left| G_\sigma(\rho) \otimes \frac{\partial}{\partial \rho} \oint_{\rho, \tilde{r}_1, \tilde{r}_2} \frac{Y_{r, \bullet}}{2\pi\rho} ds d\rho \right|, \quad (4.17)$$

where  $r = \{r_1, r_2\}, s = \{s_1, s_2\}$  are multiindices with the row and column indices,  $\bullet$  denotes all corresponding spectral indices,  $\tilde{r}$  the radius center,  $\rho$  is the radius,  $Y_{r, \bullet}$  is the  $r$ -th multispectral (color) eye pixel,  $\otimes$  denotes multispectral convolution, and  $G_\sigma(\rho)$  denotes a 3D Gaussian filter of identical scale  $\sigma$  in all spectral planes (see example of output values from this operator in Figure 4.13). The circle integral is not taken for full circle but only for degrees from  $0^\circ$  to  $45^\circ$  and from  $135^\circ$  to  $360^\circ$ . This is to better deal with possible upper eyelid occlusions in image (which would otherwise obviously obstructed the correct localization of the iris region). The next step is the pupil border detection in the red spectral channel to separate iris region. The inner circle representing pupil border is found (see Fig. 7.3, odd columns images) in a similar way as the iris location described above

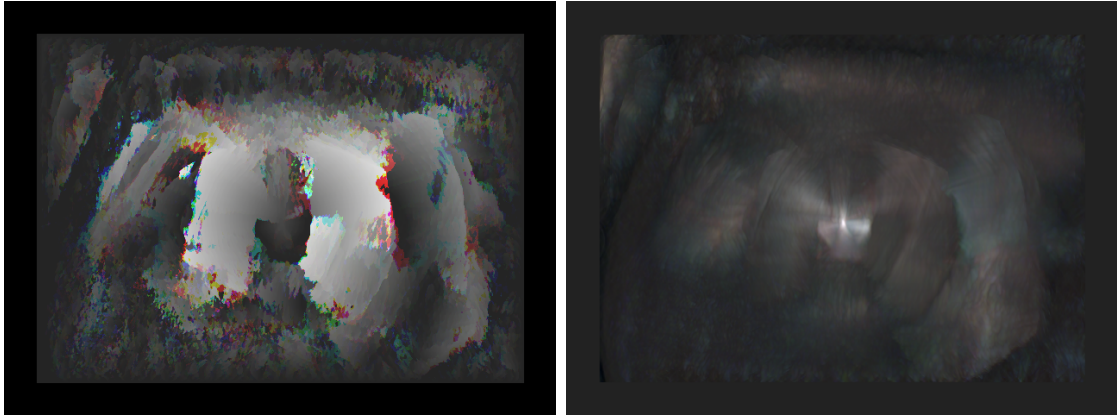


Figure 4.13: Output of multispectral integrodifferential operator (left image is  $\rho$  (radius) of maximum value in that pixel, right image is  $\max_{\rho, \tilde{r}_1, \tilde{r}_2}$  (maximum operator value) in that pixel).

but in its respective smaller area. The pupil is detected using the original (unmodified) Daugman operator [Dau93] inside the iris region. The detected iris region is then verified by checking the candidate pupil region mean with comparison of the closest left and right neighborhood iris regions. This is to deal with possible mislocalization of the iris border.

### 4.3.4 Iris Occlusions and Reflection Detection

Once we locate the iris region, this region is then normalized to rectangular shape [Dau93] and we subsequently search (see Fig.2.1 scheme) for each of the selected defects as it is illustrated in Fig.4.12. The rare cases of completely missing irises (Fig.4.12-d)) are solved using a simple thresholding in the generalized Hough transformation space. Possible occlusions are searched in the red spectral channel and reflections in the blue spectral channel, respectively. The results of all three steps (upper and lower eyelid and reflections) are binary masks that are again combined to one mask which is the method result.

#### 4.3.4.1 Upper Eyelid

The upper eyelid (Fig.4.12-a) is detected using vertically swapped image so that a potential upper eyelid is completely located in the center of image (otherwise it would be split in half at the corners of normalized iris image). Subsequently the rays from  $0^\circ$  to  $180^\circ$  from the top center point are drawn (Fig.4.14-a). These rays are convolved with differential kernel and the maxima is located on each of them (Fig.4.14-b) and lower maxima values are removed as potential outliers (Fig.4.14-c). The third order fitted polynomial then denotes the upper eyelid occlusion region border (Fig.4.14-d).

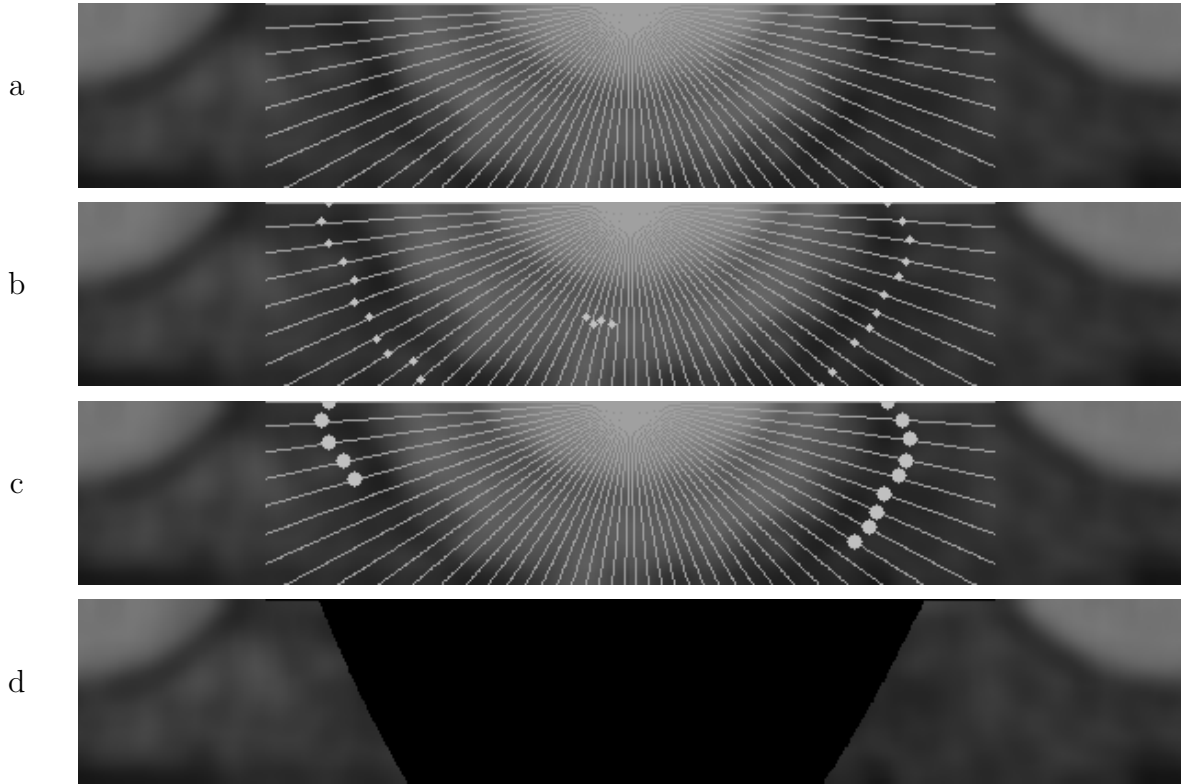


Figure 4.14: Upper eyelid detection steps in the red spectral channel.

#### 4.3.4.2 Lower Eyelid

Most iris images are not obstructed with the lower eyelid. The occasional lower eyelid occlusions (Fig.4.2-a) are detected using mean and standard deviation estimates  $\mu_{le}$  and  $\sigma_{le}$  of the top center region of normalized iris image (Figure 4.15-c). Rows are in the range of  $r_1 \in \langle 0; \frac{N}{2} \rangle$  and columns  $r_2 \in \langle \frac{M}{4}; \frac{3M}{4} \rangle$ , where  $N$  ( $M$ ) is number of rows (columns) in the normalized iris image. If the standard deviation is larger than 25% of  $\mu_{le}$ , i.e.,  $\sigma_{le} > \frac{\mu_{le}}{4}$  then the lower eyelid is detected by simple thresholding with the threshold  $\tau = \mu + \frac{\sigma_{le}}{2}$  (Figure 4.15-c). The topmost central region is detected as the lower eyelid in the resulting binarized image (Figure 4.15-c).

#### 4.3.4.3 Iris Reflections

The precise localization of reflections (Fig.4.12-c) in the fine scale normalized iris is based on fusion of similar (without dilatation) adaptive thresholding as in Section 4.3.3 and detection based on the multispectral Markovian iris texture model (see Section 4.1.5).



Figure 4.15: Thresholding for lower eyelid detection.

## 4.4 Methods Summary

In this chapter, we presented three methods for iris occlusion detection, each is suitable for a different type of data. But all deal with images acquired under visible light, in unconstrained conditions and they generally do not expect cooperation of the scanned person. Although all of them was tested on images in visible spectrum, our methods can be easily modified to accept monospectral images.

The first method works particularly well with close-up images of the eye. It is fast, straightforward method, that works best with simple occlusions of all types. Though the segmented eye should be in straight position and without glasses. The method also expects that there won't be widespread reflections across significant part of the eye. It was tested on our own ground truth masks of the UBIRIS database (7.1) and part of the UBIRIS.v2 database (same part that was used in worldwide NICE.I contest).

The second method is more complex, it consists of many submethods specialized for different occlusion types. It is also more suitable for challenging and complicated capture conditions. The eye should be in close-up position as in previous method, this one though deals well with eyes that are heavily occluded, with big reflections or partially closed. It was tested on the UBIRIS.v2 database and successfully compared with methods from the NICE.I contest.

The third method is a step towards iris localization in general images. It deals with images not containing only eye itself but can deal with photos with large parts of the face. The photos can be taken by user themselves without any complicated cooperation. The method also can deal with many light reflections from moisture drops that are often apparent on the closeup faces. It was tested on the UBIRIS.v2 and the MICHE databases, specifically the latter contains exactly that large parts of faces.





# Iris Recognition

*This chapter will detail our approach to the iris recognition. Firstly we describe some ‘prerecognition’ methods that can quickly rule out dissimilar irises. Then our approach to iris texture feature representation and classification will be described.*

## 5.1 Our Approach

We are currently aiming to propose method for iris recognition task that will be comparable with the top performing participants of the NICE.II contest (6.3). From the contest results (Tab. 5.1), it can be seen that no individual feature representation method is able to outperform others solely by itself. And that the fusion of several disjunctive feature representation methods (in sense of used iris features) along with some methods that can add another type of information (periocular, outside from iris area) is needed to develop successful iris recognition method. The overview of our method can be seen in Figure 5.1.

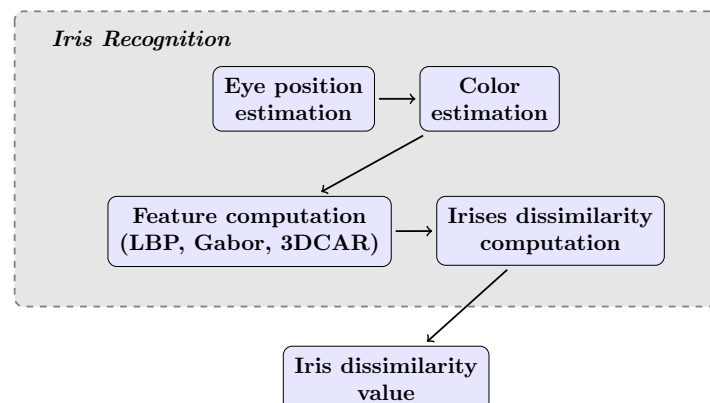


Figure 5.1: Schema of iris recognition method.



Figure 5.2: Examples of eyes with visible position (right, left, right).

## 5.2 Determining Eye Position

The recognition of the left/right eye can be useful supplemental feature that can help recognize iris classes (i.e. when comparing left eye with right eye, it is impossible to have positive match, since every person have different texture for left and right eye). So, we've developed a method that is capable to recognize this property.

As can be seen in iris images in Figure 5.2, the eyelashes are typically on the far side of eye (from center of face) and are noticeably more dense than on the other side of eye. We've utilized this property and estimated the eye position with the following equations:

$$R_l = [c_x - 3\rho, c_y - \rho, 2\rho, \rho] , \quad (5.1)$$

$$R_r = [c_x + \rho, c_y - \rho, 2\rho, \rho] , \quad (5.2)$$

$$\mu_{R_k} = \frac{1}{2\rho^2} \sum_{r_1, r_2}^{R_k} I(r_1, r_2) , \quad (5.3)$$

$$\sigma_{R_k} = \sqrt{\frac{1}{2\rho^2} \sum_{r_1, r_2}^{R_k} (I(r_1, r_2) - \mu_{R_k})^2} , \quad (5.4)$$

where both  $R_l$  and  $R_r$  are areas on the left and the right side of the eye ( $[x, y, height, width]$ ,  $x$  and  $y$  are coordinates for the top left corner and  $height$  and  $width$  are sizes of the area).  $c_x$  and  $c_y$  are coordinates of the eye centre and the  $\rho$  is iris radius. For each area, the standard deviation  $\sigma_{R_k}$  is computed. They are then compared against each other and the bigger standard deviation denotes the eye position.

This method works best in the red channel because the difference between sclera and skin is least visible here. The difference between skin and eyelashes is most apparent here which is also advantageous for the method.



## 5.3 Color Histogram

Similarly to the previous section, the eye color can also serve as rule out principle. For this approach, we utilized histograms of iris texture. The histograms are computed from the normalized iris and the iris occlusion mask (so only true iris pixels are used). Correlation of those two histograms is then computed (5.5).

$$d(H_a, H_b) = \frac{\sum_i (H_a(i) - \bar{H}_a)(H_b(i) - \bar{H}_b)}{\sqrt{\sum_i (H_a(i) - \bar{H}_a)^2 \sum_i (H_b(i) - \bar{H}_b)^2}} \quad (5.5)$$

$$\bar{H}_k = \frac{1}{N} \sum_i H_k(i) \quad (5.6)$$

where  $H_k$  is a histogram,  $H_k(i)$  is particular bin from histogram and  $N$  is number of bins in histogram. The resulting dissimilarity value is  $d(H_a, H_b)$ . As the output of this method is not a particular iris color but rather difference in color of two irises, it is needed to utilize the additional threshold to rule out iris with different color. This threshold was derived experimentally. It is also possible to add the output of this method to classification to better differentiate dissimilar irises.

## 5.4 Textural Features

We are analyzing the iris image itself by different texture features. Namely LBP and Gabor filters (see Sections 2.1.10 and 2.1.11 for brief explanation of those methods) and 3D CAR features as explained in the previous chapter (4.1.4). The iris image with occlusion mask (again, only true pixels are used) is transformed to the matrix (corresponding to the image pixels) of feature vectors given the used method. The vectors are then used for per pixel classification (see next section, 5.5).

### 5.4.1 Local Binary Pattern Features

We are utilizing standard LBP features, not rotation invariant (as presented in [POX00]). Because even in case of capturing person with rotated head (and thus rotated eye), thanks to the normalization stage, the normalized iris texture will still have the same orientation (see Figure 5.3). It will only be shifted in  $x$  axis. So in this case, it is advantageous to use rotation variant features which will thus be more descriptive.

The LBP features are computed on each spectral channel separately and than joined to one feature vector. On normalized iris with size  $200 \times 50$ , we used LBP parameters as  $P = 8, R = 3$ . These parameters are supposedly highly dependent on mentioned normalized iris size.

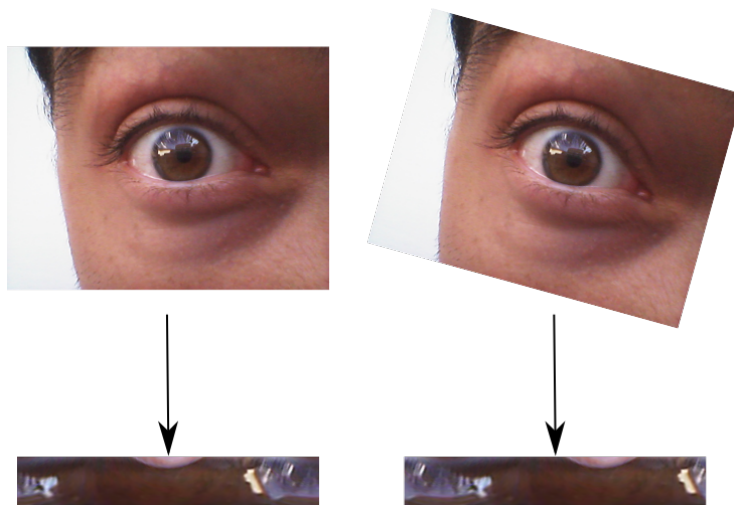


Figure 5.3: Impact of rotation to iris normalization.

### 5.4.2 Gabor Filters

As Gabor filters have numerous parameters that have to be set (see 2.1.11), we discretized those parameters and run wide range of experiments to determine best possible parameters combination.

Our parameters ranged:

$$\begin{aligned} 1/\lambda &= 0.1 \dots 2.0, \text{ step } 0.2 , \\ \theta &= 0 \dots \pi, \text{ step } \pi/4 , \\ \psi &= 0 \dots \pi, \text{ step } \pi/4 , \\ b &= 0.6 \dots 2.0, \text{ step } 0.2 , \end{aligned}$$

for each combination of parameters we constructed a Gabor kernel. The kernel was then convolved with each channel of the normalized irises from the UBIRIS.v2 database. For each iris, the matrix with Gabor feature vectors was constructed as described at beginning of the parent section (5.4).

This set of matrices was then compared pairwise and distance of each pair was computed. The distances of intra-class pairs and the distances of inter-class pairs were separated and compared as described in 6.3. As the purpose of this comparison was not to get the best possible iris dissimilarity value but we were rather interested in maximal dissimilarity value across all those values. The values are thus unoptimized, but it should nonetheless give us the Gabor kernel with highest discriminability across all irises. The example of 2D graphs with one changing parameter (others are fixed) can be seen in Figure 5.4. The best kernels can be seen in Figure 5.5.

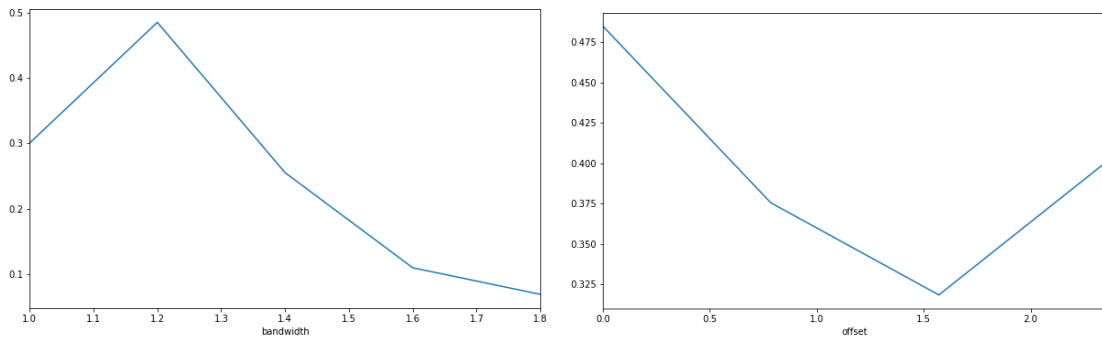


Figure 5.4: Graphs for estimating Gabor kernel. On  $x$  axis is changing parameter value, on  $y$  axis is result discriminability value.

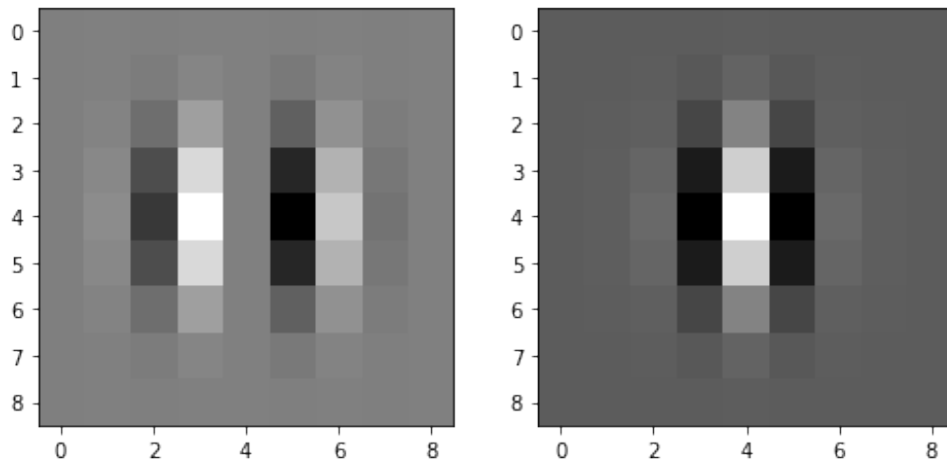


Figure 5.5: Best estimated Gabor kernels (real and imaginary part).

### 5.4.3 CAR Model

As we stated in previous chapter (Section 4.1.4), our assumption was, that the iris texture can be represented by the adaptive 3D causal simultaneous auto-regressive model. We are also using this assumption to form the iris texture representation for recognition. It can be also convenient in a way that we do not have to analyze iris again as we did it in previous step. Thus all analysis is faster.

For the occlusion detection, we used the prediction error (Equation 4.12) which was good choice for differentiating between two classes ('iris texture' and 'other parts'). But for further classification we need to use more descriptive parameters. We thus chose the model parameters  $A$  (Equation 4.3). In contrast with the prediction error which is only one value, the  $A$  matrix have  $x^2 * n$  values where  $x$  is a number of spectral channels and  $n$  is a size of the neighborhood. So in case of three spectral channels (RGB) and three neighbors, the parameter vector length for one direction is  $3^2 * 3 = 27$ .

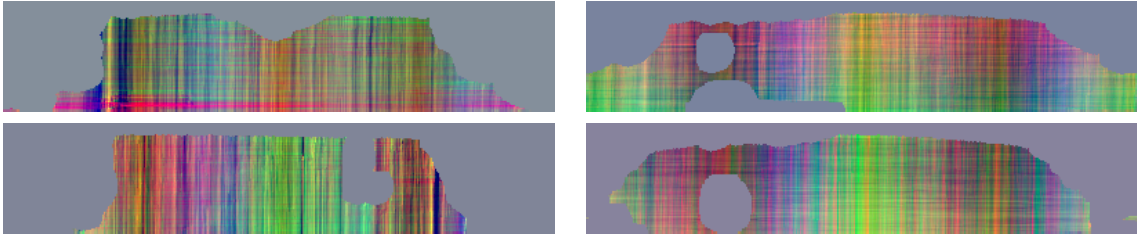


Figure 5.6: PCA transformation of 3DCAR (4.1.4) parameters. Top three dimensions mapped to RGB channels.

We experimented with all main directions (row-wise and top-down, row-wise and down-top, the same for columns and similar variations for diagonal directions,  $4x$ ). Eight directions in total. When each direction add 27 values, the parameter vector length can quickly add up. We thus ended with using two directions, the ‘left→right, top→down’ and ‘down→top, right→left’. The examples of top three dimensions from PCA transformation of those parameters (mapped to RGB channels) can be seen in Figure 5.6. In the top left image in bottom left corner can be clearly seen impact of badly segmented occlusion mask on the parameters.

## 5.5 Iris Classification

Generally, a iris classification involves usage of some well known classifier (SVM, Bayes, ...). As we want to compare our method with other top results, we need to use some form of benchmark that would allow such comparison. We chose well known NICE.II contest that have challenging, public data and contains state-of-the-art results (see Section 6.3 for description and Table 5.1 for top results).

Our setup is thus same as theirs. We are comparing two normalized iris images (with occlusion masks) to each other. Each iris is represented as the matrix of feature vectors where each vector corresponds to each pixel in normalized iris. And each vector is created from concatenated feature vectors of individual feature extraction methods described above (5.4).

Computation of dissimilarity value works as follow:

1. The iris images (and their feature vectors) are divided into regions of chosen size (Figure 5.7). On each region and each iris, the k-nearest neighbors (KNN) classifier is initialized, Figure 5.7-a. Note that KNN here only serves as fast nearest neighbor

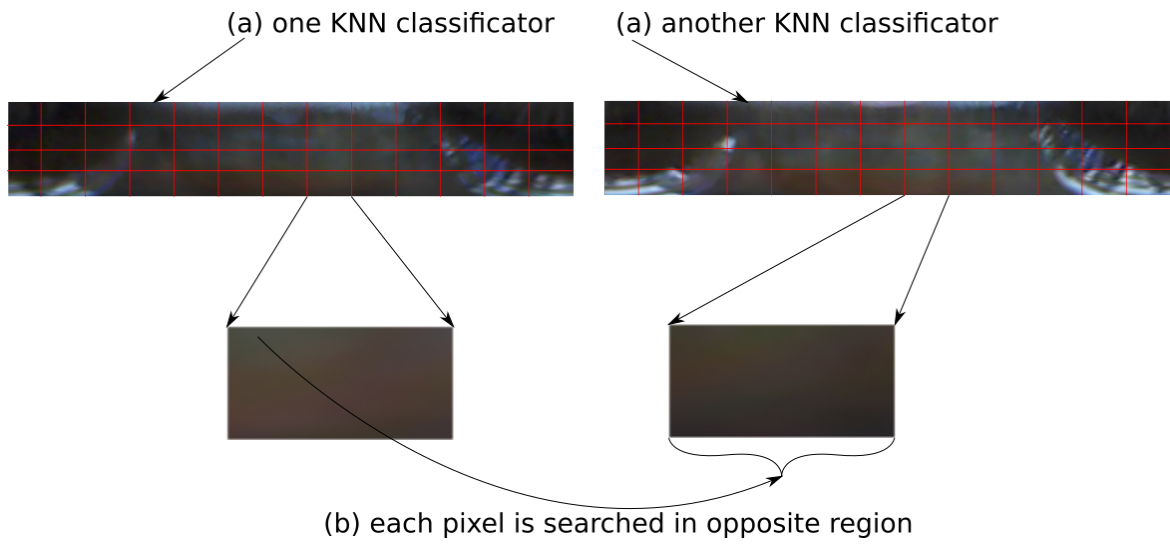


Figure 5.7: Schema of classification method.

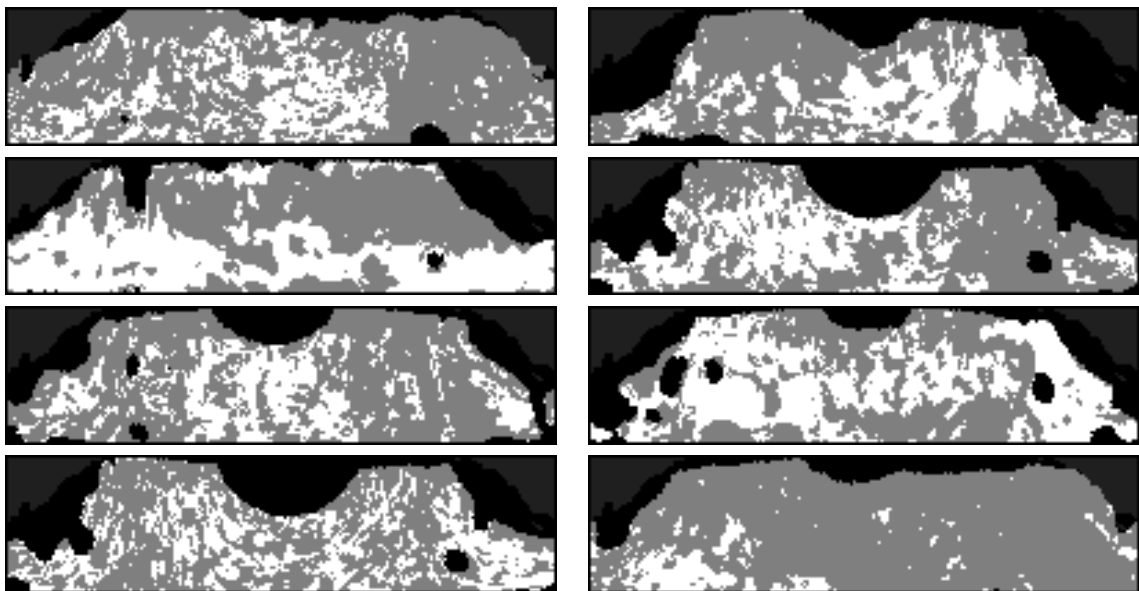


Figure 5.8: Examples of per pixel classification result images.

Rank	Author	Dissimilarity score
1	Tan <i>et al.</i> [Tan+12]	2.5748
2	Wang <i>et al.</i> [Wan+12]	1.8213
3	Santos & Hoyle [SH12]	1.7786
4	Shin <i>et al.</i> [Shi+12]	1.6398
5	Li <i>et al.</i> [LLZ12]	1.4758
6	Marsico <i>et al.</i> [MNR12]	1.2565
7	Li & Ma [LM12]	1.1892
8	Szewczyk <i>et al.</i> [Sze+12]	1.0931

Table 5.1: Top eight alternative results from the Noisy Iris Challenge Evaluation Contest (NICE.II) [PA12].

search as it contains only one class.

$$\gamma^j(r_1, r_2) = [p_0, p_1, \dots, p_n] , \quad (5.7)$$

$$R_i^j(r_1, r_2) = \gamma^j(s_1 + r_1, s_2 + r_2) , \quad (5.8)$$

$$s_1 = w(i \bmod m) , \quad (5.9)$$

$$s_2 = h \frac{i}{m} , \quad (5.10)$$

where  $R_i$  is  $i$ -th iris region,  $j$   $j$ -th iris,  $r_1, r_2$  coordinates,  $w, h$  width, height respective and  $m$  denotes number of regions in one row. Thus  $\gamma^j(r_1, r_2)$  represents one feature vector and  $n$  feature vector length.

2. Next, the cross-classification is performed. For each pixel, its feature vector is searched in corresponding region in opposite iris, Figure 5.7-b. Then the distance from the returned nearest pixel (feature vector) from opposite region is computed by the Euclidean distance (function denoted by  $\Delta$ ). This step ends with two distance masks (one for each iris).

$$\delta_i^j(r_1, r_2) = \Delta(\text{KNN}_i^k(R_i^j(r_1, r_2)), R_i^j(r_1, r_2)) , \quad (5.11)$$

$$\Delta(\vec{a}, \vec{b}) = \sqrt{\sum_{l=0}^n (a_l - b_l)^2} , \quad (5.12)$$

where  $\text{KNN}_i^k$  is KNN classifier from the  $k$ -th iris and  $i$ -th region and  $\delta_i^j(r_1, r_2)$  is minimal Euclidean distance for the  $j$ -th iris,  $i$ -th region.

3. The distance is then thresholded. The threshold value was estimated with the least squares method from the selected training sample from the UBIRIS.v2 database. The training sample consisted of 10 irises from same class that were selected and the

threshold experimentally derived.

$$T_i^j(r_1, r_2) = \begin{cases} 1 & \text{if } \delta_i^j(r_1, r_2) > \theta \\ 0 & \text{if } \delta_i^j(r_1, r_2) \leq \theta \end{cases}, \quad (5.13)$$

where  $T_i^j(r_1, r_2)$  is the thresholded value for  $r_1, r_2$  pixel,  $i$ -th iris and  $j$ -th region and  $\theta$  is the threshold value.

4. This way, the classification mask for each iris is obtained (the resulting examples can be seen in Figure 5.8, a so called per-pixel classification mask). The white pixels denotes the distance value below threshold, the gray pixels then the distance above threshold and the black pixels were not considered for classification due to the occlusion mask.
5. The confidence of each mask is then computed. Confidence is ratio of white pixels to sum of white and gray pixels. The iris Dissimilarity value is a sum of  $1 - \text{confidence}$  of both masks.

$$d = 2 - \frac{w^j}{o^j} + \frac{w^k}{o^k}, \quad (5.14)$$

$$w^j = \sum_i \sum_{r_1, r_2} T_i^j(r_1, r_2), \quad (5.15)$$

$$o^j = \sum_{r_1, r_2} M^j(r_1, r_2), \quad (5.16)$$

where  $d$  is the resulting dissimilarity value,  $w^j$  sum of white pixels,  $o^j$  sum of all classified pixels and  $M^j$  is occlusion mask.

## 5.6 Method Summary

The method results are highly dependent on the estimated parameters and chosen feature extraction methods. Namely regions size  $w, h$  and threshold value  $\theta$ . We are still improving our results and aim to outperform current top methods from the NICE.II contest.





---

# Iris Biometrics Evaluation

*This chapter describes a standard evaluation of a biometric system along with the description of different iris contests that we are using for comparison.*

## 6.1 Performance Evaluation

Evaluation of biometric recognition systems, is mainly compared by several kinds of measures [MW02b] [Way99]:

### 6.1.1 Basic Criteria

The  $p$  denotes class acceptance and  $n$  denotes class rejection.

- True positive (TP)  
The outcome from a prediction is  $p$  and the actual value is also  $p$ .
- False positive (FP, also *Type I error*)  
The outcome from a prediction is  $p$  and the actual value is  $n$ .
- True negative (TN)  
When both the prediction outcome and the actual value are  $n$ .
- False negative (FN, also *Type II error*)  
When the prediction outcome is  $n$  while the actual value is  $p$ .

### 6.1.2 Advanced Criteria

- TPR (true positive rate / recall / sensitivity)

$$TPR = \frac{TP}{TP+FN}$$

The probability that the system correctly matches the input sample to a matching class in the database. It is the percent of valid inputs which are correctly accepted.

- FPR / FAR / FMR (false positive rate / false accept rate / false match rate / fall-out)

$$FPR = \frac{FP}{FP+TN}$$

The probability that the system incorrectly matches the input sample to a non-matching class in the database. It is the percent of invalid inputs which are incorrectly accepted.

- TNR (true negative rate / specificity)

$$TNR = \frac{TN}{FP+TN}$$

The probability that the system successfully detect a non-matching sample to any class in the database. It is the percent of invalid inputs which are correctly rejected.

- FNR / FRR / FNMR (false negative rate / false reject rate / false non-match rate / miss rate)

$$FNR = \frac{FN}{TP+FN}$$

The probability that the system fails to detect a match between the input sample and a matching class in the database. It is the percent of valid inputs which are incorrectly rejected.

- ROC (receiver operating characteristic)

See 6.1.3 for description.

- EER / ECR (equal error rate / crossover error rate)

The rate at which both FAR and FRR errors are equal. The value of the EER can be easily obtained from the ROC curve. The EER is a quick way to compare the accuracy of approaches with different ROC curves. In general, it can be said that the approach with the lowest EER is most accurate.

### 6.1.3 ROC Plot

The ROC plot is a visual characterization of the trade-off between the FAR and the FRR (see Figure 6.1). In general, the matching algorithm performs a decision based on a threshold which determines how close to a class the input needs to be for it to be considered a match. If the threshold is reduced, there will be less false non-matches but more false accepts. Correspondingly, a higher threshold will reduce the FAR but increase the FRR. A common variation is the Detection error trade-off (DET), which is obtained using normal deviate scales on both axes. This more linear graph illuminates the differences for higher performances (rarer errors).

ROC analysis provides tools to select possibly optimal models and to discard suboptimal ones independently from (and prior to specifying) the cost context or the class distribution.

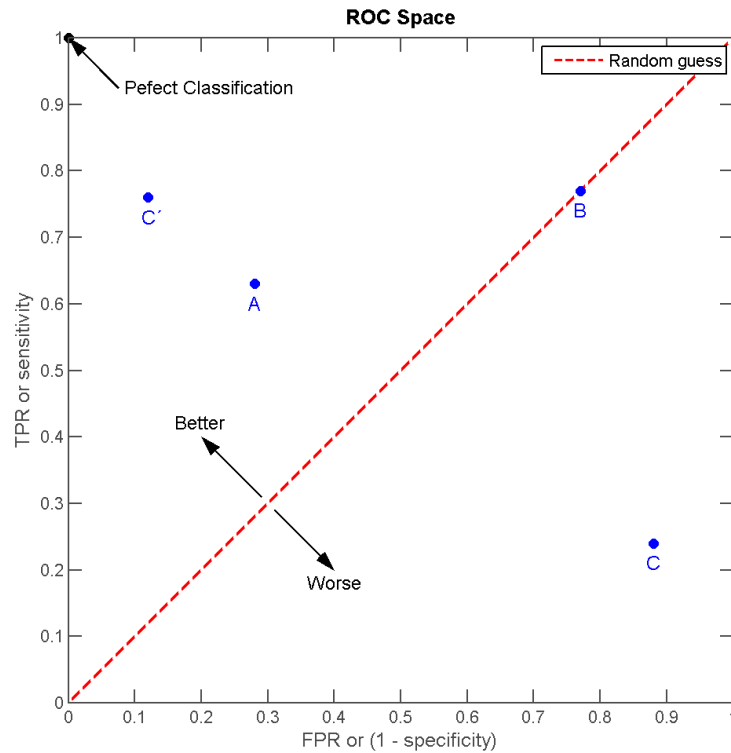


Figure 6.1: Example of ROC curve<sup>1</sup>.

ROC analysis is related in a direct and natural way to cost/benefit analysis of diagnostic decision making.

## 6.2 NICE.I Contest

All iris contests at that time (2009) focused only on recognition accuracy and were using images taken under controlled environment (occlusion free image taken under longer period of time for good iris texture). They were also taken in NIR spectrum. E.g., the *Iris Challenge Evaluation, ICE*. However, those highly restricted imaging conditions clearly reduces the range of domains where the iris recognition can be applied.

So the NICE.I contest was created with these factors in mind. The contest was run on the subset of UBIRIS.v2 database (Section 3.3.3) which contains highly noisy eye images. The participants had 500 training images and a disjoint test set of 500 images was used to measure the pixel-by-pixel agreement between the binary maps made by each participant

<sup>1</sup>Source: [https://en.wikipedia.org/wiki/Receiver\\_operating\\_characteristic](https://en.wikipedia.org/wiki/Receiver_operating_characteristic)

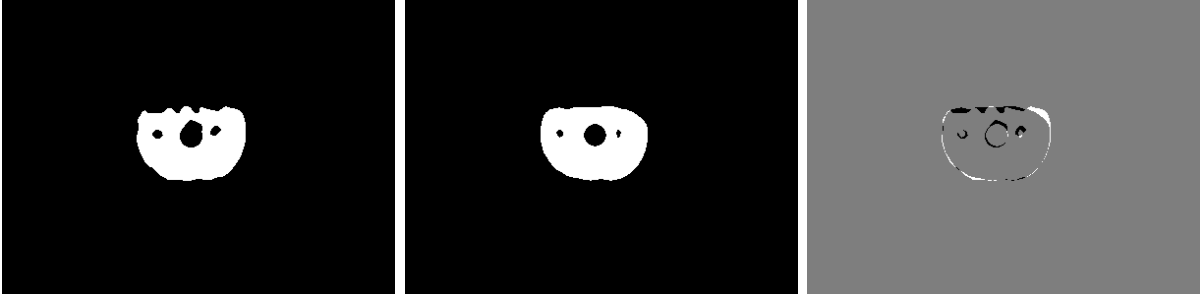


Figure 6.2: Left is the ground truth image, center is method result image and right is diff image from the first two.

( $X$ ) and the ground-truth data ( $G$ ), manually built by the NICE.I organizers [PA07] (see Figure 6.2).

The contest exclusively evaluates the iris segmentation and occlusion detection stages, allowing the independent evaluation of these tasks from the iris encoding and recognition algorithms. The contest evaluation was done by the following equation:

$$\text{Error} = \frac{1}{nn_r n_c} \sum_{k=1}^n \sum_{s_1=1}^{n_r} \sum_{s_2=1}^{n_c} {}^k X_{s_1} \otimes {}^k G_{s_2}, \quad (6.1)$$

where  $\otimes$  is the logic XOR operator,  $n_r, n_c, n$  are the number of rows, columns, and testing images, respectively.  ${}^k X$  is image output mask form benchmarked method and  ${}^k G$  is ground truth mask for that image.

### 6.3 NICE.II Contest

The NICE.II contest [PA12] complemented its predecessor in terms of the traditional pattern recognition stages, evaluating different signature encoding and matching strategies. All the participants used the exact same segmented data, which were automatically obtained according to the highest performing method in the NICE.I. Sixty-seven participants from thirty countries registered in the contest 1 and received a training set composed of 1000 images and the corresponding binary iris segmentation masks. The task was to construct a binary executable that receives (by command-line parameters) a pair of iris samples and their iris segmentation masks and outputs a text file containing a score that corresponds to the dissimilarity between the irises. This score  $d$  should be a metric, i.e., it should meet the following conditions:

1.  $d(I, I) = 0$
2.  $d(I_1, I_2) = 0 \Rightarrow I_1 = I_2$
3.  $d(I_1, I_2) + d(I_2, I_3) \geq d(I_1, I_3)$

In the evaluation, disjoint sets of 1000 unseen images and the corresponding segmentation masks were used to rank participants. The  $\mathbb{I} = I_1, \dots, I_n$  is a set of iris images,  $\mathbb{M} = M_1, \dots, M_n$  their binary iris segmentation masks and  $id(\cdot)$  the identity function on an image. An one-against-all comparison scheme yields a set of match  $\mathbb{D}^I = d_1^i, \dots, d_m^i$  and of non-match  $\mathbb{D}^E = d_1^e, \dots, d_m^e$  dissimilarity scores, respectively, for the cases where  $id(I_i) = id(I_j)$  and  $id(I_i) \neq id(I_j)$ . As suggested by Daugman, for two-choice decisions (e.g., match/ non-match) the decidability index  $d'$  measures how well separated the two types of distributions are, and recognition errors correspond to their overlap area:

$$d' = \frac{|\mu_E - \mu_I|}{\sqrt{\frac{\sigma_E^2 + \sigma_I^2}{2}}} \quad (6.2)$$

where  $\mu_I = \frac{\sum_i d_i^I}{k}$  and  $\mu_E = \frac{\sum_i d_i^E}{m}$  are the means of the two distributions and  $\sigma_I = \frac{\sum_i (d_i^I - \mu_I)}{k-1}$  and  $\sigma_E = \frac{\sum_i (d_i^E - \mu_E)}{m-1}$  their standard deviations. The participants were ranked according to their decidability scores, and the best eight were invited to publish in special *Pattern Recognition Letters* issue (see their results in Table 7.3).

## 6.4 Mobile Iris Challenge Evaluation I Contest

MICHE I contest taken form of special PRL issue in 2015. It included MICHE database (Section 3.3.4) which was used in our third method (Section 4.3). The contest was focused on following themes:

- Iris detection on mobile devices.
- Iris segmentation on mobile devices.
- Iris biometric recognition on mobile devices.
- Applications of iris biometrics on mobile devices.

The detailed description of this contest can be found in special Pattern Recognition Letters issue (Volume 57, published 1 May 2015). Mainly in the introduction article [Edi+15].



---

## Proposed Methods Results

*This chapter is showing results which we were able to achieve with the proposed methods for detecting occlusions. It showcases tables comparison with other competing methods, example iris masks as method results and also presents our achievements in public recognition of our methods.*

### 7.1 Results for Method ‘Fast Occlusion Detection on Eye Images’

The method is described in Section 4.1. It was initially developed for the UBIRIS database and because there were no ground truth masks for iris occlusions for this database, we had to produce our own. We handmade ground truth masks for samples of first 20 classes from UBIRIS database. They are now publicly available at <http://iris.utia.cas.cz/>. Examples of those masks can be seen in Figure 8.5.

The method is quite simple, it essentially uses the Daugman’s integrodifferential operator for locating iris and our multispectral causal autoregressive model for iris occlusion detection. Thus it is fast with comparable performance to other competing methods.

The method performance on the images can be seen at the Table 7.1. The acronyms in header are explained in the Section 6.1. In this table one can also see which type of the occlusion is present in the given image. The method performance on the UBIRIS.v2 database can be seen at the Table 7.2. At the time of publication it placed at the third rank. The examples of those results can be seen in Figure 7.1.

### 7.2 Results for Method ‘Robust Occlusion Detection in Challenging Images’

The second method is described in Section 4.2. It was made and tested on ground truth data from the UBIRIS.v2 database. We acquired those from organizers of the NICE.I

## 7. PROPOSED METHODS RESULTS



Figure 7.1: Eye images and the corresponding detected occlusions masks in the first method (UBIRIS database). Above the iris image in odd column is name of the iris in database. For numerical results of selected irises see Table 7.1.



7.2. Results for Method ‘Robust Occlusion Detection in Challenging Images’

UBIRIS images	occlusions types	FP [%]	FN [%]	TP+TN [%]
Img_1_1_1	bc	1.00	10.56	88.44
Img_1_2_1	abc	8.13	5.25	86.62
Img_2_1_1	abc	8.83	2.81	88.36
Img_2_2_1	abc	14.40	3.49	82.11
Img_3_1_1	abc	5.04	2.93	92.04
Img_3_2_1	abc	3.16	3.60	93.23
Img_4_1_1	abc	31.79	2.20	66.01
Img_4_2_1	abc	15.51	1.77	82.72
Img_5_1_1	abc	3.08	8.22	88.70
Img_5_2_1	bc	5.94	1.09	92.97
Img_6_1_1	abc	2.83	3.07	94.10
Img_6_2_1	abc	12.67	7.39	79.95
Img_7_1_1	abc	7.41	4.66	87.93
Img_7_2_1	abc	32.75	2.35	64.89
Img_8_1_1	ab	0.44	4.36	95.20
Img_8_2_1	b	1.52	3.33	95.15
Img_9_1_1	abc	11.17	0.91	87.93
Img_10_1_1	abc	4.40	1.96	93.64
Img_11_1_1	abc	4.05	4.91	91.03
Img_11_2_1	abc	6.42	2.24	91.34
Img_12_1_1	abc	1.11	8.57	90.32
Img_12_2_1	abc	0.81	6.46	92.73
Img_13_1_1	abc	11.01	2.46	86.53
Img_13_2_1	abc	30.93	1.16	67.91
Img_14_1_1	abc	8.41	5.93	85.66
Img_15_1_1	abc	0.18	6.08	93.74
Img_15_2_1	abc	13.05	3.90	83.05
Img_16_1_1	ab	12.85	5.74	81.40
Img_16_2_1	bc	13.45	2.37	84.19
Img_17_1_1	ab	9.84	3.68	86.48
Img_18_1_1	abc	4.46	5.00	90.54
Img_18_2_1	abc	24.19	3.70	72.11
Img_19_1_1	ab	0.11	2.53	97.36
Img_19_2_1	bc	12.81	4.47	82.72
Img_20_1_1	abc	9.27	2.48	88.25
Img_20_2_1	abc	18.94	0.18	80.87
overall perf.		9.78	3.94	86.38

Table 7.1: The first method performance overview on the UBIRIS database (a eyelid, b reflection, c eyelash). Percentages are to all image pixels. For image results for selected irises see Figure 7.1.

Rank	Method	No. par.	Error $E_1$	$E_2$
1	<b>2. &amp; 3. method</b> [HK14; HK15]	7	<b>0.0124</b>	0.042
2	Tan <i>et al.</i> [THS10]	9	0.0131	-
3	Sankowski <i>et al.</i> [San+10]	6	0.0162	0.060
4	<b>1. Method</b> [HK13]	2	<b>0.0168</b>	0.061
5	Almeida [Alm10]	5	0.0180	-
6	Tan & Kumar [TK12]	x	0.0190	-
7	Li <i>et al.</i> [Li+10]	4	0.0224	0.068
8	Jeong <i>et al.</i> [Jeo+10]	3	0.0282	0.144
9	Chen <i>et al.</i> [Che+10]	5	0.0297	0.165
10	Scotti & Labbati [LS10]	12	0.0301	0.116
11	Luengo-Oroz <i>et al.</i> [LOFA10]	7	0.0305	-

Table 7.2: The Noisy Iris Challenge Evaluation Contest [PA10] top eight results (from 97 participants) on the contest UBIRIS.v2 database compared with the presented methods and [TK12].

contest (described in Section 6.2). The method is more complicated than the first one but it also acquired the first place in comparison to other NICE.I methods (see Table 7.2).

Examples of method results can be seen in Figure 7.2. The first column is a source image, the second is a ground truth from the NICE.I contest. The third column is a method result and last is a difference between the ground truth and the result (second and third columns). The  $E_1$  displayed in the fourth column in Table 7.2 is computed exactly from that column.

### 7.3 Results for Method ‘Robust Occlusion Detection in Face Images’

The method is described in Section 4.3. It is mainly an upgrade from the previous method and it is expanded to correctly detect iris images from the MICHE database. It was published in the special issue *MICHE I* (as *Mobile Iris CHallenge Evaluation I*). And was used as the best segmentation algorithm for generating ground truth masks for the *MICHE II* (as *Mobile Iris CHallenge Evaluation II*).

The result on the NICE.I dataset are essentially the same as the previous method (see Table 7.2). But the results on the MICHE database are far better. Unfortunately because of lack of ground truth masks for this database we can not provide numeric performance. But the algorithm itself is publicly available for download<sup>1</sup> for contest participants to use and try themselves.

<sup>1</sup>Link for method download: [http://biplab.unisa.it/MICHE/MICHE-II/PRL\\_Haindl\\_Krupicka.zip](http://biplab.unisa.it/MICHE/MICHE-II/PRL_Haindl_Krupicka.zip)

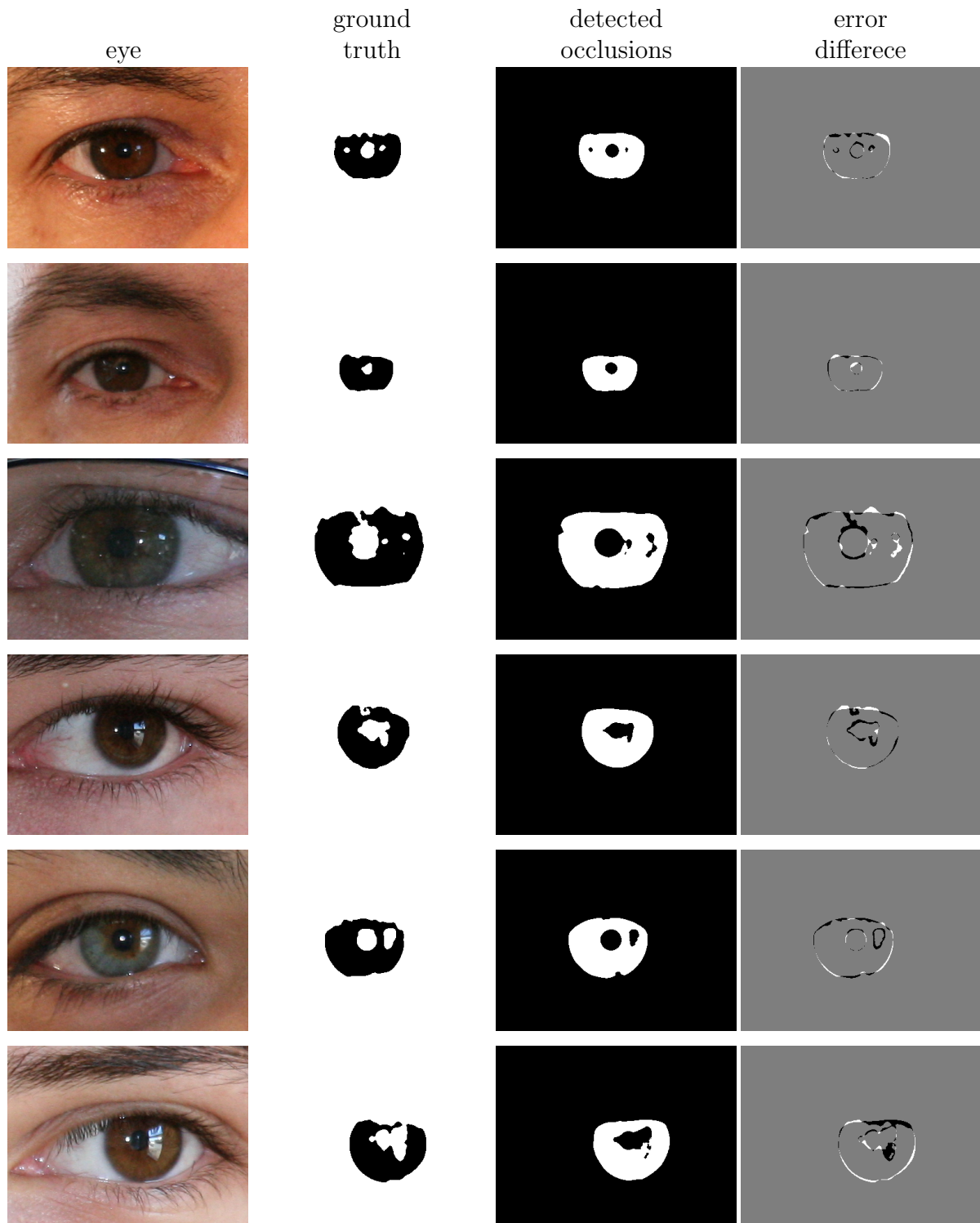


Figure 7.2: Eye images, ground truth, detected occlusions masks, and their comparison with the ground truth in the second method (UBIRIS.v2 database).

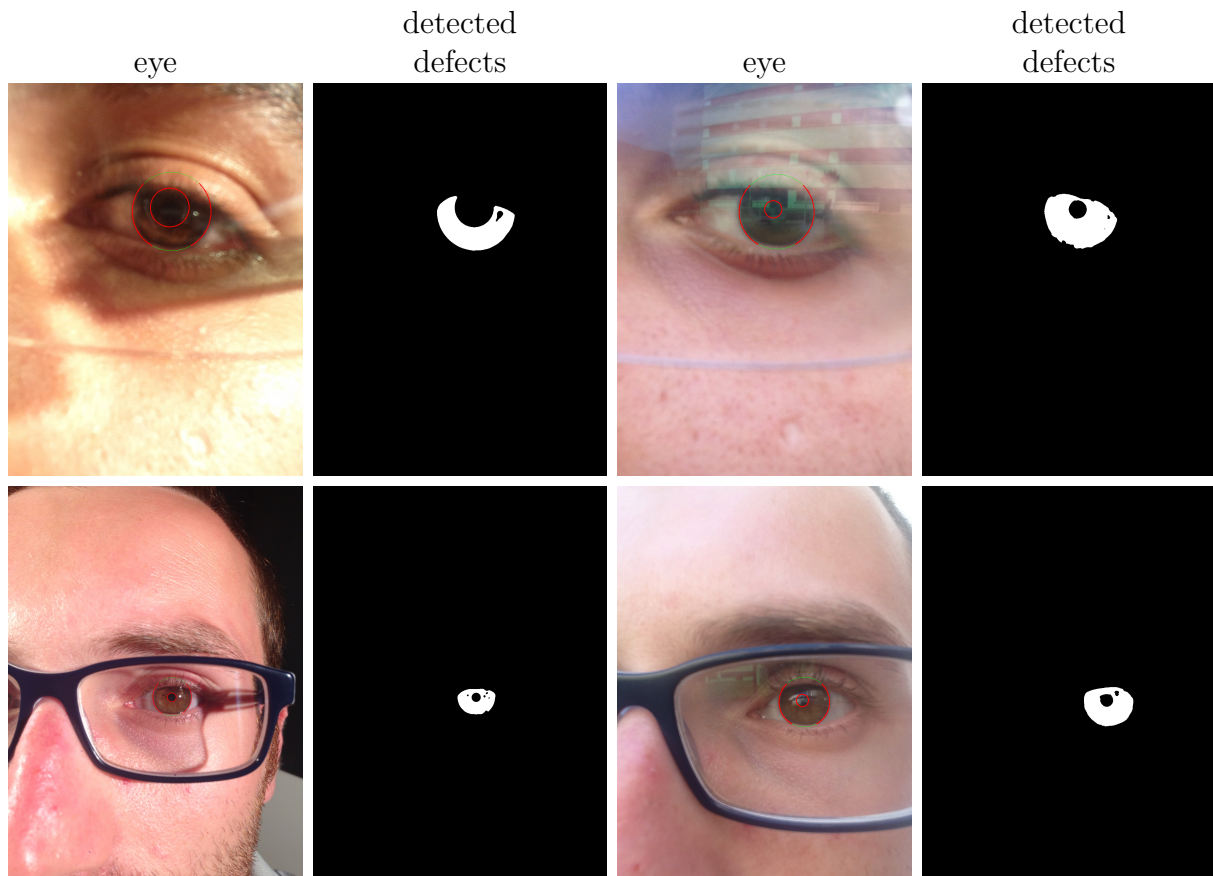


Figure 7.3: Selected eye images from the MICHE database and their detected defects (the third method, MICHE database).

## 7.4 Iris Recognition

This section contains current results which are among top results when comparing to the NICE.II contest 6.3.

### 7.4.1 Rule-out Methods

In Sections 5.2 and 5.3 we introduced two methods for a quick detection of inter-class iris comparisons. But to measure their performances we needed to evaluate their results. To compare them with other top performing methods from the NICE.II contest we interpreted their output as dissimilarity score as follow:

**Eye Position:** The resulting dissimilarity value of this method was set to 0 if irises were on same side and to 1 if they were not.

**Eye Color:** For the color histograms, we used directly the value from the histogram distance.

Rank	Author	Dissimilarity score
1	Tan <i>et al.</i> [Tan+12]	2.5748
2	Wang <i>et al.</i> [Wan+12]	1.8213
3	Santos & Hoyle [SH12]	1.7786
4	Shin <i>et al.</i> [Shi+12]	1.6398
5	Li <i>et al.</i> [LLZ12]	1.4758
6	Marsico <i>et al.</i> [MNR12]	1.2565
7	Li & Ma [LM12]	1.1892
8	<i>Methods 5.3 and 5.2 combined</i>	<i>1.1460</i>
9	Szewczyk <i>et al.</i> [Sze+12]	1.0931
10	<i>Color histogram (Section 5.3)</i>	<i>0.8736</i>
11	<i>Eye position (Section 5.2)</i>	<i>0.7285</i>

Table 7.3: Top eight results from the Noisy Iris Challenge Evaluation Contest [PA12] (NICE.II) compared with our individual step results.

**Eye Position and Color Combined:** When combined, as our intention was to only prove effectiveness of both features, we simply used experimentally derived normalization constant for histogram features and sum their value with the position dissimilarity value.

In the Table 7.3 can be seen results of our two methods for ruling out iris images from comparison (before any computation of advanced iris features). Both of them individually are a bit behind the contestants results. But when both methods combined, even without computing any subsequent features, they easily outperform the last contestant. It is thus viable way to improve the overall performance of iris recognition.

## 7.4.2 Iris Textural Features

Our actual results are currently not at the first place in comparison with other NICE.II contestants. We are thus still improving our method to outperform them.

Examples of irises convolved with Gabor kernels can be seen in 7.6. Similarly, the examples of LBP features computed from irises can be seen in 7.6. And visualization of 3DCAR parameters (4.1.4) can be seen in Figure 7.5. Visualization is done by PCA transformation with top three dimensions mapped to RGB channels.

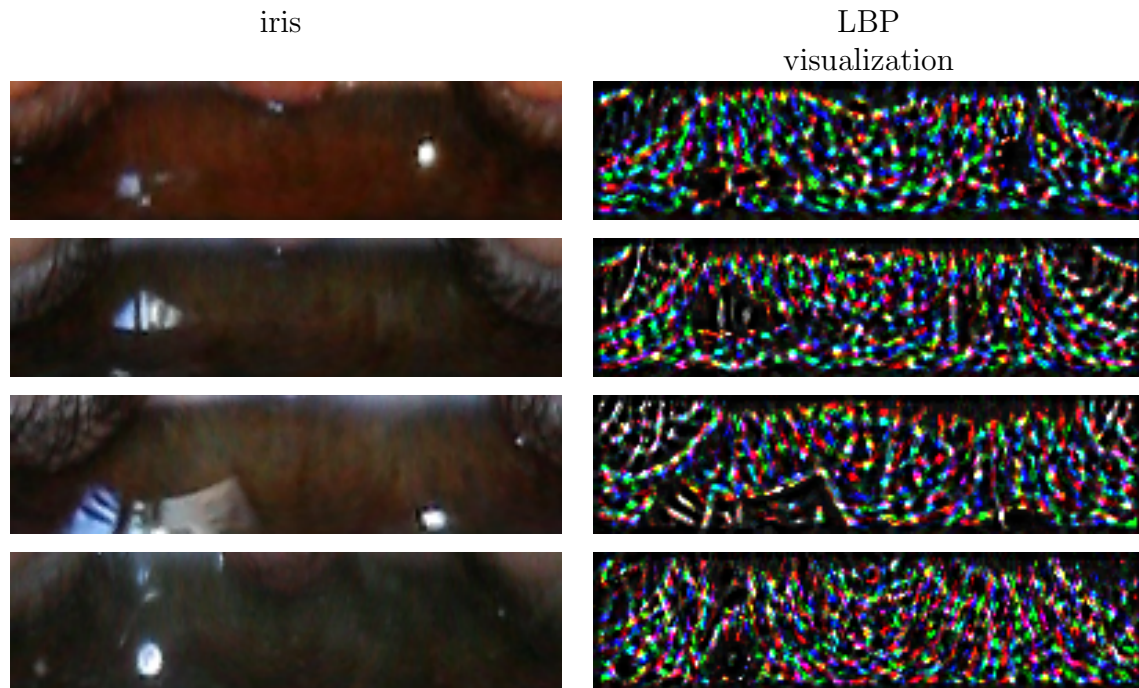


Figure 7.4: Examples of LBP feature extraction on iris images.

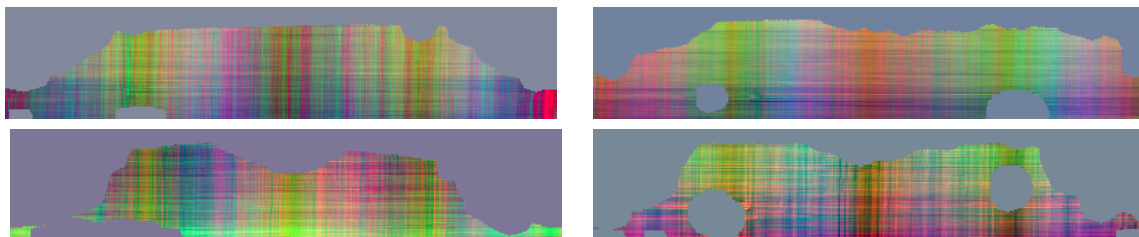


Figure 7.5: Examples of PCA visualized 3DCAR (4.1.4) parameters. Top three dimensions mapped to RGB channels.

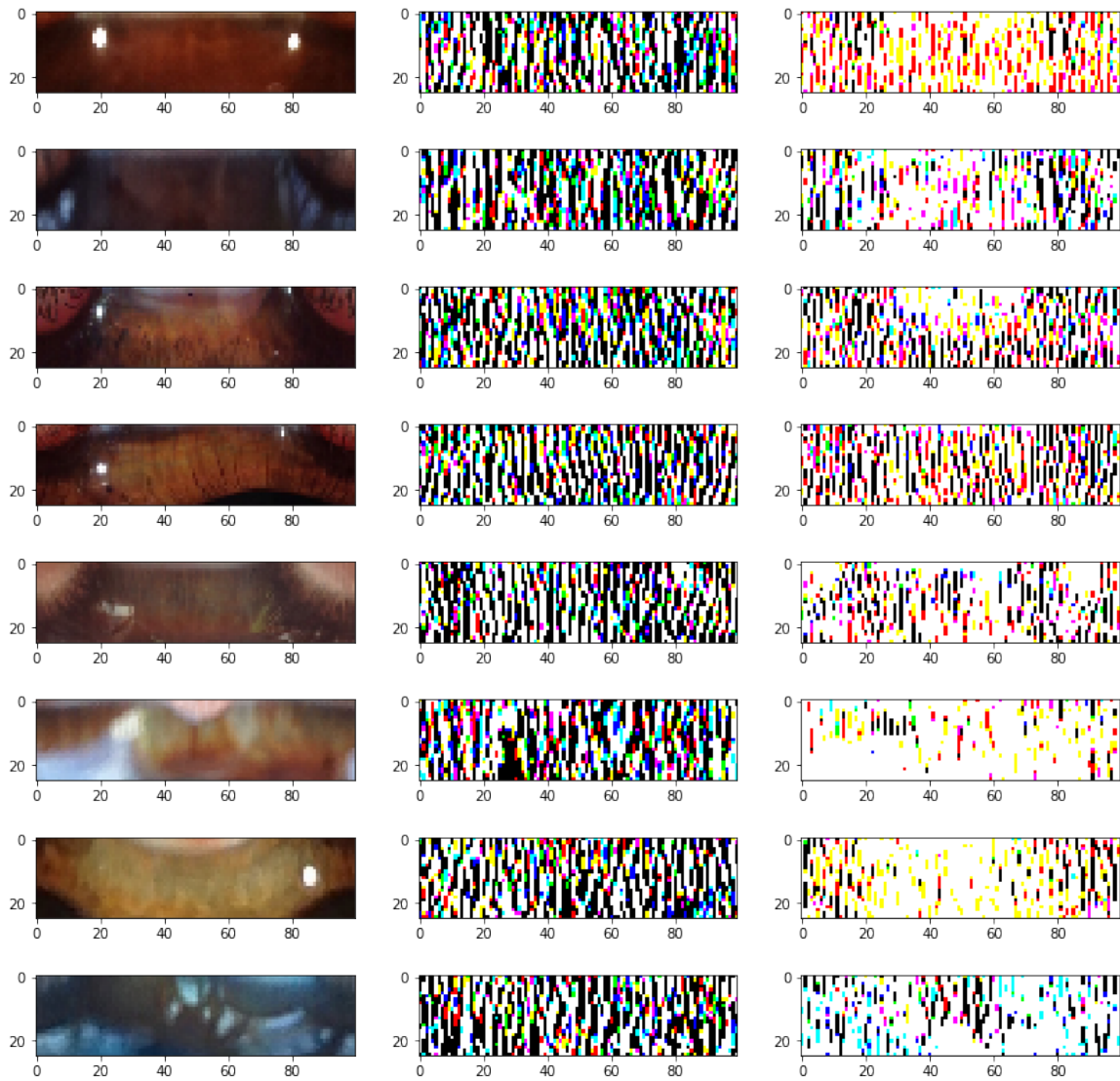


Figure 7.6: Examples of irises convolved with Gabor kernels. The first column is input iris, the second is real part of a kernel and the third is imaginary part of a kernel.





---

## Developed Software

*Apart from the presented methods themselves (Chapters 4 and 5) we were able to accomplish additional results which are presented in this chapter. Firstly is described a software that was implemented in the process of developing our methods. Next, the UBIRIS ground truth dataset will be showed.*

### 8.1 Created Software

In this section is a description of the software we've developed while working on our methods. The main contribution is in form of the Iris library that contains the implementation of all methods we presented in Chapters 4 and 5. Our source code for programs we implemented is about 19000 lines long.

As nobody can implement all by himself, number of open source programs were used. These are the main ones:

- OpenCV – <https://opencv.org/>
- Boost – <http://www.boost.org/>
- Qt Toolkit – <https://www.qt.io/>
- Jupyter Notebook – <https://jupyter.org/>

The OpenCV library is a general image processing library with already implemented many (performance optimized) methods. It is also valued for its image representation format *Mat* that greatly eases matrix manipulation.

The Boost library was used due to its cross-platform features (i.e. for file manipulation regardless of operating system).

The Qt Toolkit is known for its simplicity in creating user interfaces and ability to run same code on Windows or Linux OS.

The Jupyter Notebook greatly eases development, especially in conjunction with Python which allows for rapid development of new methods and further experimenting.

```
<?xml version="1.0" encoding="utf-8"?>
<iris-recognition>
  <logging-severity>info</logging-severity>
  <process>
    <draw-graph>>false</draw-graph>
    <save-log>>false</save-log>
    <iris-mask>>true</iris-mask>
    <without-defects>>false</without-defects>
    <debug>>false</debug>
    <output-dir>./tmp</output-dir>
    <auto-find>>false</auto-find>
    <save-additional-info>>true</save-additional-info>
  </process>
```

Figure 8.1: First few lines from configuration file.

### 8.1.1 Iris Library

The Iris library is implemented in the C++ programming language. It is a standard C++ library that could be compiled as a static or dynamic library and used in other projects. It was programmed to be cross-platform and we experimentally verified that it can run at least on Windows and Linux OS. We used it mainly in two projects that served as user interface (described in Section 8.1.3) and as an console interface suitable for automated processing (described in Section 8.1.2).

The important library we used was also VR library. It is an internal library of our department where various advanced mathematical methods are implemented. We used mainly aforementioned *multispectral causal autoregressive model*. But there are many other models that can be utilized in future development.

### 8.1.2 Console Application

The console application was used for batch processing and for testing the various parameters that we wanted to try. It usually runs on Linux server over several hours, processing whole databases, possibly several times trying out different versions of our method. It is a command line program that takes parameters file, parses it and calls methods from Iris library. The configuration file is in XML format and is loaded with the help of methods from the *Boost* library that correctly parses and process it's parameters. Example of this file can be seen in Figure 8.1.

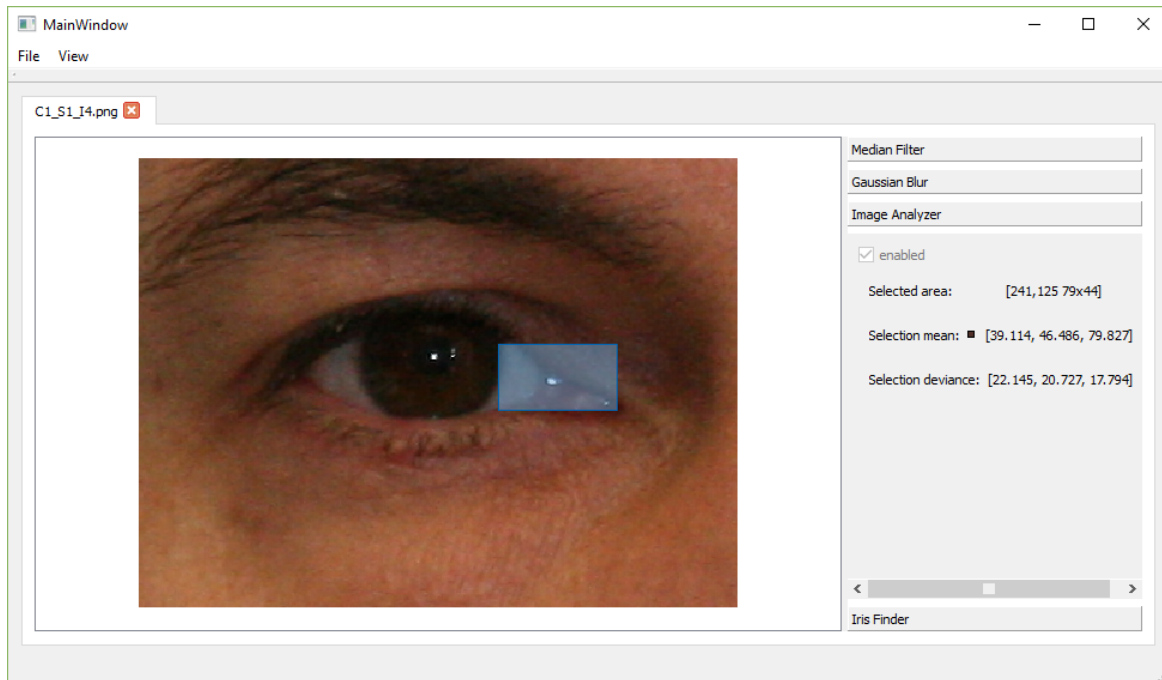


Figure 8.2: Screenshot from our ImageProcessing application.

### 8.1.3 Windows Application

Over the course of developing our methods. We also created a graphical application to help us experiment with iris images. See the screenshot in Figure 8.2. This application serves for experimenting with input images or intermediate results of each method (see Figure 8.3 for example).

It can be used for a quick view and manipulation of source image (or any other result of some method). We can run several image processing methods (gaussian blur, thresholding, canny detector, resize, ...) in any order to quickly see how image reacts and changes, what can be interesting paths to take the developed method further. Example of simple analysis of image area can be seen in Figure 8.2.

It uses our Iris library, graphical interface itself is build on open source version of the QT toolkit (can be downloaded at product website <https://www.qt.io/>). It's programmed in C++ and we successfully run it on Windows and Linux platforms. Source codes have about 2700 lines of code.

## 8.2 Ground Truth Masks for UBIRIS Database

When we began to implement our first method, it quickly became apparent that we need some form of ground truth data to evaluate its performance. We searched for datasets with iris occlusions masks that we could use. But only one we were able to find is the one

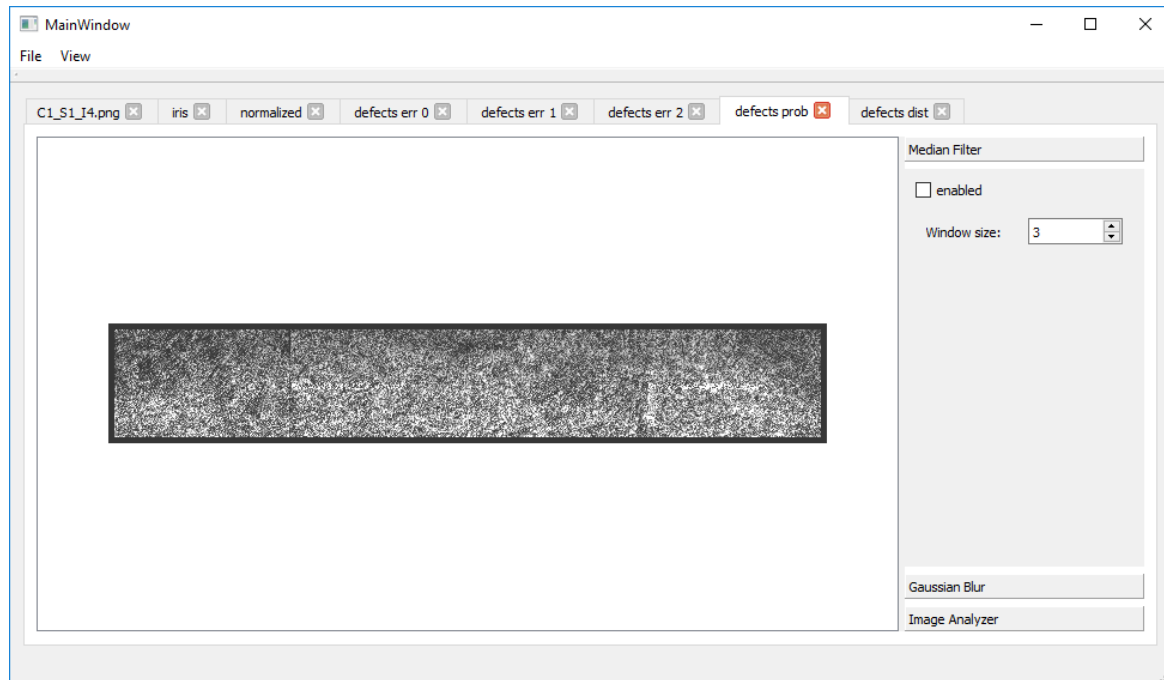
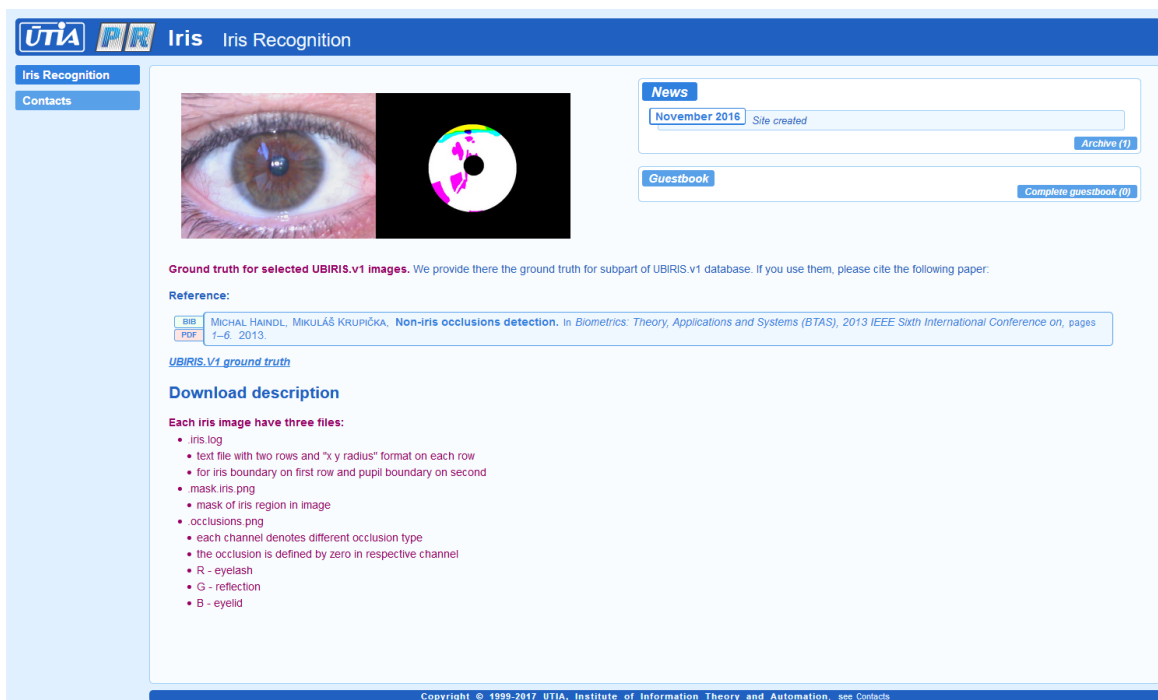


Figure 8.3: Example of results of occlusion detection task in application.

mentioned in Hugo Proença’s dissertation thesis [Pro06] and despite our effort we were not able to obtain this dataset. We thus needed to create our own.

It contains 36 iris occlusions masks. Each mask is an color image with three channels (RGB) and each of these channels denotes one type of occlusion. The occlusions are defined by zero in respective channel (R - eyelash, G - reflection, B - eyelid). Examples are shown in figure 8.5. Our database is unique in a way that our ground truth data are separated to different types of occlusion. There is no other database to our knowledge with similar data. It can be used to better understanding and evaluation of different algorithms how well they can grasp various types of occlusions.

The dataset is publicly available at <http://iris.utia.cas.cz/> (see Figure 8.4). However note that these are only the ground truth masks without original images as we do not have the rights to share those. It is therefore necessary to obtain those from their official website at <http://iris.di.ubi.pt/ubiris1.html>.



The screenshot shows a web page titled "Iris Recognition" with a logo for "UTIA PR". The page features a navigation menu with "Iris Recognition" and "Contacts". The main content area displays two images: a photograph of a human eye and a corresponding ground truth mask where the iris is highlighted in a rainbow color and the pupil is black. To the right, there are sections for "News" (dated November 2016) and "Guestbook". Below the images, the text reads: "Ground truth for selected UBIRIS.v1 images. We provide there the ground truth for subpart of UBIRIS.v1 database. If you use them, please cite the following paper." A reference is provided: "MICHAL HAINDL, MIKULÁŠ KRUPÍČKA, Non-iris occlusions detection. In *Biometrics: Theory, Applications and Systems (BTAS), 2013 IEEE Sixth International Conference on*, pages 1-6. 2013." A link for "UBIRIS.V1 ground truth" is also present. A "Download description" section lists the files provided for each iris image: iris.log (text file with two rows and "x y radius" format), mask.iris.png (mask of iris region), and occlusions.png (occlusion channels for eyelash, reflection, and eyelid).

**Ground truth for selected UBIRIS.v1 images.** We provide there the ground truth for subpart of UBIRIS.v1 database. If you use them, please cite the following paper:

**Reference:**

BTAS MICHAL HAINDL, MIKULÁŠ KRUPÍČKA, **Non-iris occlusions detection**. In *Biometrics: Theory, Applications and Systems (BTAS), 2013 IEEE Sixth International Conference on*, pages 1-6. 2013.

[UBIRIS.V1 ground truth](#)

**Download description**

**Each iris image have three files:**

- iris.log
  - text file with two rows and "x y radius" format on each row
  - for iris boundary on first row and pupil boundary on second
- mask.iris.png
  - mask of iris region in image
- occlusions.png
  - each channel denotes different occlusion type
  - the occlusion is defined by zero in respective channel
  - R - eyelash
  - G - reflection
  - B - eyelid

Copyright © 1999-2017 UTIA, Institute of Information Theory and Automation, see Contacts

Figure 8.4: Screen from <http://iris.utia.cas.cz/> web.

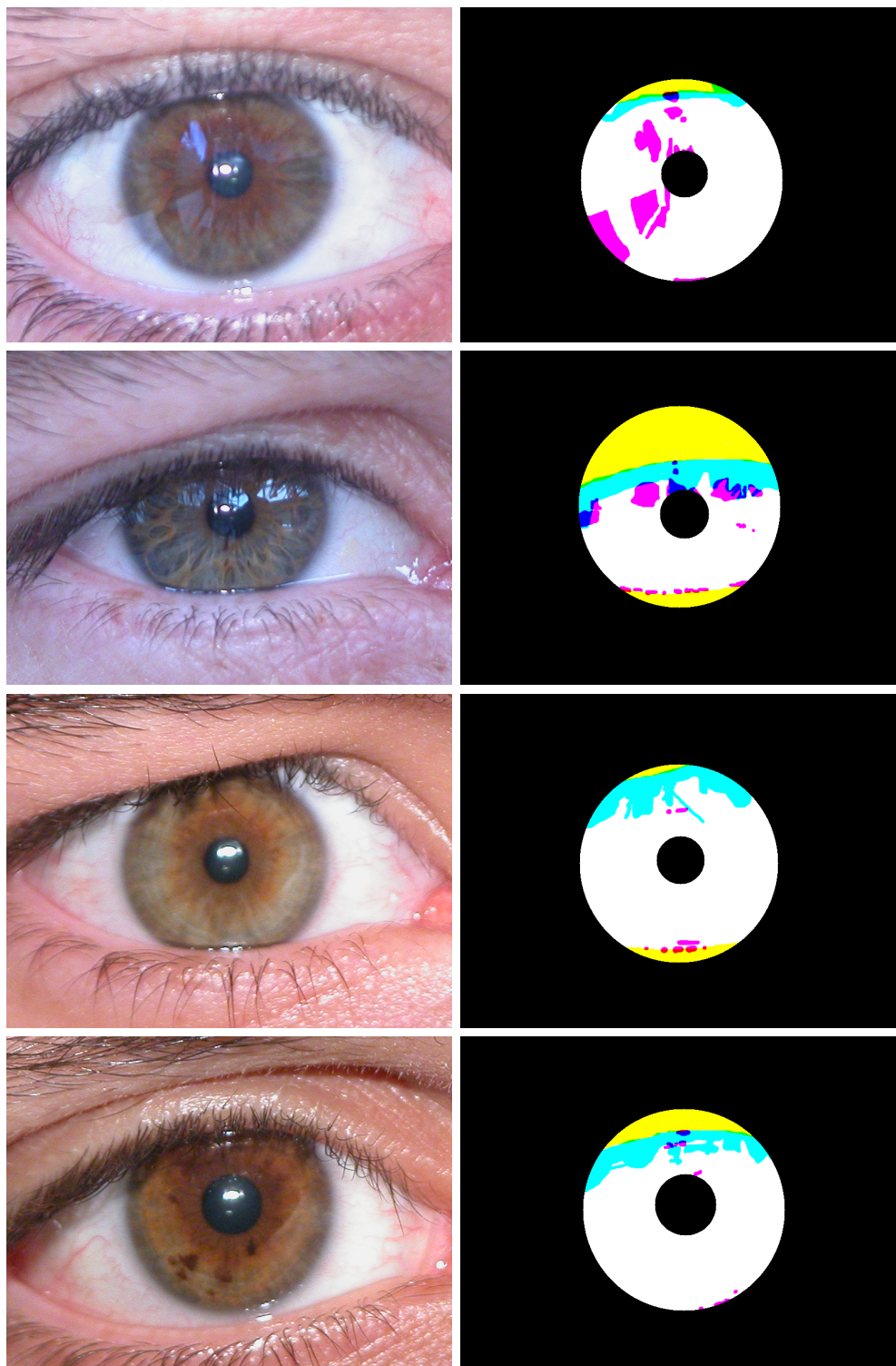


Figure 8.5: Publicly available ground truth masks of UBIRIS database (downloadable from <http://iris.utia.cas.cz/>).

---

# Conclusions

*This chapter summarizes our contributions and most important findings. It also discusses future work.*

## 9.1 Summary

**Introduction** In the first chapter, motivation for this thesis is described along with the introduction to biometric identification. Particularly biometric identification based on iris. Then each step of the iris recognition system is described with its own specifics and challenges. The chapter concludes with the description of the problem we've tried to solve. The goals which we've tried to achieve and the structure of the thesis are both communicated.

**State-of-the-Art** The second chapter introduces the reader to the necessary theoretical background. It thoroughly describes each step of the iris recognition pipeline and surveys the current State-of-the-Art of each step. Additionally it points to other surveys of the iris processing methods and also surveys the iris quality metric articles.

**Iris Databases** The third chapter surveys the available iris databases and gives an overview of each along with image samples for the several of them. It focuses specifically on the color iris image databases. The chapter concludes with discussion about choosing databases for our experiments. The important part is also the table with comparison of each database presented and their properties summarized.

**Iris Occlusions Detection** In the fourth chapter we presented our main contributions for iris occlusions detection in form of three methods. These methods were developed over the course of last years, and they are gradually rising in complexity but also have better results than the previous one. With the second method we achieved the first place in comparison with 97 other competing algorithms from the *NICE.I* contest from all over

the world. The third method was submitted to the *MICHE I* and subsequently used in the *MICHE II* as the ground truth generation method for other contestants. In the last method we presented the multispectral modification to the widely used integrodifferential operator.

**Iris Recognition** The fifth chapter describes our approach to the iris recognition. Firstly we described two ‘prerecognition’ methods that can quickly rule out dissimilar irises. Then our approach to iris texture features representation was described.

**Iris Biometrics Evaluation** In the sixth chapter, the reader is introduced to evaluation of biometric systems along with the description of different iris contests that we are using for comparison. As the NICE.I contest is the only widespread contest with iris occlusions ground truth masks it is used to evaluate all of our occlusion detection methods.

**Achieved Results of Proposed Methods** The seventh chapter is showing results which we were able to achieve with the proposed methods for detecting occlusions. It showcases tables comparison with other competitive methods, example image masks as well as method results. It also presents our achievements in public recognition of our methods.

**Developed Software** In the eight chapter the supplementary results which we were able to accomplish are detailed. Firstly is described software that was implemented in the process of developing our methods. And next, the UBIRIS ground truth dataset is showed with reasoning why it was created.

## 9.2 Contributions of the Dissertation Thesis

1. Overview of the recent state-of-the-art in the iris recognition area in all related fields.
2. Overview of the iris image databases with detailed description of their properties and the table with comparison of each database presented and their properties summarized.
3. Three novel methods for detecting iris occlusions. They range from most simple one (also the fastest) to more complex combined from several algorithms focused on specialized tasks. The first one uses our own publicly available ground truth database. The second method achieved the first place in comparison with 97 other competing methods from the worldwide *NICE.I* contest. And the third method was submitted to the *MICHE I* and was subsequently used as the ground truth generation method for contestants in the following contest (*MICHE II*). In the last method, we presented the multispectral modification of the widely used integrodifferential operator.



4. Novel approach to iris recognition. Consisting of preprocessing steps to rule out negative iris images followed with combination of feature representation and dissimilarity computing method for pairs of iris images.
5. The ground truth masks for iris occlusions made publicly available to measure performance between different methods. The mask for one iris image is in fact three masks for three different types of occlusions. It enables more in depth look to algorithms performance.

## 9.3 Future Work

Topics for future research:

- Automatic adaptation on different visual conditions and environmental surroundings.
- Descriptive general multispectral iris recognition method.
- Detection of fake irises.
- Computer aided eye diseases diagnosis.
- Eye disease progress monitoring.
- Iris detection in general visual scenes (security cameras, ...).
- Further improved iris recognition to become the leading method.



---

## Bibliography

- [Aba+17] A. F. Abate, S. Barra, L. Gallo and F. Narducci. ‘Kurtosis and skewness at pixel level as input for SOM networks to iris recognition on mobile devices’. In: *Pattern Recognition Letters* 91.Supplement C (2017). Mobile Iris CHallenge Evaluation (MICHE-II), pp. 37–43. ISSN: 0167-8655.
- [Adl60] F. H. Adler. ‘Physiology of the Eye. Clinical Application’. In: *Proceedings of the Royal Society of Medicine* 53.11 (1960), p. 980.
- [Agi+17a] N. Aginako, G. Echeagaray, J. Martínez-Otzeta, I. Rodríguez, E. Lazkano and B. Sierra. ‘Iris matching by means of Machine Learning paradigms: A new approach to dissimilarity computation’. In: *Pattern Recognition Letters* 91.Supplement C (2017). Mobile Iris CHallenge Evaluation (MICHE-II), pp. 60–64. ISSN: 0167-8655.
- [Agi+17b] N. Aginako, M. Castrillón-Santana, J. Lorenzo-Navarro, J. M. Martínez-Otzeta and B. Sierra. ‘Periocular and iris local descriptors for identity verification in mobile applications’. In: *Pattern Recognition Letters* 91.Supplement C (2017). Mobile Iris CHallenge Evaluation (MICHE-II), pp. 52–59. ISSN: 0167-8655.
- [AH03] J. M. H. Ali and A. E. Hassainen. ‘An iris recognition system to enhance e-security environment based on wavelet theory’. In: *AMO-Advanced Modeling and Optimization* 5.2 (2003), pp. 93–104.
- [Ahm+17] N. U. Ahmed, S. Cvetkovic, E. H. Siddiqi, A. Nikiforov and I. Nikiforov. ‘Combining iris and periocular biometric for matching visible spectrum eye images’. In: *Pattern Recognition Letters* 91.Supplement C (2017). Mobile Iris CHallenge Evaluation (MICHE-II), pp. 11–16. ISSN: 0167-8655.
- [Ahu+17] K. Ahuja, R. Islam, F. A. Barbhuiya and K. Dey. ‘Convolutional neural networks for ocular smartphone-based biometrics’. In: *Pattern Recognition Letters* 91.Supplement C (2017). Mobile Iris CHallenge Evaluation (MICHE-II), pp. 17–26. ISSN: 0167-8655.

- [Alm10] P. de Almeida. ‘A knowledge-based approach to the iris segmentation problem’. In: *Image and Vision Computing* 28.2 (2010), pp. 238–245. ISSN: 0262-8856.
- [AS06] A. Abhyankar and S. Schuckers. ‘Active shape models for effective iris segmentation’. In: *Proc. SPIE Conf. Biometric Technol. Human Identif. III*. 2006, 62020H.
- [Bal81] D. Ballard. ‘Generalizing the Hough transform to detect arbitrary shapes’. In: *Pattern Recognition* 13.2 (1981), pp. 111–122. ISSN: 0031-3203.
- [Bar+15] S. Barra, A. Casanova, F. Narducci and S. Ricciardi. ‘Ubiquitous iris recognition by means of mobile devices’. In: *Pattern Recognition Letters* 57. Supplement C (2015). Mobile Iris CHallenge Evaluation part I (MICHE I), pp. 66–73. ISSN: 0167-8655.
- [BB98] W. W. Boles and B. Boashash. ‘A human identification technique using images of the iris and wavelet transform’. In: *Signal Processing, IEEE Transactions on* 46.4 (Apr. 1998), pp. 1185–1188. ISSN: 1053-587X.
- [BD08] C. Belcher and Y. Du. ‘A selective feature information approach for iris image-quality measure’. In: *IEEE Transactions on Information Forensics and Security* 3.3 (2008), pp. 572–577.
- [Ber86] A. Bertillon. *La couleur de l’iris*. Masson, 1886.
- [BHF08] K. W. Bowyer, K. Hollingsworth and P. J. Flynn. ‘Image understanding for iris biometrics: A survey’. In: *Computer vision and image understanding* 110.2 (2008), pp. 281–307.
- [BHF13] K. W. Bowyer, K. P. Hollingsworth and P. J. Flynn. ‘A survey of iris biometrics research: 2008–2010’. In: *Handbook of iris recognition*. Springer, 2013, pp. 23–61.
- [BI98] A. Blake and M. Isard. *Active contours*. London: Springer London, 1998, p. 309. ISBN: 978-1-4471-1557-1.
- [BT05] A. K. Bachoo and J.-R. Tapamo. ‘Texture detection for segmentation of iris images’. In: *Proceedings of the 2005 annual research conference of the South African institute of computer scientists and information technologists on IT research in developing countries*. South African Institute for Computer Scientists and Information Technologists. 2005, pp. 236–243.
- [Can86] J. Canny. ‘A Computational Approach to Edge Detection’. In: *Pattern Analysis and Machine Intelligence, IEEE Transactions on PAMI*-8.6 (1986), pp. 679–698. ISSN: 0162-8828.
- [CDJ05] Y. Chen, S. C. Dass and A. K. Jain. ‘Localized iris image quality using 2-D wavelets’. In: *Advances in Biometrics* (2005), pp. 1–6.

- 
- [CFC10] C. F. Costa Filho and M. G. Costa. ‘Iris segmentation exploring color spaces’. In: *Image and Signal Processing (CISP), 2010 3rd International Congress on*. Vol. 4. IEEE. 2010, pp. 1878–1882.
- [Che+10] Y. Chen, M. Adjouadi, C. Han, J. Wang, A. Barreto, N. Rishe and J. Andrian. ‘A highly accurate and computationally efficient approach for unconstrained iris segmentation’. In: *Image and Vision Computing* 28.2 (2010), pp. 261–269. ISSN: 0262-8856.
- [CHH09] W.-S. Chen, R.-H. Huang and L. Hsieh. ‘Iris recognition using 3D co-occurrence matrix’. In: *International Conference on Biometrics*. Springer. 2009, pp. 1122–1131.
- [Cui+04] J. Cui, Y. Wang, T. Tan and L. Ma. ‘A fast and robust iris localization method based on texture segmentation’. In: *SPIE Defense and Security* (2004).
- [CW02] T. A. Camus and R. Wildes. ‘Reliable and fast eye finding in close-up images’. In: *Pattern Recognition, 2002. Proceedings. 16th International Conference on*. Vol. 1. IEEE. 2002, pp. 389–394.
- [Dau01] J. Daugman. ‘Iris Recognition The colored part of the eye contains delicate patterns that vary randomly from person to person, offering a powerful means of identification’. In: *American scientist* 89.4 (2001), pp. 326–333.
- [Dau04] J. Daugman. ‘How iris recognition works’. In: *IEEE Transactions on Circuits and Systems for Video Technology* 14.1 (Jan. 2004), pp. 21–30. ISSN: 1051-8215.
- [Dau06] J. Daugman. ‘Probing the uniqueness and randomness of IrisCodes: Results from 200 billion iris pair comparisons’. In: *Proceedings of the IEEE* 94.11 (2006), pp. 1927–1935.
- [Dau07] J. Daugman. ‘New Methods in Iris Recognition’. In: *Systems, Man, and Cybernetics, Part B: Cybernetics, IEEE Transactions on* 37.5 (Oct. 2007), pp. 1167–1175. ISSN: 1083-4419.
- [Dau85] J. G. Daugman. ‘Uncertainty relation for resolution in space, spatial frequency, and orientation optimized by two-dimensional visual cortical filters’. In: *JOSA A* 2.7 (1985), pp. 1160–1169.
- [Dau93] J. Daugman. ‘High confidence visual recognition of persons by a test of statistical independence’. In: *Pattern Analysis and Machine Intelligence, IEEE Transactions on* 15.11 (1993), pp. 1148–1161. ISSN: 0162-8828.
- [DD01] J. Daugman and C. Downing. ‘Epigenetic randomness, complexity and singularity of human iris patterns’. In: *Proceedings of the Royal Society of London B: Biological Sciences* 268.1477 (2001), pp. 1737–1740.
- [DIE04] Y. Du, R. Ives and D. Etter. ‘A new approach to iris pattern recognition’. In: *Proceedings of SPIE* (2004), pp. 1–12.

- [DM] M. Dobes and L. Machala. *UPOL iris database*. <http://www.inf.upol.cz/iris/>. [Online; accessed 15-May-2012].
- [DSF05] V. Dorairaj, N. A. Schmid and G. Fahmy. ‘Performance evaluation of iris-based recognition system implementing pca and ica encoding techniques’. In: *Proc. SPIE*. Vol. 5779. 2005, pp. 51–58.
- [Du06] Y. Du. ‘Using 2D log-Gabor spatial filters for iris recognition’. In: *SPIE*. Vol. 6202. 2006, p. 62020.
- [Edi+15] G. Editors, M. D. Marsico, M. Nappi and H. Proença. ‘Guest editorial introduction to the special executable issue on ”Mobile Iris CHallenge Evaluation part I (MICHE I)”’. In: *Pattern Recognition Letters* 57.Supplement C (2015). Mobile Iris CHallenge Evaluation part I (MICHE I), pp. 1–3. ISSN: 0167-8655.
- [FB11] S. P. Fenker and K. W. Bowyer. ‘Experimental evidence of a template aging effect in iris biometrics’. In: *Applications of Computer Vision (WACV), 2011 IEEE Workshop on*. IEEE. 2011, pp. 232–239.
- [Fie+10] J. Fierrez, J. Galbally, J. Ortega-Garcia, M. R. Freire, F. Alonso-Fernandez, D. Ramos, D. T. Toledano, J. Gonzalez-Rodriguez, J. A. Siguenza, J. Garrido-Salas et al. ‘BiosecuRID: a multimodal biometric database’. In: *Pattern Analysis & Applications* 13.2 (2010), pp. 235–246.
- [FS89] I. Fogel and D. Sagi. ‘Gabor filters as texture discriminator’. In: *Biological cybernetics* 61.2 (1989), pp. 103–113.
- [GD17] C. Galdi and J.-L. Dugelay. ‘FIRE: Fast Iris REcognition on mobile phones by combining colour and texture features’. In: *Pattern Recognition Letters* 91.Supplement C (2017). Mobile Iris CHallenge Evaluation (MICHE-II), pp. 44–51. ISSN: 0167-8655.
- [GN11] K. Grabowski and A. Napieralski. ‘Hardware architecture optimized for iris recognition’. In: *IEEE Transactions on Circuits and Systems for Video Technology* 21.9 (2011), pp. 1293–1303.
- [Hai12] M. Haindl. ‘Visual Data Recognition and Modeling Based on Local Markovian Models’. In: *Mathematical Methods for Signal and Image Analysis and Representation*. Ed. by L. Florack, R. Duits, G. Jongbloed, M.-C. Lieshout and L. Davies. Vol. 41. Computational Imaging and Vision. Springer London, 2012. Chap. 14, pp. 241–259. ISBN: 978-1-4471-2353-8.
- [He+09] Z. He, T. Tan, Z. Sun and X. Qiu. ‘Toward Accurate and Fast Iris Segmentation for Iris Biometrics’. In: *Pattern Analysis and Machine Intelligence, IEEE Transactions on* 31.9 (Sept. 2009), pp. 1670–1684. ISSN: 0162-8828.
- [HK13] M. Haindl and M. Krupička. ‘Non-iris occlusions detection’. In: *Biometrics: Theory, Applications and Systems (BTAS), 2013 IEEE Sixth International Conference on*. IEEE. 2013, pp. 1–6.

- [HK14] M. Haindl and M. Krupička. ‘Accurate Detection of Non-Iris Occlusions’. In: *Signal-Image Technology and Internet-Based Systems (SITIS), 2014 Tenth International Conference on*. IEEE. 2014, pp. 49–56.
- [HK15] M. Haindl and M. Krupička. ‘Unsupervised detection of non-iris occlusions’. In: *Pattern Recognition Letters* 57 (2015), pp. 60–65.
- [HLC02] Y.-P. Huang, S.-W. Luo and E.-Y. Chen. ‘An efficient iris recognition system’. In: *Machine Learning and Cybernetics, 2002. Proceedings. 2002 International Conference on*. Vol. 1. November. 2002, 450–454 vol.1. ISBN: 0780375084.
- [Hou59] P. V. Hough. ‘Machine analysis of bubble chamber pictures’. In: *Conf. Proc.* Vol. 590914. 1959, pp. 554–558.
- [HSD73] R. M. Haralick, K. Shanmugam and I. H. Dinstein. ‘Textural features for image classification’. In: *Systems, Man and Cybernetics, IEEE Transactions on* 3.6 (1973), pp. 610–621.
- [HSH15] Y. Hu, K. Sirlantzis and G. Howells. ‘Improving colour iris segmentation using a model selection technique’. In: *Pattern Recognition Letters* 57. Supplement C (2015). Mobile Iris CHallenge Evaluation part I (MICHE I), pp. 24–32. ISSN: 0167-8655.
- [Hua+04] J. Huang, Y. Wang, T. Tan and J. Cui. ‘A new iris segmentation method for recognition’. In: *Pattern Recognition, 2004. ICPR 2004. Proceedings of the 17th International Conference on*. Vol. 3. 0. IEEE, 2004, pp. 554–557. ISBN: 0769521282.
- [HŠ92] M. Haindl and S. Šimberová. ‘A multispectral image line reconstruction method’. In: *Theory & Applications of Image Analysis* (1992), pp. 306–315.
- [IGE04] R. W. Ives, A. J. Guidry and D. M. Etter. ‘Iris recognition using histogram analysis’. In: *Signals, Systems and Computers, 2004. Conference Record of the Thirty-Eighth Asilomar Conference on*. Vol. 1. IEEE. 2004, pp. 562–566.
- [Jeo+10] D. S. Jeong, J. W. Hwang, B. J. Kang, K. R. Park, C. S. Won, D.-K. Park and J. Kim. ‘A new iris segmentation method for non-ideal iris images’. In: *Image and Vision Computing* 28.2 (2010), pp. 254–260. ISSN: 0262-8856.
- [JM03] Joaquim de Mira Jr. and J. Mayer. ‘Image feature extraction for application of biometric identification of iris—a morphological approach’. In: *Computer Graphics and Image Processing, 2003. SIBGRAPI 2003. XVI Brazilian Symposium on*. IEEE. 2003, pp. 391–398.
- [JRN11] A. Jain, A. Ross and K. Nandakumar. ‘Introduction to biometrics: A textbook’. In: *Springer Publishers* (2011).

- [Kal+10] N. D. Kalka, J. Zuo, N. A. Schmid and B. Cukic. ‘Estimating and fusing quality factors for iris biometric images’. In: *IEEE Transactions on Systems, Man, and Cybernetics-Part A: Systems and Humans* 40.3 (2010), pp. 509–524.
- [KBC09] N. Kalka, N. Bartlow and B. Cukic. ‘An automated method for predicting iris segmentation failures’. In: *Biometrics: Theory, Applications, and Systems, 2009. BTAS’09. IEEE 3rd International Conference on*. IEEE. 2009, pp. 1–8.
- [KGC10] J. Koh, V. Govindaraju and V. Chaudhary. ‘A robust iris localization method using an active contour model and hough transform’. In: *Pattern Recognition (ICPR), 2010 20th International Conference on*. IEEE. 2010, pp. 2852–2856.
- [KGS07] E. Krichen, S. Garcia-Salicetti and B. Dorizzi. ‘A new probabilistic iris quality measure for comprehensive noise detection’. In: *Biometrics: Theory, Applications, and Systems, 2007. BTAS 2007. First IEEE International Conference on*. IEEE. 2007, pp. 1–6.
- [KIG06] L. R. Kennell, R. W. Ives and R. M. Gaunt. ‘Binary morphology and local statistics applied to iris segmentation for recognition’. In: *Image Processing, 2006 IEEE International Conference on*. IEEE. 2006, pp. 293–296.
- [Kim+04] J. Kim, S. Cho, J. Choi and R. J. Marks II. ‘Iris recognition using wavelet features’. In: *The Journal of VLSI Signal Processing* 38.2 (2004), pp. 147–156.
- [KZ03] W.-K. Kong and D. Zhang. ‘Detecting eyelash and reflection for accurate iris segmentation’. In: *International Journal of Pattern Recognition and Artificial Intelligence* 17.6 (2003), pp. 1025–1034.
- [LCF02] L. W. Liam, A. Chekima and L. C. Fan. ‘Iris recognition using self-organizing neural network’. In: *2002. SCORed 2002. Student Conference on Research and Development (2002)*, pp. 169–172.
- [Li+10] P. Li, X. Liu, L. Xiao and Q. Song. ‘Robust and accurate iris segmentation in very noisy iris images’. In: *Image and Vision Computing* 28.2 (2010), pp. 246 –253. ISSN: 0262-8856.
- [Lim+01] S. Lim, K. Lee, O. Byeon and T. Kim. ‘Efficient iris recognition through improvement of feature vector and classifier’. In: *ETRI journal* 23.2 (2001), pp. 61–70.
- [LLZ12] P. Li, X. Liu and N. Zhao. ‘Weighted co-occurrence phase histogram for iris recognition’. In: *Pattern Recognition Letters* 33.8 (2012). Noisy Iris Challenge Evaluation II - Recognition of Visible Wavelength Iris Images Captured At-a-distance and On-the-move, pp. 1000 –1005. ISSN: 0167-8655.



- [LM12] P. Li and H. Ma. ‘Iris recognition in non-ideal imaging conditions’. In: *Pattern Recognition Letters* 33.8 (2012). Noisy Iris Challenge Evaluation II - Recognition of Visible Wavelength Iris Images Captured At-a-distance and On-the-move, pp. 1012–1018. ISSN: 0167-8655.
- [LOFA10] M. A. Luengo-Oroz, E. Faure and J. Angulo. ‘Robust iris segmentation on uncalibrated noisy images using mathematical morphology’. In: *Image and Vision Computing* 28.2 (2010), pp. 278–284. ISSN: 0262-8856.
- [LS10] R. D. Labati and F. Scotti. ‘Noisy iris segmentation with boundary regularization and reflections removal’. In: *Image and Vision Computing* 28.2 (2010), pp. 270–277. ISSN: 0262-8856.
- [Ma+03] L. Ma, T. Tan, Y. Wang and D. Zhang. ‘Personal identification based on iris texture analysis’. In: *Pattern Analysis and Machine Intelligence, IEEE Transactions on* 25.12 (2003), pp. 1519–1533. ISSN: 0162-8828.
- [Ma+04] L. Ma, T. Tan, Y. Wang and D. Zhang. ‘Efficient iris recognition by characterizing key local variations’. In: *IEEE Transactions on image processing* 13.6 (2004), pp. 739–750.
- [Mar+15] M. D. Marsico, M. Nappi, D. Riccio and H. Wechsler. ‘Mobile Iris Challenge Evaluation (MICHE)-I, biometric iris dataset and protocols’. In: *Pattern Recognition Letters* 57 (2015). Mobile Iris CHallenge Evaluation part I (MICHE I), pp. 17–23. ISSN: 0167-8655.
- [Mar80] S Marčelja. ‘Mathematical description of the responses of simple cortical cells’. In: *JOSA* 70.11 (1980), pp. 1297–1300.
- [MKP01] A. Muroň, P. Koiš and J. Pospíšil. ‘Identification of persons by means of the Fourier spectra of the optical transmission binary models of the human irises’. In: *Optics Communications* 192.3–6 (2001), pp. 161–167. ISSN: 0030-4018.
- [MNR12] M. D. Marsico, M. Nappi and D. Riccio. ‘Noisy Iris Recognition Integrated Scheme’. In: *Pattern Recognition Letters* 33.8 (2012). Noisy Iris Challenge Evaluation II - Recognition of Visible Wavelength Iris Images Captured At-a-distance and On-the-move, pp. 1006–1011. ISSN: 0167-8655.
- [MRSASR01] D. Martin-Roche, C. Sanchez-Avila and R. Sanchez-Reillo. ‘Iris recognition for biometric identification using dyadic wavelet transform zero-crossing’. In: *Security Technology, 2001 IEEE 35th International Carnahan Conference on* (2001), pp. 272–277.
- [MRZ07] D. M. Monro, S. Rakshit and D. Zhang. ‘DCT-based iris recognition’. In: *IEEE Transactions on Pattern Analysis and Machine Intelligence* 29.4 (2007), pp. 586–595.
- [MW02a] L. Ma and Y. Wang. ‘Iris recognition based on multichannel Gabor filtering’. In: *Proc. Fifth Asian Conf. Computer* 59825105 (2002), pp. 1–5.

- [MW02b] A. J. Mansfield and J. L. Wayman. ‘Best practices in testing and reporting performance of biometric devices’. In: (2002).
- [MWT02] L. Ma, Y. Wang and T. Tan. ‘Iris recognition using circular symmetric filters’. In: *Pattern Recognition, 2002. Proceedings. 16th International Conference on*. Vol. 2. IEEE. 2002, pp. 414–417.
- [NFS10] K. Nguyen, C. Fookes and S. Sridharan. ‘Fusing shrinking and expanding active contour models for robust iris segmentation’. In: *Information Sciences Signal Processing and their Applications (ISSPA), 2010 10th International Conference on*. IEEE. 2010, pp. 185–188.
- [NN04] K. Nishino and S. K. Nayar. ‘Eyes for relighting’. In: *ACM Transactions on Graphics (TOG)*. Vol. 23. 3. ACM. 2004, pp. 704–711.
- [OPH94] T. Ojala, M. Pietikainen and D. Harwood. ‘Performance evaluation of texture measures with classification based on Kullback discrimination of distributions’. In: *Pattern Recognition, 1994. Vol. 1-Conference A: Computer Vision & Image Processing., Proceedings of the 12th IAPR International Conference on*. Vol. 1. IEEE. 1994, pp. 582–585.
- [PA05] H. Proença and L. A. Alexandre. ‘UBIRIS: A noisy iris image database’. In: *13th International Conference on Image Analysis and Processing - ICIAP 2005*. Vol. LNCS 3617. Cagliari, Italy: Springer, 2005, pp. 970–977. ISBN: 3540288694.
- [PA06] H. Proença and L. A. Alexandre. ‘A Method for the Identification of Noisy Regions in Normalized Iris Images’. In: *18th International Conference on Pattern Recognition (ICPR’06)* 4 (2006), pp. 405–408.
- [PA07] H. Proença and L. Alexandre. ‘The NICE.I: Noisy Iris Challenge Evaluation - Part I’. In: *Biometrics: Theory, Applications, and Systems, 2007. BTAS 2007. First IEEE International Conference on*. Sept. 2007, pp. 1–4.
- [PA10] H. Proença and L. A. Alexandre. ‘Introduction to the Special Issue on the Segmentation of Visible Wavelength Iris Images Captured At-a-distance and On-the-move’. In: *Image and Vision Computing* 28.2 (2010). Segmentation of Visible Wavelength Iris Images Captured At-a-distance and On-the-move, pp. 213–214. ISSN: 0262-8856.
- [PA12] H. Proença and L. A. Alexandre. ‘Introduction to the Special Issue on the Recognition of Visible Wavelength Iris Images Captured At-a-distance and On-the-move’. In: *Pattern Recognition Letters* 33.8 (2012). Noisy Iris Challenge Evaluation II - Recognition of Visible Wavelength Iris Images Captured At-a-distance and On-the-move, pp. 963–964. ISSN: 0167-8655.

- [Phi+10] P. J. Phillips, W. T. Scruggs, A. J. O’Toole, P. J. Flynn, K. W. Bowyer, C. L. Schott and M. Sharpe. ‘FRVT 2006 and ICE 2006 Large-Scale Experimental Results’. In: *IEEE Transactions on Pattern Analysis and Machine Intelligence* 32 (2010), pp. 831–846. ISSN: 0162-8828.
- [POX00] M. Pietikäinen, T. Ojala and Z. Xu. ‘Rotation-invariant texture classification using feature distributions’. In: *Pattern Recognition* 33.1 (2000), pp. 43–52.
- [Pro+10] H. Proença, S. Filipe, R. Santos, J. Oliveira and L. Alexandre. ‘The UBIRIS.v2: A Database of Visible Wavelength Images Captured On-The-Move and At-A-Distance’. In: *IEEE Trans. PAMI* 32.8 (Aug. 2010), pp. 1529–1535.
- [Pro06] H. Proença. ‘Towards non-cooperative biometric iris recognition’. In: *University of Beira Interior, Department of Computer* October (2006).
- [Pro11] H. Proença. ‘Quality assessment of degraded iris images acquired in the visible wavelength’. In: *Information Forensics and Security, IEEE Transactions on* 6.1 (2011), pp. 82–95.
- [Raj+15] K. B. Raja, R. Raghavendra, V. K. Vemuri and C. Busch. ‘Smartphone based visible iris recognition using deep sparse filtering’. In: *Pattern Recognition Letters* 57.Supplement C (2015). Mobile Iris CHallenge Evaluation part I (MICHE I), pp. 33–42. ISSN: 0167-8655.
- [Raj+17] K. B. Raja, R. Raghavendra, S. Venkatesh and C. Busch. ‘Multi-patch deep sparse histograms for iris recognition in visible spectrum using collaborative subspace for robust verification’. In: *Pattern Recognition Letters* 91.Supplement C (2017). Mobile Iris CHallenge Evaluation (MICHE-II), pp. 27–36. ISSN: 0167-8655.
- [Rat+16] A. Rattani, R. Derakhshani, S. K. Saripalle and V. Gottemukkula. ‘ICIP 2016 Competition on Mobile Ocular Biometric Recognition’. In: *IEEE International Conference on Image Processing (ICIP) 2016, Challenge Session on Mobile Ocular Biometric Recognition*. 2016.
- [RC03] N Ritter and J. Cooper. ‘Locating the iris: A first step to registration and identification’. In: *Proceedings of the 9th IASTED International Conference on Signal and Image processing*. ACTA Press/IASTED. 2003, pp. 507–512.
- [Rei+13] D. Reid, S. Samangoei, C. Chen, M. Nixon and A. Ross. ‘Soft biometrics for surveillance: an overview’. In: *Machine learning: theory and applications*. Elsevier (2013), pp. 327–352.
- [RUW13] C. Rathgeb, A. Uhl and P. Wild. *Iris biometrics: from segmentation to template security*. Vol. 59. Springer Science & Business Media, 2013.
- [San+06] W. Sankowski, K. Grabowski, M. Zubert and M. Napieralska. ‘Iris Finder–Program For Reliable Iris Localization In Images Taken Under Visible Light’. In: *Journal of Medical Informatics & Technologies Selected full texts* 10 (2006), pp. 125–132.

- [San+10] W. Sankowski, K. Grabowski, M. Napieralska, M. Zubert and A. Napieralski. ‘Reliable algorithm for iris segmentation in eye image’. In: *Image and Vision Computing* 28.2 (2010), pp. 231–237. ISSN: 0262-8856.
- [San+15] G. Santos, E. Grancho, M. V. Bernardo and P. T. Fiadeiro. ‘Fusing iris and periocular information for cross-sensor recognition’. In: *Pattern Recognition Letters* 57.Supplement C (2015). Mobile Iris CHallenge Evaluation part I (MICHE I), pp. 52–59. ISSN: 0167-8655.
- [SASRMR02] C. Sanchez-Avila, R. Sanchez-Reillo and D. de Martin-Roche. ‘Iris-based biometric recognition using dyadic wavelet transform’. In: *Aerospace and Electronic Systems Magazine, IEEE* 17.10 (2002), pp. 3–6.
- [SH12] G. Santos and E. Hoyle. ‘A fusion approach to unconstrained iris recognition’. In: *Pattern Recognition Letters* 33.8 (2012). Noisy Iris Challenge Evaluation II - Recognition of Visible Wavelength Iris Images Captured At-a-distance and On-the-move, pp. 984–990. ISSN: 0167-8655.
- [Shi+12] K. Y. Shin, G. P. Nam, D. S. Jeong, D. H. Cho, B. J. Kang, K. R. Park and J. Kim. ‘New iris recognition method for noisy iris images’. In: *Pattern Recognition Letters* 33.8 (2012). Noisy Iris Challenge Evaluation II - Recognition of Visible Wavelength Iris Images Captured At-a-distance and On-the-move, pp. 991–999. ISSN: 0167-8655.
- [SR09] S. Shah and A. Ross. ‘Iris segmentation using geodesic active contours’. In: *IEEE Transactions on Information Forensics and Security* 4.4 (2009), pp. 824–836.
- [Sze+12] R. Szewczyk, K. Grabowski, M. Napieralska, W. Sankowski, M. Zubert and A. Napieralski. ‘A reliable iris recognition algorithm based on reverse biorthogonal wavelet transform’. In: *Pattern Recognition Letters* 33.8 (2012). Noisy Iris Challenge Evaluation II - Recognition of Visible Wavelength Iris Images Captured At-a-distance and On-the-move, pp. 1019–1026. ISSN: 0167-8655.
- [Tan+12] T. Tan, X. Zhang, Z. Sun and H. Zhang. ‘Noisy iris image matching by using multiple cues’. In: *Pattern Recognition Letters* 33.8 (2012). Noisy Iris Challenge Evaluation II - Recognition of Visible Wavelength Iris Images Captured At-a-distance and On-the-move, pp. 970–977. ISSN: 0167-8655.
- [Tel04] A. Telea. ‘An image inpainting technique based on the fast marching method’. In: *JOURNAL OF GRAPHICS TOOLS*. 9.1 (2004), pp. 23–34.
- [THS10] T. Tan, Z. He and Z. Sun. ‘Efficient and robust segmentation of noisy iris images for non-cooperative iris recognition’. In: *Image and vision computing* 28.2 (2010), pp. 223–230.
- [Tis+02] C. Tisse, L. Martin, L. Torres and M. Robert. ‘Person identification technique using human iris recognition’. In: *Proc. Vision Interface*. i. Citeseer. 2002, pp. 294–299.

- [TK12] C.-W. Tan and A. Kumar. ‘Unified Framework for Automated Iris Segmentation Using Distantly Acquired Face Images’. In: *Image Processing, IEEE Transactions on* 21.9 (2012), pp. 4068–4079. ISSN: 1057-7149.
- [VJ01] P. Viola and M. Jones. ‘Rapid object detection using a boosted cascade of simple features’. In: *Proceedings of the 2001 IEEE Computer Society Conference on Computer Vision and Pattern Recognition. CVPR 2001* 1 (2001), pp. I-511–I-518.
- [VSN05] M. Vatsa, R. Singh and A. Noore. ‘Reducing the false rejection rate of iris recognition using textural and topological features’. In: *International Journal of Signal Processing* 2.2 (2005), pp. 66–72.
- [Wan+12] Q. Wang, X. Zhang, M. Li, X. Dong, Q. Zhou and Y. Yin. ‘Adaboost and multi-orientation 2D Gabor-based noisy iris recognition’. In: *Pattern Recognition Letters* 33.8 (2012). Noisy Iris Challenge Evaluation II - Recognition of Visible Wavelength Iris Images Captured At-a-distance and On-the-move, pp. 978–983. ISSN: 0167-8655.
- [Way+09] J. Wayman, N. Orlans, Q. Hu, F. Goodman, A. Ulrich and V. Valencia. ‘Technology assessment for the state of the art biometrics excellence roadmap’. In: *Mitre Technical Report* (2009).
- [Way99] J. L. Wayman. ‘Error rate equations for the general biometric system’. In: *Robotics & Automation Magazine, IEEE* 6.1 (1999), pp. 35–48.
- [Wil97] R. P. Wildes. ‘Iris recognition: an emerging biometric technology’. In: *Proceedings of the IEEE* 85.9 (1997), pp. 1348–1363. ISSN: 0018-9219.
- [Yao+06] P. Yao, J. Li, X. Ye, Z. Zhuang and B. Li. ‘Iris recognition algorithm using modified log-gabor filters’. In: *Pattern Recognition, 2006. ICPR 2006. 18th International Conference on*. Vol. 4. IEEE. 2006, pp. 461–464.
- [ZDB09] Z. Zhou, Y. Du and C. Belcher. ‘Transforming traditional iris recognition systems to work in nonideal situations’. In: *IEEE Transactions on Industrial Electronics* 56.8 (2009), pp. 3203–3213.
- [ZS08] J. Zuo and N. Schmid. ‘An Automatic Algorithm for Evaluating the Precision of Iris Segmentation, IEEE Second Int’. In: *Conf. on Biometrics Theory, Applications and Systems (BTAS 08) Sep.* 2008.
- [ZS10] J. Zuo and N. A. Schmid. ‘On a methodology for robust segmentation of nonideal iris images’. In: *IEEE Transactions on Systems, Man, and Cybernetics, Part B (Cybernetics)* 40.3 (2010), pp. 703–718.
- [ZTW00] Y. Zhu, T. Tan and Y. Wang. ‘Biometric personal identification based on iris patterns’. In: *Pattern Recognition, 2000. Proceedings. 15th International Conference on*. Vol. 2. IEEE. 2000, pp. 801–804.

## BIBLIOGRAPHY

---

- [ZYY05] Z. Zheng, J. Yang and L. Yang. ‘A robust method for eye features extraction on color image’. In: *Pattern Recognition Letters* 26.14 (2005), pp. 2252–2261.
- [Cen] Center for Biometrics and Security Research. *CASIA iris database*. <http://biometrics.idealtest.org/findTotalDbByMode.do?mode=Iris>. [Online; accessed 15-May-2012].
- [Mul] Multimedia university. *MMU iris database*. <http://pesona.mmu.edu.my/~ccte0/>. [Online; accessed 15-May-2012].
- [Uni] University of Bath. *BATH iris database*. <http://www.smartsensors.co.uk/information/bath-iris-image-database/>. [Online; accessed 15-May-2012].

---

## Reviewed Publications of the Author Relevant to the Thesis

- [A.1] M. Haindl and M. Krupička. Non-iris occlusions detection. In: *Biometrics: Theory, Applications and Systems (BTAS), 2013 IEEE Sixth International Conference on*. IEEE. 2013. 1-6.

The paper has been cited in:

- K. Hajari and K. Bhojar. ‘A review of issues and challenges in designing Iris recognition Systems for noisy imaging environment’. In: *Pervasive Computing (ICPC), 2015 International Conference on*. IEEE. 2015, pp. 1-6.
  - M. Yahiaoui. Modèles statistiques avancés pour la segmentation non supervisée des images dégradées de l’iris’. PhD thesis. Université Paris-Saclay, 2017.
- [A.2] M. Haindl and M. Krupička. Accurate Detection of Non-Iris Occlusions. In: *Signal-Image Technology and Internet-Based Systems (SITIS), 2014 Tenth International Conference on*. IEEE. 2014. 49-56.
- [A.3] M. Haindl and M. Krupička. Unsupervised detection of non-iris occlusions. In: *Pattern Recognition Letters 57*. 2015. 60-65.

The paper has been cited in:

- A. F. Abate, S. Barra, F. D’Aniello and F. Narducci. ‘Two-Tier Image Features Clustering for Iris Recognition on Mobile’. In: *International Workshop on Fuzzy Logic and Applications*. Springer. 2016, pp. 260-269.
- A. Abate, S. Barra, L. Gallo and F. Narducci. ‘SKIPSOM: Skewness & kurtosis of iris pixels in Self Organizing Maps for iris recognition on mobile devices’. In: *Pattern Recognition (ICPR), 2016 23rd International Conference on*. IEEE. 2016, pp. 155-159.

- A. F. Abate, S. Barra, L. Gallo and F. Narducci. ‘Kurtosis and skewness at pixel level as input for SOM networks to iris recognition on mobile devices’. In: *Pattern Recognition Letters* 91 (2017), pp. 37-43.
- A. F. Abate, S. Barra, G. Fenu, M. Nappi and F. Narducci. ‘A Lightweight Mamdani Fuzzy Controller for Noise Removal on Iris Images’. In: *International Conference on Image Analysis and Processing*. Springer. 2017, pp. 93-103.
- R. T. Al-Zubi, K. A. Darabkh and N. Al-Zubi. ‘Effect of Eyelid and Eyelash Occlusions on a Practical Iris Recognition System: Analysis and Solution’. In: *International Journal of Pattern Recognition and Artificial Intelligence* 29.08 (2015), p. 1556016.
- N. Aginako, J. Martínez-Otzerta, B. Sierra, M. Castrillón-Santana and J. Lorenzo-Navarro. ‘Local descriptors fusion for mobile iris verification’. In: *Pattern Recognition (ICPR), 2016 23rd International Conference on*. IEEE. 2016, pp. 165-169.
- N. Aginako, M. Castrillón-Santana, J. Lorenzo-Navarro, J. M. Martínez-Otzeta and B. Sierra. ‘Periocular and iris local descriptors for identity verification in mobile applications’. In: *Pattern Recognition Letters* 91 (2017), pp. 52-59.
- N. U. Ahmed, S. Cvetkovic, E. H. Siddiqi, A. Nikiforov and I. Nikiforov. ‘Using fusion of iris code and periocular biometric for matching visible spectrum iris images captured by smart phone cameras’. In: *Pattern Recognition (ICPR), 2016 23rd International Conference on*. IEEE. 2016, pp. 176-180.
- N. U. Ahmed, S. Cvetkovic, E. H. Siddiqi, A. Nikiforov and I. Nikiforov. ‘Combining iris and periocular biometric for matching visible spectrum eye images’. In: *Pattern Recognition Letters* 91 (2017), pp. 11-16.
- K. Ahuja, R. Islam, F. A. Barbhuiya and K. Dey. ‘A preliminary study of CNNs for iris and periocular verification in the visible spectrum’. In: *Pattern Recognition (ICPR), 2016 23rd International Conference on*. IEEE. 2016, pp. 181-186.
- K. Ahuja, R. Islam, F. A. Barbhuiya and K. Dey. ‘Convolutional neural networks for ocular smartphone-based biometrics’. In: *Pattern Recognition Letters* 91 (2017), pp. 17-26.
- M. Arsalan, H. G. Hong, R. A. Naqvi, M. B. Lee, M. C. Kim, D. S. Kim, C. S. Kim and K. R. Park. ‘Deep Learning-Based Iris Segmentation for Iris Recognition in Visible Light Environment’. In: *Symmetry* 9.11 (2017), p. 263.
- M. Castrillón-Santana, M. De Marsico, M. Nappi, F. Narducci and H. Proença. ‘Mobile iris challenge evaluation ii: results from the ICPR competition’. In: *Pattern Recognition (ICPR), 2016 23rd International Conference on*. IEEE. 2016, pp. 149-154.



- G. Cheng, W. Yang, D. Zhang and Q. Liao. ‘A Fast and Accurate Iris Segmentation Approach’. In: International Conference on Image and Graphics. Springer. 2015, pp. 53-63.
  - C. N. Devi. ‘Automatic segmentation and recognition of iris images: With special reference to twins’. In: Signal Processing, Communication and Networking (ICSCN), 2017 Fourth International Conference on. IEEE. 2017, pp. 1-5.
  - M. De Marsico, M. Nappi and H. Proença. ‘Results from MICHE II-Mobile Iris CHallenge Evaluation II’. In: Pattern Recognition Letters 91 (2017), pp. 3-10.
  - C. Galdi and J.-L. Dugelay. ‘Fusing iris colour and texture information for fast iris recognition on mobile devices’. In: Pattern Recognition (ICPR), 2016 23rd International Conference on. IEEE. 2016, pp. 160-164.
  - C. Galdi and J.-L. Dugelay. ‘FIRE: Fast Iris REcognition on mobile phones by combining colour and texture features’. In: Pattern Recognition Letters 91 (2017), pp. 44-51.
  - F. Jan. ‘Segmentation and localization schemes for non-ideal iris biometric systems’. In: Signal Processing 133 (2017), pp. 192-212.
  - S. Memar Zadeh and A. Harimi. ‘Iris localization by means of adaptive thresholding and Circular Hough Transform’. In: Journal of AI and Data Mining 5.1 (2017), pp. 21-28.
  - A. Rattani and R. Derakhshani. ‘Ocular biometrics in the visible spectrum: A survey’. In: Image and Vision Computing 59 (2017), pp. 1-16.
  - F. A. Santos et al. ‘Uma solução baseada no reconhecimento de íris para proteção de dados em dispositivos móveis’. In: (2016).
  - X. Wang, Y. He, K. Pei, M. Liang and J. He. ‘Combining Multiple Color Components for Efficient Visible Spectral Iris Localization’. In: Chinese Conference on Biometric Recognition. Springer. 2016, pp. 366-373.
- [A.4] M. Krupička and M. Haindl. Iris Recognition. In: *DAR 2011 Mariánská*. 2011.
- [A.5] J. Filip, R. Vávra, M. Haindl, P. Žid, M. Krupička and V. Havran. BRDF slices: Accurate adaptive anisotropic appearance acquisition In: *Proceedings of the IEEE Conference on Computer Vision and Pattern Recognition*. 2013. pp 1468-1473.

The paper has been cited in:

- D. Antensteiner and S. Štolc. ‘Full BRDF Reconstruction Using CNNs from Partial Photometric Stereo-Light Field Data’. In: Proceedings of the IEEE Conference on Computer Vision and Pattern Recognition Workshops. 2017, pp. 13-21.
- K. J. Dana. ‘Capturing Computational Appearance: More than meets the eye’. In: IEEE Signal Processing Magazine 33.5 (2016), pp. 70-80.

- J. S. Kautz. ‘In-Situ Cameras for Radiometric Correction of Remotely Sensed Data’. PhD thesis. The University of Arizona, 2017.
  - B. Raymond. ‘Contrôle de l’apparence des matériaux anisotropes’. PhD thesis. Bordeaux, 2016.
  - C. Schwartz, R. Sarlette, M. Weinmann, M. Rump and R. Klein. ‘Design and implementation of practical bidirectional texture function measurement devices focusing on the developments at the University of Bonn’. In: *Sensors* 14.5 (2014), pp. 7753-7819.
  - M. Weinmann and R. Klein. ‘Advances in geometry and reflectance acquisition (course notes)’. In: *SIGGRAPH Asia 2015 Courses*. ACM. 2015, p. 1.
- [A.6] J. Filip, R. Vávra and M. Krupička. ‘Rapid material appearance acquisition using consumer hardware. In: *Sensors* 14.10 (2014) 2014. pp 19785-19805.

The paper has been cited in:

- J. Čáap, J. Hošek, V. Havran, Š. Němcová and K. Macúchová. ‘Optomechanical design of rotary kaleidoscope for bidirectional texture function acquisition’. In: *Applied Optics* 56.26 (2017), pp. 7373-7384.
- D. Den Brok, H. C. Steinhausen, M. B. Hullin and R. Klein. ‘Multiplexed acquisition of bidirectional texture functions for materials’. In: *Proc. of SPIE-IS&T Vol 9398* (2015), 93980F-1.
- W. Dong, H.-L. Shen, X. Du, S.-J. Shao and J. H. Xin. ‘Spectral bidirectional texture function reconstruction by fusing multiple-color and spectral images’. In: *Applied optics* 55.36 (2016), pp. 10400-10408.
- D. Guarnera, G. C. Guarnera, A. Ghosh, C. Denk and M. Glencross. ‘Brdf representation and acquisition’. In: *Computer Graphics Forum*. Vol. 35. 2. Wiley Online Library. 2016, pp. 625-650.
- D. Guarnera, G. C. Guarnera, A. Ghosh, I. Hall and M. Glencross. ‘Capturing and representing brdfs for virtual reality’. In: *SIGGRAPH ASIA 2016 Courses*. ACM. 2016, p. 5.
- V. Havran, J. Hošek, Š. Němcová, J. Čáap and J. Bittner. ‘Lightdrum—Portable Light Stage for Accurate BTF Measurement on Site’. In: *Sensors* 17.3 (2017), p. 423.
- J. Hošek, V. Havran, Š. Němcová, J. Bittner and J. Čáap. ‘Optomechanical design of a portable compact bidirectional texture function measurement instrument’. In: *Applied Optics* 56.4 (2017), pp. 1183-1193.
- H. C. Steinhausen, R. Martín, D. den Brok, M. B. Hullin and R. Klein. ‘Extrapolation of bidirectional texture functions using texture synthesis guided by photometric normals’. In: *SPIE/IS&T Electronic Imaging*. International Society for Optics and Photonics. 2015, 93980A-93980A.

- H. C. Steinhausen, D. den Brok, M. B. Hullin and R. Klein. ‘Extrapolating Large-Scale Material BTFs under Cross-Device Constraints.’ In: VMV. 2015, pp. 143-150.
  - X. Zhang, L. Yang, S. Cui and T. Wu. ‘YUV-based material modeling from a single image’. In: Image and Signal Processing, BioMedical Engineering and Informatics (CISP-BMEI), International Congress on. IEEE. 2016, pp. 801-805.
  - X. Zhanga, S. Cui, H. Cuia, L. Yangb and T. Wub. ‘Material appearance acquisition from a single image’. In: Seventh International Conference on Electronics and Information Engineering. International Society for Optics and Photonics. 2017, 103221E-103221E.
- [A.7] J. Filip, R. Vávra, M. Havlíček and M. Krupička. Predicting Visual Perception of Material Structure in Virtual Environments. In: *Computer Graphics Forum. Vol. 36. 1.* Wiley Online Library. 2017. 89-100.

The paper has been cited in:

- R. Martín, M. Weinmann and M. B. Hullin. ‘Digital transmission of subjective material appearance’. In: (2017).
- K. Vanhoey, B. Sauvage, P. Kraemer and G. Lavoué. ‘Visual Quality Assessment of 3D Models: On the Influence of Light-Material Interaction’. In: ACM Transactions on Applied Perception (TAP) 15.1 (2017), p. 5.



---

## Remaining Publications of the Author Relevant to the Thesis

- [A.8] Krupička, Mikuláš *Iris recognition*. Ph.D. Minimum Thesis, Faculty of Information Technology, Prague, Czech Republic, 2012.